EFFICIENT SPACE-TIME SIGNALLING

EFFICIENT SPACE-TIME SIGNALLING SCHEMES: COHERENT AND NON-COHERENT SCENARIOS

By

RAMY H. GOHARY, B.Sc., M.Sc.

APRIL 2006

A Thesis

Submitted to the Department of Electrical & Computer Engineering

and the School of Graduate Studies

in Partial Fulfilment of the Requirements

for the Degree of

Doctor of Philosophy

McMaster University

DOCTOR OF PHILOSOPHY (2006) — McMaster University

(Electrical & Computer Engineering) — Hamilton, Ontario

TITLE:	Efficient Space-Time Signalling Schemes: Coherent and Non-Coherent Scenarios
AUTHOR:	Ramy H. Gohary B.Sc. (Communications and Electronics Engineering) Assiut University, Assiut, Egypt M.Sc. (Communications and Electronics Engineering) Cairo University, Giza, Egypt
SUPERVISOR:	Timothy N. Davidson, Associate Professor
NUMBER OF PAGES:	xiv, 165

Dedications

To the memory of my father,

to my mother,

my siblings,

my wife,

and my daughter Lina.

Abstract

In this thesis we develop new practical transmission and detection techniques for wireless multiple-input multiple-output (MIMO) communication systems operating over frequency-flat block Rayleigh fading channels. Both the coherent scenario where the fading coefficients are known at the receiver but not at the transmitter and the non-coherent scenario where these coefficients are not known at either the transmitter or the receiver are considered.

For coherent systems, we develop a design method for a class of codes known as Linear Dispersion (LD) codes. This class of codes subsumes several standard designs and can be used with systems that have an arbitrary number of transmit and receive antennas. We show that for systems that employ a large number of transmit antennas, LD codes constructed from random unitary coding matrices become asymptotically optimum from different design perspectives, viz., Minimum Mean Square Error (MMSE), mutual information and average Pairwise Error Probability (PEP). Those measures have a direct impact on the detection complexity, data rate and error performance that a space-time code can achieve. Using the insight generated by the asymptotic result, we provide a structured design technique for these codes that suits a broad class of finite configurations. Although our main result is based on large systems, we demonstrate via simulations that even for small systems, our codes can support higher data rates and provide performance advantages over known designs.

Based on the asymptotic results, we also propose a row interleaving scheme. This interleaving scheme is shown to result in significant performance enhancement without incurring additional detection complexity.

For the non-coherent communication scenario we focus on wireless systems operating at moderate-to-high SNRs. At high SNRs, the capacity achieving distribution for this channel corresponds to the isotropic distribution on a Grassmann manifold. Using a subspace perturbation analysis, an appropriate metric for the distance between Grassmannian constellation points is determined. Based on this metric, a greedy technique for designing constellations that mimic the isotropic distribution is then proposed. Our numerical examples show that our choice of the metric yields constellations that outperform other designs as the data rate approaches the high SNR non-coherent capacity limit. In addition to the proposed constellation design technique, we use the subspace perturbation analysis to develop an efficient suboptimum detector. The performance of this detector is comparable to that of the maximum likelihood detector, but it requires considerably less computational effort. Finally, seeing as the pairwise error probability (PEP) is indicative of the system performance at high SNR, we derive an exact expression for this quantity. As compared to other PEP expressions, our expression is easier to compute and can be used to extract more insight into the key parameters that affect the high SNR performance of the non-coherent system.

Acknowledgments

As my Ph.D. program at McMaster university comes to an end, I look back in time and I see people whose input to my progress and my life is unmistakable. Regrettably, I will not be able to mention all of them nor will I be able to give those who I mention the full merit of their doings. I have been surrounded by great loving people who would share in full the happiness of my graduation.

I am particularly indebted to my late father. His ability to overlook details and to have a clear vision of the global picture has always guided me through my struggles. His sincere love and hearty support are things that I truly miss. He helped me to discern my way to engineering. My heart and mind are set on not disappointing him.

Without her love and confidence in me, I would not have made it. She taught me how to explore my options and to trust my instincts. Mom, I am so grateful to you.

As to my wife, Lili, I am grateful to her for she willingly put up with my mood swings on the days when my Ph.D. work was not going as I would have hoped for.

Another person who had a great influence on me is N. Shonbo. I am indebted to his sincere friendship and his generous contribution in teaching me many valuable skills. I am indebted to my siblings Cherine, Heba, Hisham and Abla, for they have always been a wonderful example of perseverance and determination. I am also indebted to my bosom friends H. Saad and W. Samir for their uninterrupted support throughout the previous years.

I would like to thank my math teachers Mr. K. Haleem and Mr. A. Ishak for being

the first to introduce me to the elegance and beauty of math. I would also like to thank my professors in the Electrical and Computer Engineering (ECE) department at Assiut University, Egypt, for conscientiously providing the engineering background that has later proven invaluable. I would also like to thank my supervisors during the M.Sc. program, Dr. E. K. Al-Hussaini and Dr. H. Mourad of the ECE department at Cairo university, Egypt, for enriching my background in communication engineering.

I am indebted to the land and people of this magnanimous country, Canada. The inviting warmth of Canadians made me feel at home from the very first day in this land. Canada has offered me the chance not only to learn, but to enjoy learning.

I would like to thank the ECE department of McMaster university for the research facilities and healthy atmosphere it provides for its students. I would like to thank our administrative and technical staves. In particular, I would like to thank Mrs. H. Jachna for the moral support she has always provided to us, the students. I would also like to thank Mrs. C. Gies for she has been our refuge each time we were stranded with the paper work. Her sense of humour adds a pleasant ingredient to our department. I would like to thank Mr. T. Greenlay and Mr. C. Coroiu for keeping our systems up and running. They have always been there each time the machines gave us trouble.

I would like to thank all my friends and colleagues in the department for the continuous discussions that have certainly enhanced my scope of knowledge. I would also like to thank my dear friend, D. Agueev. Our walks by the lake and his sharp crisp comments have always been a great source of relief and enlightenment.

I would like to thank Dr. W. Hanley and Dr. A. Rosner of the French department for giving me access to the riches of the French language.

I would like to express my deepest gratitude to Dr. T. Luo for all the help and guidance he generously provided. I would also like to thank the members of my supervisory committee, Dr. M. K. Wong and Dr. N. Balakrishnan for their insightful

comments during the committee meetings. I owe special thanks to Dr. M. Min-Oo for all the discussions we used to have in his office. His questions and comments during these sessions have contributed a great deal to my understanding.

Finally, I would like to thank my supervisor and my friend, Dr. T. N. Davidson. During the past four years I had the privilege and the honour of being Dr. Davidson's student. As a supervisor, his sound counsel has always guided me. He enriched my knowledge with stimulating and fruitful discussions. As a friend, his friendship has always been generous and giving. He listened when I was worried and supported at the time of need. Dr. Davidson, I still have a lot to learn from your lofty standards and your decent subtlety. There is not much to say other than "Thank You".

Contents

List of Figures

Chapter 1

Introduction

The focus of this thesis is the development of transmission and reception strategies for multiple-input multiple-output (MIMO) wireless communication systems. These systems possess many desirable features that render them attractive for applications that require the reliable transfer [1] of high data rates [2] between the communicating terminals. We begin by introducing the principles of wireless MIMO systems, their features and limitations.

1.1 Communication over the wireless channel

Communication systems operating over wireless channels possess the attractive feature of maintaining flexible connectivity between the communicating terminals [3] without requiring the installation of costly wireline networks. However, in order for this connectivity to be both efficient and reliable, the system designer has to take into account the inherent way in which the information carrying signal propagates, as well as the time-varying nature of the wireless medium over which these systems operate [4]. In particular, the information carrying waves emitted from the transmitter impinge on surrounding objects in a way that causes the portion of waves that reach

the receiver to travel along different paths. Signals traveling along different paths undergo different attenuations, phase rotations and possibly different time delays. Waves arriving at the receiver at approximately the same time instant may combine constructively, resulting in high signal levels, or destructively, resulting in low signal levels. This signal level fluctuation phenomenon is known as fading [5] and is one of the key features that characterize the wireless communication medium. In addition to signal level fluctuation, if the length of the propagation paths taken by the waves differ significantly, the information carrying waves experience different time delays. This causes the signals that were transmitted at different time instants to interfere with each other at the receiver, resulting in the so called intersymbol interference [4].

In addition to the difficulties that follow from multipath propagation and time-variance, the fact that the wireless medium can be shared by other services and users that operate in the same frequency band produces another source of impairment. In particular, the signals from these extrinsic sources interfere with the desired signal at the receiver and reduce the reliability of detection.

In spite of the challenges it presents, the multipath propagation mechanism that is inherent of wireless communication channels can actually be exploited to serve the communication process. In order to see that, consider a scenario in which the transmitter launches possibly different representations of the same message signal along multiple paths simultaneously. Even if one of these paths happens to undergo atypical attenuation, the remaining paths will still provide a detectable signal to the receiver [1]. On the other hand, from a data rate perspective, if for the moment we ignore the interference between paths, each path can be regarded as a separate channel. Hence, one can increase the data rate that can be supported by a single channel by transmitting independent data over different paths. Thus one can see that the flow of information along multiple paths can be exploited either to subsidize the reliability of the wireless communication link or to increase the data rate. In fact,

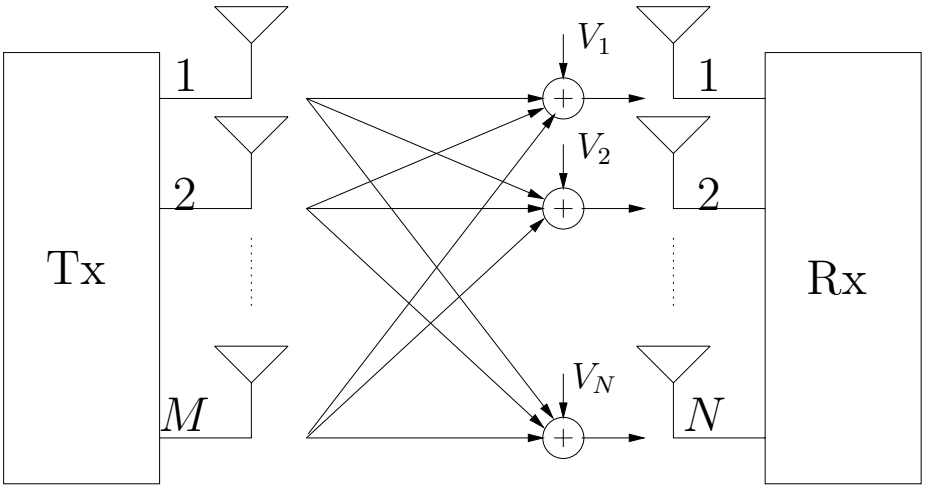

Figure 1.1: Multiple antenna system.

realizing these two gains is not exclusive. Indeed, it was shown in [6, 7] that there is a certain trade-off that governs the rate at which the achievable data rate and the reliability can be simultaneously increased.

1.2 Wireless MIMO Systems

In order to realize the potential advantages of multipath propagation, the information carrying signal must be transmitted along multiple paths in a controlled manner. One way to do so is by utilizing multiple transmit and receive antennas. In particular, let us assume that the transmitter is equipped with M antennas and that the receiver is equipped with N antennas. This setup is depicted in Figure 1.1. The arrows in this figure denote the MN signal paths that connect the transmitter and the receiver. In general, the path between the i-th transmit and the j-th receive antenna can comprise several subpaths [5], where each subpath is typically characterized by two parameters that depend on the length and nature of this subpath; a complex scalar gain and a non-negative delay. The received signal from the ij-th path is the sum of all the signals components in the constituent subpaths. Hence, each path resembles a finite

impulse response (FIR) filter[1] whose frequency response is a complex gain function that characterizes the path [5]. If the bandwidth occupied by the signal is narrow enough so that the frequency response of each path is essentially constant within this band, the complex gain function of each path can be well approximated by a complex scalar in the band of interest [3]. In this case the channel is said to be frequency-flat. On the other hand, if the bandwidth occupied by the signal is not sufficiently small to justify the approximation of the complex gain function of each path by a complex scalar, the channel is said to be frequency-selective. In the frequency-selective case it is possible to decompose the wideband signal into components that occupy non-overlapping narrow frequency subbands. If the decomposition of the wideband signal is sufficiently fine, the channel within each of these subbands can be considered to be frequency-flat [8,9]. For this reason we will restrict our attention to frequency-flat propagation, where the complex gain functions are assumed to be complex scalars.

Depending on the nature of the propagation environment and the mobility of the transmitter and the receiver, the complex gain functions can vary with time. The rate at which these functions vary is one of the basic parameters that describe the wireless channel. For instance, if the variations of the gain functions over a few signalling intervals is small, the channel is said to be slowly-fading. Otherwise, if the gain functions vary within one signalling interval, it is called fast-fading. Throughout this thesis we will restrict our attention to a subclass of slowly-fading frequency-flat channels. This subclass comprises channels that remain essentially constant for a few signalling intervals and then take on independent values. This subclass is called block-fading and will be described in Chapter 2 in more detail. We will refer to the time interval during which the gain functions remain approximately constant as the coherence time of the channel. This parameter plays a central role in selecting an

[1]The main difference between a conventional FIR filter and a composite signal path is that the tap delays of the FIR filter are integer multiples of the signalling interval, whereas for a signal path the delays associated with subpaths are arbitrary.

appropriate signalling strategy that can benefit from the potential advantages that a given communication scenario can offer.

In addition to the distortion that the signal undergoes due to fading, the signal at the receiver is affected by a number of parasitic factors. These factors are due to the thermal noise that is introduced by the electronic devices involved in the signal conditioning stages that precede information recovery. The overall effect of these parasitic factors can be modelled by an additive term that can be usually assumed to be statistically independent of both the transmitted signal and the propagation channel. In Figure 1.1 we denote this additive noise term at the i-th receive antenna by V_i.

One of the goals of using multiple transmit and receive antennas is to provide the receiver with diverse representations of the transmitted signal. This goal can be achieved if the wireless channel is richly scattered. In this case, the complex path gains become statistically independent. This causes the transmitted signal to undergo independent fading along each propagation path and hence provides the receiver with statistically independent variants of the information carrying signal. If the channel is not sufficiently scattered, several signal paths may fade in a similar way resulting in reduced diversity of the received signal.

Field measurements show that, in a richly scattered environment, statistical independence between the complex path gains can be approximately achieved when the antenna elements of both the transmitter and the receiver are spaced sufficiently apart; typically the antenna elements are placed on a rectangular lattice with spacing that ranges between 0.5λ and 10λ, where λ is the carrier wavelength [10, 11]. For example, with a 5 GHz carrier frequency, λ is only about 6 cm. This indicates that when the frequency of the carrier signal is sufficiently high, typically available space can easily accommodate several well-spaced antenna elements.

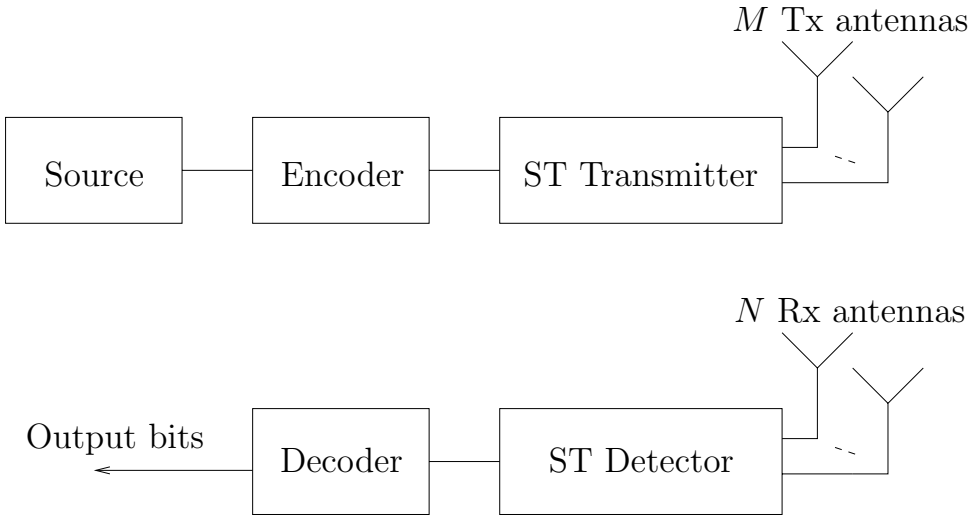

Figure 1.2: A generic MIMO communication system.

1.3 Space-Time signalling

In communication systems in which the transmitter has only one antenna element, data is encoded over the time axis, which is usually partitioned into slots that represent a signalling frame. However, in systems in which the transmitter is equipped with multiple antenna elements data can be jointly encoded; spatially over the transmit antennas and temporally over the time axis. In this case, the encoding surface is partitioned into space-time slots, where each slot represents a specific transmit antenna and a specific signalling interval. In order to show how encoding over space and time can be performed jointly, in this section we describe the basic building blocks of a generic MIMO communication system model. A block diagram of such a system is shown in Figure 1.2. Consider the scenario where an information source generates data in the form of raw bits. The raw bits are encoded and fed to the multiple antenna transmitter which parses the encoded data stream into blocks. In order for these data blocks to be transmitted over a wireless medium, the transmitter maps each block of

bits to a corresponding space-time channel symbol using a mapper, where a space-time channel symbol represents a particular assignment of signalling waveforms to each space-time slot. The set of all admissible channel symbols is usually called a space-time code [3]. The signalling waveforms output from the space-time encoder are then amplified and fed to the transmit antennas that radiate these signals in the respective space-time slots.

At the receiver side the transmission process is reversed. The receiver first detects the transmitted waveforms using a space-time detector. These waveforms are then demapped to produce a stream of data bits. This stream is then passed to the decoder which produces a stream of bits that corresponds to the original stream of raw bits[2].

We now consider different signalling strategies. To begin with, we recall that the coherence time of the wireless channel is the time interval during which the channel remains essentially constant. The length of this time interval is an important element in determining the appropriate signalling strategy. In one scenario, the coherence time is assumed to be long [8] enough for the transmitter to send many pilot symbols to the receiver. Since these pilot symbols are known at the receiver, they can be used to generate accurate estimates of the channel parameters. If the coherence time is sufficiently long, the receiver can feed back the channel knowledge it has just acquired to the transmitter over a separate feedback channel. In this scenario, the coherence time is said to be long if the amount of time required to acquire the channel knowledge at the communication terminals is negligible compared to the overall coherence time. Now that the transmitter has perfect channel information, it can use this information to organize its transmission strategy in such a way that maximizes the amount of data being transfered reliably over the link. The receiver for its part exploits the channel information to perform efficient detection of the received signal.

[2]For the simplicity of exposition, we have only considered disjoint detection and decoding. However, these two processes can be interlinked. An instance of an iterative detection technique to do that can be found in [12].

While the scenario of perfect channel knowledge at both the receiver and the transmitter allows for the reliable transfer of high data rates, the resources that are needed to realize this scenario are often hard to accommodate [13]. In particular, even if we assume that a separate channel is available for the receiver to feed accurate channel parameters back to the transmitter, the mobility of the transmitter and/or the receiver usually limits the coherence time, and the channel may change significantly before the receiver manages to convey its channel knowledge to the transmitter. This situation gives rise to a more practical communication model. In this model, the receiver is assumed to be able to estimate the channel accurately, but no channel information is fed back to the transmitter [13]. An interesting feature that this model shares with the previous one is that the maximum data rate that can be communicated over the MIMO channel is achieved by linearly structured space-time coding techniques [14, 15]. Because in this scenario the receiver has access to an accurate channel model that facilitates the process of data recovery, this communication model is usually referred to as coherent [16].

In the coherent communication model the coherence time is assumed to be long enough to warrant neglecting the fraction of the transmission time required for the receiver to acquire an accurate model of the channel in comparison with the overall transmission time. In many practical situations the variations in the channel parameters are quite fast, and the time required for the receiver to acquire a reasonably accurate channel model may consume a significant portion of the available time for communication. This problem becomes more pronounced in systems that employ a large number of transmit antennas [6]. For these instances, the communication scenario may be better described by a model in which neither the transmitter nor the receiver has any channel information available *a priori*. This communication model is usually referred to as non-coherent [16]. Similar to the coherent channel case, in this scenario the transmitter can still send pilot symbols for the receiver to identify

the channel parameters and perform coherent detection. However, unlike the coherent channel model, this procedure is properly accounted for in the design of the non-coherent communication system.

In addition to the communication models described in this section, there are other interesting models in which the receiver and possibly the transmitter have access to partial channel information [13, 17]. However, these models are beyond the scope of this thesis and will be considered in future work.

1.4 Thesis Outline

The focus of this thesis is on the design of space-time encoding and detection techniques for both the coherent and the non-coherent communication scenarios. In all cases we assume that the transmitter has no access to channel information.

We begin in Chapter 2 by reviewing the fundamental limits of space-time wireless communication systems. The goal of this chapter is to provide the relevant definitions that will be used in subsequent chapters. This chapter also includes an overview of different classes of space-time coding techniques, their advantages and limitations. A key issue that arises in space-time communication contexts is the complexity of optimum detection strategies and methods for implementing efficient suboptimum detectors. We include in this chapter a brief description of a class of practical detectors known as sphere detectors [18]. This class of detectors exploits the linear structure of the input signals to perform coherent detection. Under certain conditions the performance of these detectors can be quite close to that of optimum maximum likelihood detectors, but with significantly reduced computational complexity. An underlying principle of these detectors will be used in Chapter 5 to develop an efficient suboptimum detection strategy for non-coherent channels. While the purpose of Chapter 2 is to summarize known results and conventional space-time coding techniques, the main contributions

of this thesis are included in Chapters 3, 4 and 5. In order to maintain the continuity of flow, most of the proofs are presented in the appendices.

In Chapter 3, we consider communication over coherent space-time channels using a class of general space-time codes called Linear Dispersion (LD) codes [14]. This class of space-time codes subsumes many standard designs and can be applied in systems with arbitrary number of transmit and receive antennas. In this chapter we present a systematic design technique for these codes. We show that this design technique is asymptotically optimum from several practical standpoints.

In Chapter 4, we consider communication over non-coherent space-time channels. It was shown in [19] that the distribution of the input signals that maximize the rate at which data can be reliably transferred over these channels is isotropic on the compact Grassmann manifold. In this chapter we begin by arguing that an appropriate metric for measuring the distance between Grassmannian constellation points is given by the chordal Frobenius norm. We then use this metric to develop a practical greedy algorithm for designing Grassmannian constellations. The constellations designed using this algorithm are shown to perform well in practice.

A major drawback of non-coherent space-time communication systems follows from the nonlinear fashion in which the optimal space-time signals are structured. This feature inhibits the use of efficient suboptimal techniques like sphere detectors in the detection process. In order to promote the practical application of Grassmannian signalling over non-coherent channels, in Chapter 5 we address the problem of detecting Grassmannian signals efficiently. We propose a novel efficient suboptimal detector. The performance of this detector is close to that of the optimum maximum likelihood detector but requires considerably less computational power.

Chapter 6 concludes the thesis and suggests a few directions for future research.

Chapter 2

Principles of space-time communications

This chapter provides an introduction to the fundamentals of wireless MIMO communication systems. A space-time signalling scheme is given by a set of signalling waveforms $\{u_{ij}(t)\}$, where each of these waveforms is localized in a specific space-time slot; see Section 1.3. That is, the signal transmitted from the j-th antenna can be written as $\sum_i u_j(t - iT_s)$, where $1/T_s$ is the symbol rate. In a practical communication system, the signalling waveforms are required to meet specific limitations on the bandwidth of the available communication channel as well as to be resilient against timing errors that result from imperfect synchronization at the receiver. A standard technique to confine the signalling waveforms to the allocated bandwidth while maintaining practical robustness against timing errors is to use a pulse-shaping waveform $p(t)$ that is independent of both the space-time slot and the data content of the waveform. Using this technique, the signalling waveforms can be expressed as $\{u_{ij}(t) = p(t)s_{ij}(t)\}$, where $s_{ij}(t)$ is the information-carrying waveform. Typically, $p(t)$ is chosen to be a root-raised cosine waveform, which is a pulse-shaping waveform

whose autocorrelation satisfies the Nyquist criterion required for zero intersymbol interference (ISI). In comparison with other conventional choices of waveforms whose autocorrelations satisfy the Nyquist criterion, a root-raised cosine waveform has the advantage of being quite resilient to small timing errors that result for inaccurate synchronization at the receiver [5].

Having considered an appropriate choice of the pulse-shaping waveforms, we now consider the second constituent of the signalling waveforms; i.e., the information-carrying waveforms $\{s_{ij}(t)\}$. The function space occupied by these waveforms can be represented by a set of orthogonal functions $\{\phi_k(t)\}$ that form a basis for this space. Hence, each signalling waveform can be written as a distinct linear combination of the basis functions. That is, for any real signal $s_{ij}(t)$ one can write

$$s_{ij}(t) = \sum_k s_{ij}^k \phi_k(t). \tag{2.1}$$

A standard choice for the basis functions in (2.1) is the pair of quadrature sinusoidal waveforms $\cos(2\pi f_c t)$ and $\sin(2\pi f_c t)$, where f_c is the carrier frequency. When the quadrature sinusoidal waveforms are chosen as basis functions, each waveform in the space-time code, $s_{ij}(t)$, can be represented by one complex scalar, s_{ij}, that specifies the amplitude and the phase of the sinusoid. This characterization of the signalling waveforms will give rise to the space-time communication model we describe below.

In a space-time communication system that uses quadrature sinusoidal waveforms, the set of complex scalars, $\{s_{ij}\}$, that represent the information-carrying signals in (2.1) is typically endowed with some embedded structure that enables the space-time scheme to satisfy a set of desirable signalling properties. Typically, these properties include the ability of the code to support high data rates [15], to be resilient to possible adverse channel conditions, and to be easily detectable [20].

Consider the scenario where M transmit antennas are used to transmit data in

blocks, where each block spans T time slots. In the sequel, a time slot will be referred to as a channel use. Using complex scalars to represent the phases and amplitudes of the signalling waveforms in the TM space-time slots, one can represent any particular assignment of waveforms in a specific $T \times M$ block by a complex-valued $M \times T$ matrix S. We will refer to each of these matrices as a space-time codeword and the set of all admissible waveform assignments as the space-time codebook, $\mathcal{S}$.

As mentioned in Chapter 1, we will only consider the case of flat-fading channels. That is, the case in which the complex channel gain function from each transmit antenna to each receive antenna can be represented by a complex scalar. Assuming that the receiver has N receive antennas, one can represent the channel coefficients in the form of an $N \times M$ matrix H. The $N \times T$ received signal Y can be written as,

$$Y = HS + V, \tag{2.2}$$

where $S \in \mathcal{S}$ and V is an $N \times T$ matrix that represents the noise samples. Apart from scaling factors that will be assigned to either the noise term or signal term, we will be using this generic model throughout the thesis.[1] In the next section we will review the fundamental limits of space-time signalling schemes that can be represented by this model.

2.1 Fundamental limits of space-time signalling

In order to assess the performance of a given signalling scheme, it is useful to have fundamental benchmarks against which the performance of different schemes can be measured. One of the critical benchmarks in communication theory is given by the channel capacity [21]. The channel capacity can be thought of as a tight upper bound on the maximum data rate that can be reliably communicated over the channel [21].

[1] For convenience, in Chapters 4 and 5 we will use the transposed version of this model.

This quantity is a characteristic property of the channel and is equal to the maximum mutual information $I(S;Y)$ between the input signal S and the output signal Y [21], where the maximization is carried over all admissible distributions of the input signal.

Before providing mathematical expressions for the channel capacities for the communication scenarios of interest, we will define an important class of channels that can be used to represent many practical communication scenarios [20].

Definition 2.1 (Block-Fading Channel) *A communication channel that is represented by a random matrix, H, is said to be a block-fading channel with coherence time T if for each block of T channel uses the channel assumes an independent realization.*

The average mutual information between the input and the output of this channel is given by

$$I(S;Y) = \mathrm{E}_H\{I(S;Y|H)\}, \tag{2.3}$$

where $\mathrm{E}_\chi\{\cdot\}$ denotes mathematical expectation over χ. If we allow the information to be encoded across blocks, the maximum data rate that can be reliably communicated over this channel is equal to the maximum average mutual information between the input, S, and the output, Y. This quantity is called the ergodic channel capacity [2, 13].

Definition 2.2 (Ergodic Capacity) *The ergodic capacity of a block-fading channel is defined as the maximum average rate that can be communicated over this channel. In particular,*

$$C = \max_{p(S)\in\mathcal{P}} I(S;Y) = \max_{p(S)\in\mathcal{P}} \mathrm{E}_H\{I(S;Y|H)\}. \tag{2.4}$$

Notice that in this definition, any constraints on the input signals, S, (e.g., average or maximum power constraints) can be incorporated in the set of admissible distributions, $\mathcal{P}$.

2.1.1 Ergodic capacity of MIMO systems

The noise matrix V in (2.2) accounts for all the parasitic terms that contribute additively to the received signal. When these terms are statistically independent with zero-mean, the central limit theorem [22] asserts that the entries of V approach the zero-mean Gaussian distribution as the number of additive terms grows. Given the multitude of the parasitic elements that may affect the communication system, it is customary to assume that the entries of V have a circularly symmetric Gaussian distribution [3, 5]. That is, $V_{ij} \sim \mathcal{CN}(0, \sigma^2)$, where $\mathcal{CN}(0, \sigma^2)$ denotes the complex zero-mean circularly symmetric Gaussian distribution with variance σ^2. Under the assumption that the noise is Gaussian, the ergodic channel capacity was studied in [2] and [10] for the coherent channel and in [23] and [19] for the non-coherent one. In this section we will discuss the main results for these two cases.

Coherent MIMO systems

In Chapter 1 we have described the coherent communication scenario where the receiver knows the channel matrix, H, but the transmitter has no access to channel information. In this case, under the Gaussian assumption on the noise, it is possible to compute the maximization in (2.4) explicitly [2]. In particular, the ergodic capacity of the coherent channel is given by

$$C_{\text{coherent}} = \mathrm{E}_H\Big\{\log\big(\det(I_N + \tfrac{\rho}{M} HH^\dagger)\big)\Big\}, \tag{2.5}$$

where I_N denotes the identity matrix of size N, $(\cdot)^\dagger$ denotes the Hermitian transpose and ρ denotes the ratio of the average signal power in the received signal to the average noise power in the received signal. This quantity is usually referred to as the average signal-to-noise ratio (SNR). Using the model in (2.2) the average SNR can be written as

$$\rho = \frac{\mathrm{E}\{\|HS\|_F^2\}}{\mathrm{E}\{\|V\|_F^2\}},$$

where $\|A\|_F$ is the Frobenius norm of the matrix A.

The distribution of the input signals that achieves capacity is the circularly-symmetric complex Gaussian distribution with zero-mean and covariance $\frac{\rho}{M} I_M$ [2]. If the entries of H can be modeled as independent identically distributed (i.i.d.) complex Gaussian random variables then the expectation in (2.5) can be computed explicitly yielding a complicated expression in terms of Laguerre polynomials [2]. A deeper insight into the coherent channel capacity in that scenario can be obtained by considering a lower bound for the expression in (2.5). This bound was developed in [10] and is given by

$$C_{\text{coherent}} \geq \min(M,N) \log\left(\tfrac{\rho}{M}\right) + \sum_{i=\max(M,N)-\min(M,N)+1}^{\max(M,N)} \mathrm{E}\{\log_2(\chi^2_{2i})\}, \qquad (2.6)$$

where χ^2_{2i} is a Chi-square random variable with $2i$ degrees of freedom. This bound becomes asymptotically tight at high SNR. By comparing the bound in (2.6) with the corresponding bound for single-input single-output (SISO) antenna systems (systems for which $M = N = 1$), it can be seen that the high SNR capacity of the MIMO system is roughly $\min(M,N)$ times the high SNR capacity of the SISO system. Because one can regard the $\min(M,N)$ factor as the number of parallel data pipes available for communication, this factor is sometimes referred to as the multiplexing gain [6] or, alternatively, as the number of communication degrees of freedom of the MIMO system [19].

In Chapter 3, we will develop a practical coding technique that enables the MIMO system to communicate reliably at rates that are close to the ergodic channel capacity. The philosophy of our approach is based on the observation that as the number of transmit antennas increases, a class of linearly structured codes becomes optimal from both rate and reliability perspectives.

Non-coherent MIMO systems

The expression for the ergodic capacity of a coherent MIMO channel shows the valuable rate advantage that MIMO systems have over SISO systems. However, coherent communication over MIMO channels requires significantly more training than SISO channels [24], because the receiver will have to learn a total of MN complex channel parameters. This task may exhaust a considerable portion of the overall communication resource. In order to account for the resources that would have to be expended to identify the channel, one ought to evaluate the ergodic capacity of the non-coherent MIMO systems. That is, systems in which no channel knowledge is available at either the transmitter or the receiver; see Chapter 1.

For non-coherent systems, computing the mutual information between the system input and output in (2.3) at any SNR remains an open problem. However, in [16], using first principles, the high SNR ergodic non-coherent capacity of SISO systems was computed explicitly. Using a fundamentally different technique, the high SNR ergodic non-coherent capacity of MIMO systems with arbitrary number of receive and transmit antennas was computed in [19]. The computation in [19] revealed fundamental relationships between the basic parameters of the non-coherent MIMO system. For instance, it was shown in [19] that the optimum number of transmit antennas is given by $M = \min(\lfloor \frac{T}{2} \rfloor, N)$, where, T is the coherence time; see Definition 2.1. It was shown in [19] that increasing the number of transmit antennas beyond the number of receive antennas results in a reduction in the achievable rate, while having more receive than transmit antennas yields an SNR independent capacity gain. For any M, N and $T \geq \min(M, N) + N$, the high SNR ergodic non-coherent channel capacity is given by

$$C_{\text{non-coherent}} = M^*(1 - \tfrac{M^*}{T}) \log_2(\rho) + c_{\min(M,N),N} + o(1), \tag{2.7}$$

where M^* is the optimal number of transmit antennas, namely $M^* = \min(\lfloor \frac{T}{2} \rfloor, N, M)$,

ρ is the SNR and $o(1)$ is a term that goes to zero as the SNR goes to infinity. For $p \leq q$, the constant $c_{p,q}$ is given by

$$c_{p,q} = \frac{1}{T}\log_2\big(|\mathbb{G}_p(\mathbb{C}^T)|\big) + p(1-\tfrac{p}{T})\log_2(\tfrac{T}{\pi e p}) + (1-\tfrac{p}{T})\sum_{i=q-p+1}^{q} \mathrm{E}\{\log_2(\chi^2_{2i})\},$$

where $|\mathbb{G}_p(\mathbb{C}^T)|$ denotes the volume of the compact Grassmann manifold $\mathbb{G}_p(\mathbb{C}^T)$, and is given by

$$|\mathbb{G}_p(\mathbb{C}^T)| = \frac{\prod_{i=T-p+1}^{T} \frac{2\pi^i}{(i-1)!}}{\prod_{i=1}^{p} \frac{2\pi^i}{(i-1)!}}.$$

It was shown in [19] that at high SNR the ergodic non-coherent capacity of the MIMO system is achieved by unitarily structured input signals that are isotropically distributed on the compact Grassmann manifold. Using the expression in (2.7), it was shown in [19] that at high SNR non-coherent MIMO systems can achieve a significant fraction of the corresponding coherent MIMO system. Furthermore, the difference between the ergodic capacity of the non-coherent MIMO channel and that of the coherent one approaches zero as T goes to infinity.

Motivated by this promising result, in Chapters 4 and 5 we will consider non-coherent code designs and efficient detection techniques that make direct communication with no training over non-coherent channels more amenable to practical implementation.

2.2 Performance of MIMO systems

Having discussed the maximum data rate that can be communicated over a MIMO wireless channel, we now review the basic measures that can be used to characterize the error performance of MIMO systems.

A natural way to measure the performance of a MIMO system is to evaluate the probability of making a detection error at the receiver. That is, the probability that

the receiver decides in favour of a codeword other than the one that was transmitted. If we denote the space-time codebook by $\mathcal{C}$ and its cardinality by $|\mathcal{C}|$, then, assuming that the codewords are transmitted with equal probability, one can write the average probability of error as [5]

$$P_e = \frac{1}{|\mathcal{C}|}\sum_{i=1}^{|\mathcal{C}|} Pr\Big(\bigcup_{\substack{j=1\\ j\neq i}}^{|\mathcal{C}|} E_{ij}\Big), \tag{2.8}$$

where E_{ij} denotes the event that the receiver erroneously decides in favour of the codeword S_j instead of the transmitted codeword S_i. This expression is generally hard to compute because it requires one to know the decision region of each codeword. While identifying the boundaries of the decision regions is often manageable in SISO systems, this task becomes excessively complicated in MIMO systems as the number of signalling dimensions grows. This difficulty has resulted in the development of other performance measures that can be analytically evaluated. A particularly useful measure is the union bound [5] which can be obtained from (2.8) by upper bounding the right hand side. In particular, we have

$$\frac{1}{|\mathcal{C}|}\sum_{i=1}^{|\mathcal{C}|} Pr\Big(\bigcup_{\substack{j=1\\ j\neq i}}^{|\mathcal{C}|} E_{ij}\Big) \leq \frac{1}{|\mathcal{C}|}\sum_{i}\sum_{j} Pr(E_{ij}), \tag{2.9}$$

where the inequality in (2.9) follows from the fact that for any two events E_1 and E_2

$$Pr(E_1 \cup E_2) = Pr(E_1) + Pr(E_2) - Pr(E_1 \cap E_2) \leq Pr(E_1) + Pr(E_2).$$

The union bound can be used to identify the key parameters that affect the high SNR performance of MIMO systems [20]. In order to compute the bound in (2.9), we need to compute the probabilities $Pr(E_{ij})$ for all $i, j \in \{1, |\mathcal{C}|\}$. The probability $Pr(E_{ij})$ is called the pairwise error probability and will be denoted as $P(i \to j)$. In the next section we will give expressions for this quantity for both coherent and non-coherent MIMO systems.

2.2.1 The pairwise error probability

The pairwise error probability (PEP) is the probability that a certain codeword, say the i-th codeword, is mistaken by the receiver for the j-th codeword. In this section we will present PEP expressions and useful bounds for both coherent [20] and non-coherent [23] MIMO systems.

PEP of coherent MIMO systems

In coherent MIMO systems the channel fading coefficients are known at the receiver. We consider the case where the noise V in (2.2) is white and Gaussian with zero-mean and unit-variance [20, 25]; i.e., the entries $V_{ij} \sim \mathcal{CN}(0,1)$. Then a receiver that uses Maximum Likelihood (ML) detection would mistake the j-th codeword S_j for the i-th codeword S_i if

$$\|Y - HS_i\|_F \geq \|Y - HS_j\|_F.$$

Using this fact, along with the Gaussianity of noise, one can show that the exact PEP is given by [3]

$$\begin{aligned} P(i \to j) &= Q\big(\tfrac{d_H(S_i,S_j)}{\sqrt{2}}\big) \\ &\leq e^{-d_H^2(S_i,S_j)/4}, \end{aligned} \tag{2.10}$$

where $Q(\cdot)$ is the Q-function defined as

$$Q(x) = \tfrac{1}{\sqrt{2\pi}} \int_x^\infty e^{-\frac{u^2}{2}}\, du,$$

and $d_H(S_i, S_j) = \|H(S_i - S_j)\|_F$ is the distance between the i-th codeword and the j-th one as observed from the receiver when the channel realization is given by H. The inequality in (2.10) follows from using the Chernoff bound [5, p. 55] to show that for all $x \geq 0$, $Q(x) \leq e^{-x^2/2}$.

Averaging the right hand side of (2.10) over all possible channel realizations, we obtain an upper bound on the average PEP, $\bar{P}(i \to j)$. If the entries of the channel

realizations are assumed to be i.i.d. zero-mean unit-variance circularly-symmetric Gaussian random variables, the bound on the average pairwise error probability will be given by [20]

$$\bar{P}(i \to j) \leq \left(\left(\prod_{k=1}^{r_{i,j}} \lambda_k^{i,j} \right)^{1/r_{i,j}} \right)^{-r_{i,j}N} \left(\frac{\rho}{4}\right)^{-r_{i,j}N}, \tag{2.11}$$

where $\lambda_k^{i,j}$ denotes the k-th nonzero eigenvalue of the matrix

$$\Delta_{ij} = (S_i - S_j)^{\dagger}(S_i - S_j), \tag{2.12}$$

and $r_{i,j}$ is its rank.

The expression in (2.11) is composed of two factors. The first factor on the left of the right hand side of (2.11) is independent of the SNR. The minimum index of this factor over all possible codewords $S_i, S_j,\ i \neq j$ is called the coding gain of the MIMO system. That is,

$$\text{Coding Gain} = \min_{i,j} \left(\prod_{k=1}^{r_{i,j}} \lambda_k^{i,j} \right)^{1/r_{i,j}}.$$

The second factor reflects how the error performance behaves when the SNR increases. The minimum of the exponent of this factor over all possible codewords $S_i, S_j,\ i \neq j$ is called the diversity gain of the MIMO system.

$$\text{Diversity Gain} = N \min_{i,j} r_{i,j}.$$

In order to visualize the difference between these two factors, consider the curve where the logarithm of the average PEP is plotted against the SNR in decibels. Then, the coding gain would be responsible for horizontally shifting the whole curve, whereas the diversity gain would determine the slope of the average PEP curve at high SNR. Since the maximum value of $r_{i,j}$ in (2.11) is equal to M, the maximum diversity gain that a space-time code can achieve is equal to MN [26], which is equal to the number of independent signal paths between the transmitter and the receiver; see Figure 1.1.

Given their impact on the error performance of the system, the coding gain and the diversity gain have been at the centre of many standard space-time designs; e.g., [1,20] and [27].

PEP of non-coherent MIMO systems

In Section 2.1.1, we mentioned that rate efficient communication over non-coherent MIMO channels at high SNRs requires the space-time codewords to be unitary. In this section we will assume that this condition is satisfied and to emphasize this, we will denote the set of codewords by $\{Q_{X_i}\}$. Similar to the case of coherent MIMO communication model, we will assume that the entries of both the noise matrix V and the channel matrix H are i.i.d. zero-mean complex Gaussian random variables with unit variance. In this case, an ML detector would make an erroneous decision in favour of the j-th codeword rather than actually transmitted i-th codeword if [23]

$$\|Y^\dagger Q_{X_i}\|_F \leq \|Y^\dagger Q_{X_j}\|_F,$$

where Y is the received signal. The computation of the probability of occurrence of this event is quite involved. An exact expression for this probability was first computed in [23] and is given by

$$P(i \to j) = \sum_k \mathrm{Res}_{\omega=\imath a_k}\Big\{-\frac{1}{\omega+\imath/2}\prod_{\substack{m=1\\ \sigma_m<1}}^{M}\frac{1+\rho T/M}{(\rho T/M)^2(1-\sigma_m^2)(\omega^2+a_m^2)}\Big\}, \qquad (2.13)$$

where $\mathrm{Res}_{\omega=\imath a_k}\{\cdot\}$ denotes the residue of the expression at the point $\omega = \imath a_k$, $\imath = \sqrt{-1}$, $a_k \stackrel{\triangle}{=} \sqrt{\frac{1}{4}+\frac{1+\rho T/M}{(\rho T/M)^2(1-\sigma_k^2)}}$ and σ_k is the k-th singular value of the matrix $Q_{X_i}^\dagger Q_{X_j}$. The main advantage of the expression in (2.13) is that it provides a compact way of expressing the PEP. However, it is difficult to extract insight from this expression. In addition, this expression suffers from a numerical drawback that was pointed out in [25]. In particular, this expression can be hard to compute because the evaluation of

the residues becomes numerically unstable when the poles of the expression within the braces in (2.13) have high multiplicities. One method that uses numerical integration for computing the PEP expression in (2.13) was given in [28]. In order to avoid this numerical inconvenience, an upper bound on the exact $P(i \to j)$ was given in [25]. This bound was shown to be asymptotically tight as the SNR goes to infinity.

In Chapter 5 we will revisit the problem of computing the exact PEP. We will adopt a different approach from the one taken in [23]. The expression we derive is in the form of an absolutely convergent infinite series expansion. This series is numerically stable and provides more insight into the key parameters that control the error performance than the expression in (2.13).

2.3 Space-Time coding techniques for coherent MIMO systems

In this section and the next one we will focus on well-established coherent MIMO communication techniques. The corresponding review of established non-coherent material will be presented along with our contributions in Chapters 4 and 5. In this section we present the fundamental features of two classes of space-time block coding techniques; orthogonal designs and layered designs. In Chapter 3, we will consider a construction that encompasses these two classes and can hence be used to combine their desirable features.

In both orthogonal designs and layered designs, the data bits output from the encoder are mapped to complex scalar symbols using a labelling scheme such as Gray coding. The complex symbols are assumed to be drawn from standard constellations such as phase shift keying (PSK) or quadrature amplitude modulation (QAM). In order to generate space-time codewords, both orthogonal designs and layered designs

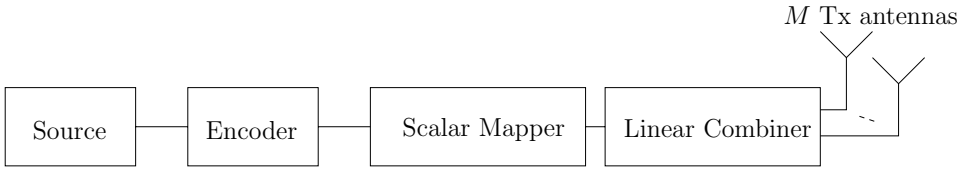

Figure 2.1: Linear Space-Time Block Transmitter

combine the scalar complex symbols in a linear fashion to produce $M \times T$ space-time blocks. In fact, both designs can be viewed as variants of the way in which the complex symbols are combined to generate the space-time codebook. Despite the similarity in the underlying framework, orthogonal designs and layered designs yield space-time codes that possess fundamentally different properties. We will now describe these techniques and their associated properties in more detail.

2.3.1 Orthogonal designs

Orthogonal designs comprise a specific means for constructing space-time codes from standard QAM or PSK constellations [26, 29]. The resulting space-time codeword matrices are constrained to be orthogonal and hence codes that are structured in this way are usually called orthogonal space-time block codes (OSTBC). It was shown in [29] and [26] that this construction possesses two remarkable advantages. Firstly, this construction guarantees that the space-time code achieves full diversity. In other words, the matrix Δ_{ij} in (2.12) has rank M for any pair of codewords $i, j \in \{1, |\mathcal{C}|\}$. As mentioned in Section 2.2.1, this implies that the probability of error versus SNR curve has the maximum slope that an uncoded MIMO system with the same antenna configuration can achieve. The second advantage that distinguishes orthogonal designs from other space-time coding techniques is the simplicity of the detection process. In particular, the orthogonal structure of this class of codes allows the complex symbols to be decoupled through linear preprocessing of the received signal without any penalty in performance. Hence, ML detection collapses to scalar detection of

individual symbols.

Despite their valuable advantages, space-time signalling using OSTBC codes suffers from a few drawbacks that restrain their application. In particular, these codes are generally not easy to construct [14] and do not even exist for certain block sizes [26,30]. In addition, constraining space-time codes to be orthogonal generally results in exhausting a significant portion of the communication degrees of freedom. That is, the benefits that follow from the orthogonal construction come at the heavy cost of reducing the data rate that can be achieved through this signalling scheme [14].

Before describing other designs, it is worth giving an example of an OSTBC code that illustrates the fundamental properties of this class of codes. For this purpose, we choose the standard scheme due to Alamouti [29] where the block size $T = 2$ and the number of transmit $M = 2$. The major part of OSTBC code designs that followed Alamouti's scheme have basically tried to generalize this scheme for larger block sizes or for scenarios where more antennas are available at the transmitter and the receiver [14, 26].

Alamouti Scheme

In this scheme we will denote the complex symbols by s_i. This scheme transmits two symbols, say s_0 and s_1, in each block, where s_0 and s_1 are drawn from a QAM (or PSK) constellation, $\mathcal{C}$. The space-time codewords $\{S\}$ are constructed as follows.

$$S(s) = \begin{bmatrix} s_0 & s_1^* \\ s_1 & -s_0^* \end{bmatrix},$$

where $s = \begin{bmatrix} s_0^* & s_1^* \end{bmatrix}^\dagger$ and $(\cdot)^*$ denotes the complex conjugate. In order to show that this scheme achieves full diversity according to the definition in Section 2.2.1, we only need to show that for a code matrix $S(\tilde{s})$ composed of any two symbols $\tilde{s}_0$ and $\tilde{s}_1$, the matrix $\Delta = \big(S(s) - S(\tilde{s})\big)^\dagger \big(S(s) - S(\tilde{s})\big)$ is full rank whenever $S(s) \neq S(\tilde{s})$. It is

easy to verify that

$$|\det(\Delta)|^2 = |\tilde{s}_0 - s_0|^2 + |\tilde{s}_1 - s_1|^2,$$

which implies that Δ is full rank for all $S(\tilde{s}) \neq S(s)$.

We now discuss the detection technique for OSTBCs. Consider the case when the number of receive antennas $N = 2$, and let the received signal matrix Y be given by (2.2) and its entries be $\{y_{ij}\}$. Consider a vectorized model of (2.2), in which the columns of the received signal matrix Y are stacked in one tall column. For the Y matrix the length of this column will be $TN = 4$. One can verify that (2.2) is equivalent to

$$\begin{aligned} y = \begin{bmatrix} y_{11} \\ y_{21} \\ y_{12}^* \\ y_{22}^* \end{bmatrix} &= \begin{bmatrix} h_{11} & h_{12} \\ h_{21} & h_{22} \\ -h_{12}^* & h_{11}^* \\ -h_{22}^* & h_{21}^* \end{bmatrix} \begin{bmatrix} s_0 \\ s_1 \end{bmatrix} + \begin{bmatrix} v_{11} \\ v_{21} \\ v_{12}^* \\ v_{22}^* \end{bmatrix}, \\ &= \mathcal{H}s + v, \end{aligned} \tag{2.14}$$

where v_{ij} denotes the ij-th entry of the noise matrix V in (2.2),

$$v = \begin{bmatrix} v_{11} \\ v_{21} \\ v_{12}^* \\ v_{22}^* \end{bmatrix} \qquad \text{and} \qquad \mathcal{H} = \begin{bmatrix} h_{11} & h_{12} \\ h_{21} & h_{22} \\ -h_{12}^* & h_{11}^* \\ -h_{22}^* & h_{21}^* \end{bmatrix}. \tag{2.15}$$

Notice that the columns of the matrix $\mathcal{H}$ are orthogonal. More specifically, $\mathcal{H}^\dagger\mathcal{H} = \|H\|^2 I$. If we let $\hat{s}_{\text{ML}}$ denote the ML decision on the complex symbols, then one can show that

$$\hat{s}_{\text{ML}} = \arg\min_{s\in\mathcal{C}^M} \big\{\|y - \mathcal{H}s\|_F\big\} = \arg\min_{s\in\mathcal{C}^M} \big\{\|\tfrac{1}{\|H\|^2}\mathcal{H}^\dagger y - s\|_F\big\}.$$

That is the ML decision on the ith symbol is given by,

$$\hat{s}_{\text{ML}_i} = \arg\min_{s_i\in\mathcal{C}} \big\{\|\tfrac{1}{\|H\|^2}[\mathcal{H}^\dagger y]_i - s_i\|_F\big\},$$

where $[\cdot]_i$ denotes the ith entry of a vector. This equation shows that, without incurring any penalty in performance, ML detection of OSTBC codes can be reduced to scalar detection by performing simple linear preprocessing on the received signal.

Having discussed the diversity and the detection of OSTBCs, it remains to compare the mutual information that can be achieved by this scheme with the ergodic channel capacity. The mutual information achieved by the orthogonal design, $I_{\text{orth}}(s;y)$ is given by [14]

$$I_{\text{orth}}(s;y) = \mathrm{E}\{\log(1+\tfrac{1}{2}\rho\|H\|^2)\}) \leq \mathrm{E}\{\log(1+\tfrac{\rho}{2}\sum_i \lambda_i)\},$$

where λ_i is the i-th eigenvalue of $H^\dagger H$. On the other hand, the ergodic MIMO channel capacity [14] is given by

$$C_{\text{coherent}} = \mathrm{E}\{\log\big(\det(I+\tfrac{\rho}{2}H^\dagger H)\big)\} = \mathrm{E}\{\sum_i \log\big(1+\tfrac{\rho}{2}\lambda_i\big)\}.$$

Since the log function is concave, then by Jensen's inequality,

$$\sum_i \log\big(1+\tfrac{\rho}{2}\lambda_i\big) \geq \log(1+\tfrac{\rho}{2}\sum_i \lambda_i), \tag{2.16}$$

where the equality holds only if at most one eigenvalue is nonzero. This observation suggests that, in the general case, orthogonal designs incur information loss. More specifically, orthogonal designs cannot achieve capacity unless either the transmitter or the receiver has one antenna.

2.3.2 Layered designs

In the previous section, we have presented a review of orthogonal designs of space-time block codes. We have highlighted some of their advantages and their limitations. We have seen that the main disadvantage of these designs follows from restricting the space-time codewords to be orthogonal. This stringent constraint means that the data

rate that can be supported by these codes is strictly less than the channel capacity whenever the number of receive antennas exceeds one; c.f. (2.16). In order to overcome this disadvantage, the space-time code must be structured in a less stringent way that allows the transmission of more independent streams of data. Layered designs form a class of space-time codes that aims at achieving this goal by allowing data to flow along parallel streams which are called layers [15, 31, 32]. The data in each layer is encoded independently of the other layers and is then parsed into blocks of length T. The blocks from all layers are passed directly to the transmit antennas in a specific order that is determined by the transmission strategy.

The way in which the encoded blocks are passed to the transmit antennas determines the detection complexity and the diversity gain that can be achieved through a certain layered design. Examples of different layering designs include the Bell Laboratories layered space-time architecture (BLAST) schemes [15,31] and threaded algebraic space-time (TAST) [32] schemes as well as the codes introduced in [27]. In this section we describe the common theme on which these techniques are based.

We begin by considering the BLAST techniques. In this class of layered designs, the input data stream is demultiplexed into M substreams; see Figure 2.2. Each substream of bits is then time encoded and mapped onto complex symbols from some QAM (or PSK) constellation. If each stream of complex symbols is transmitted directly from a fixed transmit antenna, the resulting scheme is called vertical BLAST (V-BLAST); see Figure 2.2(a). In this scheme the streams are independent and hence, the space-time codewords in this scheme have no specific structure. This implies that the rank of the matrix Δ_{ij} in (2.12) for two distinct V-BLAST codewords i and j can be as low as one [3]. On the other hand, the fact that the codewords are independent, allows the V-BLAST to achieve full multiplexing gain [6].

In V-BLAST all the coding is done over the time dimension and no coding is performed over the space dimension. This feature is the main reason that causes

V-BLAST to have a low diversity gain. In order to increase the diversity gain, a structure has to be inserted into the codewords. In other words, coding has to be done jointly over space and time. One way to do this is to subdivide each layer into bursts and, using a space-time interleaver, with each burst being transmitted from a different antenna; see Figure 2.2(b). Because this technique allows each layer to be transmitted from all the M transmit antennas, this technique has the potential to achieve full diversity while maintaining the same data rate as the V-BLAST coding scheme. Since each layer progresses in time and space simultaneously, this scheme is called diagonal BLAST (D-BLAST). Notice that in D-BLAST, coding over the time dimension is performed on bits not on symbols and the space dimension is just used to interleave the symbols from each layer.

We now describe the design principles of TAST codes [32] which fall under the category of layered designs but involve more structure than BLAST techniques. TAST codes have introduced two fundamental elements to the D-BLAST technique. The first of these elements is to watermark each layer by a carefully chosen scalar. This watermark enables different data layers to be distinguished at the receiver. The second key element introduced by TAST codes is that the symbols are encoded jointly over the space and time dimensions using a rotation matrix that rotates the vector of input symbols. Figure 2.2(c) shows a block diagram of this scheme.

The input data stream is time encoded and then mapped to complex symbols. These symbols are rotated using the matrix U and the output stream of symbols is demultiplexed into M streams which form M layers. In order to distinguish these layers, each layer is multiplied by the scalar β^g, where g is the number of the layer. In [27], it was shown that by carefully choosing the value of β, and the rotation U one can achieve full diversity. The appropriate values for β and U depend on the number of receive and transmit antennas as well as the underlying signal constellation. A systematic way for choosing these parameters for a rather wide range of antenna

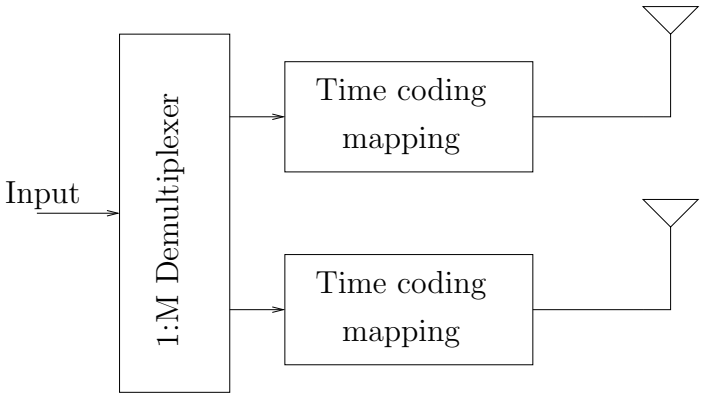

(a) V-BLAST scheme

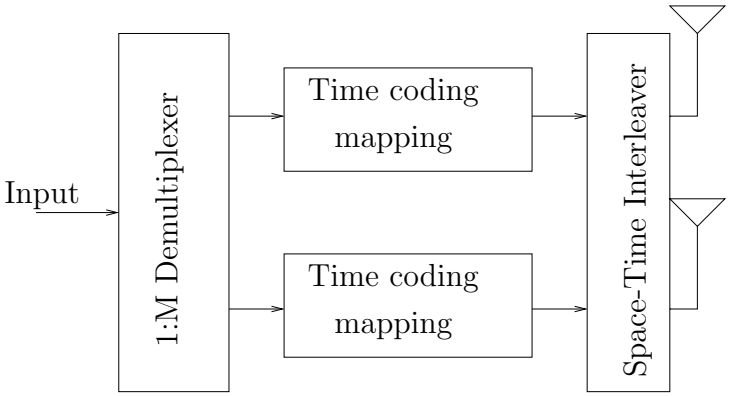

(b) D-BLAST scheme

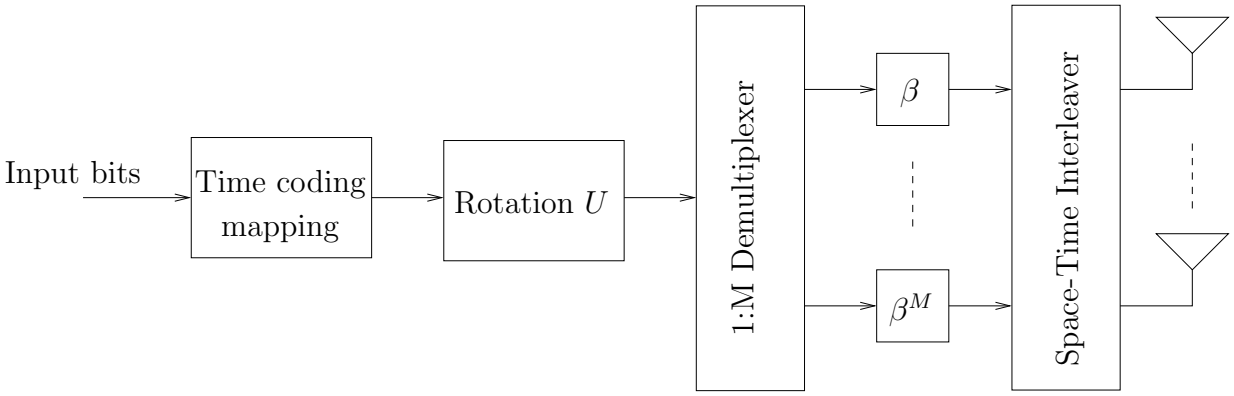

(c) TAST Coding scheme

Figure 2.2: Variants of layered designs

configurations was given in [33]. In addition to the full diversity that these codes can achieve, these codes were shown in [27] to be information lossless. That is, these codes are structured enough to attain full diversity and relaxed enough so as not to reduce the achievable data rate. In spite of their desirable features, these codes do not offer any guarantee on the coding gain. In addition, for these codes to acquire these desirable features, the block length has to be constrained to be equal to the number of transmit antennas; a strong limitation on the coding gain of this scheme when the channel coherence time is long enough to admit the transmission of large data blocks. In Chapter 3 we will touch on the performance limitations of the designs in [27].

The common theme in both orthogonal designs and layered designs is that each of these schemes can be regarded as a particular instance of combining the complex symbols in a linear fashion [14]. Given that these two classes can achieve fundamentally different goals, one might pose the question of whether it is possible to devise a generic scheme for combining the complex symbols linearly so that the resulting space-time codes achieve several design criteria at the same time. In order to answer this question, a class of linearly structured codes that subsumes both layered and orthogonal designs was developed in [14]. These codes not only subsume orthogonal and layered designs, they can also be adapted to any number of transmit and receive antenna and to any block size that is less than or equal to the coherence time of the channel. In Chapter 3, we will revisit the design problem for this class of generalized codes. By performing an asymptotic analysis we will show that when the number of transmit antennas is large it is possible for these codes to be designed so as to acquire many of the desirable features possessed by layered and orthogonal designs. Using this asymptotic result, we will provide a constellation independent design technique for generating finite size space-time codes that meet several design criteria .

2.4 Space-Time detectors

In the previous section we have discussed a variety of space-time encoding techniques for coherent MIMO systems. We have seen that the techniques that yield desirable performance characteristics require joint coding over the time and the space dimensions. In order to recover the transmitted symbols at the receiver, the detection algorithm has to exploit its knowledge about the way in which the codewords were constructed at the transmitter. For instance, we have shown in Section 2.3.1 that for orthogonal designs the receiver can exploit the orthogonality of the equivalent channel (c.f., (2.15)) to decouple the complex symbols and perform scalar detection on the decoupled data. Although OSTBCs are very attractive from the point of view of detection complexity, we have pointed out that these designs are information lossy and hence are not recommended for communication at high data rates.

We now consider the detection of codes generated using the technique of layered designs. For BLAST schemes, the independence between the data layers can be exploited in implementing an efficient suboptimum detection strategy at high SNR [15, 31]. This detection method is known as the the nulling-cancellation procedure. Assuming that the channel matrix has full column rank, in this method layers are detected sequentially by first forcing the interference from undetected layers to be zero[2] by projecting the received signal on the null space of the still undetected layers. This is step is known as the nulling step. The receiver then subtracts the interference from the already detected layers by treating the data contained therein as perfectly known. This step is known as the cancellation step. In particular, consider the case when there are M layers to be detected. In order to detect the Mth layer, the received signal is projected onto the subspace spanned by this layer which is orthogonal to the subspace spanned by the remaining $M-1$ layers. Once the signals from these

[2]It is possible to use Minimum Mean Squared Error (MMSE) filtering for interference suppression [34, 35] instead of Zero Forcing (ZF).

layers is nullified, the symbols in the Mth layer can be extracted by performing scalar detection. By treating the data in this layer as perfectly known, the receiver subtracts the interference introduced by this layer from the overall received signal. The residual received signal is now projected on the subspace spanned by the first $M-2$ layers and the symbols in the $(M-1)$th layer are then extracted by performing scalar detection on this layer. This process continues in the subsequent layers until all the M layers are detected. The order in which the layers are decoded has a major impact on the performance of the nulling-cancellation procedure. Typically this procedure processes the layers in order starting from the layer with the least interference level.

While BLAST schemes are amenable to nulling and cancellation, this detection technique does not perform well for more structured layered designs, such as TAST codes and the codes in [27]. In order to extract the potential benefits offered by these codes, joint detection of the received signal is required. Although ML detection is optimum from an error performance perspective, it incurs a computational cost that usually precludes it from practical application in the context of space-time communication where the constellation sizes are likely to be large.

In order to make the potential gains that a space-time communication system can offer available for practical applications, we need a computationally efficient detector whose performance is comparable to that of the ML detector. A class of detectors that can perform as well as ML detectors but with significantly less computational effort was developed in [18, 36]. This class is known as sphere detectors [37–40]. In the next section we will describe the principle of sphere detection and its application in space-time communication contexts.

2.4.1 Sphere detectors

Consider the situation when the vectorized signal model in (2.14) is used to describe the signal at the receive antennas of a space-time communication system when the

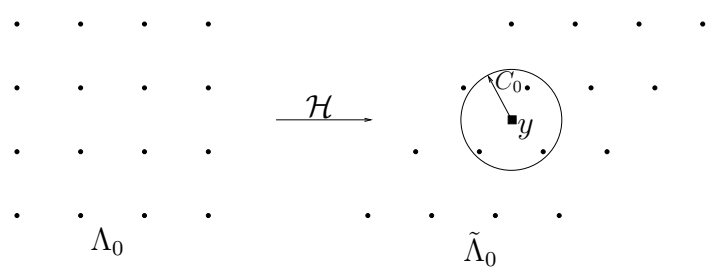

Figure 2.3: Sphere detection of the received vector y.

equivalent channel matrix $\mathcal{H}$ is known at the receiver but not at the transmitter[3].

$$y = \mathcal{H}s + v.$$

Since a complex lattice can be viewed as the Cartesian product of two real one-dimensional lattices[4], in this section we will only consider the case in which $\mathcal{H}$, y, s and v are real. The signal vector s is assumed to be drawn from some m-dimensional real discrete finite lattice Λ_0. The entries of the noise vector v are assumed to be i.i.d. white zero-mean Gaussian with a common variance [38]. Because the noise is Gaussian and white, the ML detection algorithm amounts to searching the whole lattice for the point $\hat{s} \in \Lambda_0$ that satisfies

$$\hat{s} = \arg\min_{s \in \Lambda_0} \|y - \mathcal{H}s\|, \tag{2.17}$$

which is simply the Euclidean distance between the received signal vector and a version of the transmitted signal vector that has undergone scaling and rotation by the channel. In Figure 2.3 we depict this situation. The original lattice Λ_0 is transformed by the channel $\mathcal{H}$ into a skewed lattice $\tilde{\Lambda}_0$. The received signal vector now corresponds to a point in the skewed lattice that has been shifted by the noise vector v.

Since testing all the points in Λ_0 against the ML metric in (2.17) becomes computationally expensive when the dimension of s is large, several algorithms that aim at

[3]In the rest of this section we will refer to the equivalent channel by "the channel".

[4]For example, the standard q^2-ary QAM constellation can be viewed as the Cartesian product of two q-ary pulse amplitude modulation (PAM) constellations.

avoiding this exhaustive search (at least on average) have been developed [18, 38, 40]. These algorithms are collectively known as sphere detectors. The common theme between these algorithms is to try to avoid searching the whole lattice for the point that has most likely been transmitted. In particular, these algorithms consider points that lie within a sphere that is centered at the received vector y (or some linearly processed version of it). Several versions of sphere detectors are available in the literature. These versions vary in the way the received signal is preprocessed prior to detection [38], the way in which the radius of the search sphere is selected [36, 37] and the order in which the points within the sphere are searched [38]. In Figure 2.3 the neighbourhood of y was chosen to be an m-dimensional sphere with radius C_0. In order to ensure that the transmitted lattice point lies within the search region, this radius has to be carefully chosen. It was shown [37, 41] that an appropriate choice of C_0 is crucial in controlling the complexity of the sphere detector.

One of the earliest versions of sphere detectors was developed in [36]. In this detector, the channel matrix $\mathcal{H}$ and a constant C_0 are assumed to be given. For simplicity we will only consider the case when $\mathcal{H}$ is square. (Variations of sphere detectors that include rectangular channel matrices are also available [38, 39].) The detector starts by performing a QR decomposition on the channel matrix. That is, $\mathcal{H}$ is decomposed into the product of an orthonormal matrix $\mathcal{Q}$ and an upper triangular matrix $\mathcal{R}$. Since the norm in (2.17) is invariant under orthonormal transformations, we can write (2.17) as

$$\hat{s} = \arg\min_{s\in\Lambda_0} \|\tilde{y} - \mathcal{R}s\|, \tag{2.18}$$

where $\tilde{y} = \mathcal{Q}^\dagger y$. The set of lattice points that lie within a sphere of of radius C_0 around $\tilde{y}$ is the set of points s that satisfy $\|\tilde{y} - \mathcal{R}s\| \leq C_0$. Because of the upper triangular structure, this equation implies that

$$\sum_{j=i}^{m} \left|\tilde{y}_j - \sum_{\ell=j}^{m} \mathcal{R}_{j,\ell} s_\ell\right|^2 \leq C_0, \qquad \text{for } i = 1, \ldots, m, \tag{2.19}$$

where the subscripts denote the entries in the respective matrices. The sphere detector uses (2.19) to decode the signal sequentially using a tree structured search that starts from the root at the m-th level and proceeds to the leaves at the first level[5]. If at any level of the tree the inequality in (2.19) is violated, the detector moves back to the previous node of the tree and proceeds along a different path. After spanning the whole tree, the algorithm then tests only the points that lie within the sphere for the one that yields the closest vector to $\tilde{y}$. If after spanning the tree, no points happen to lie within the sphere, the radius of the sphere C_0 can be increased and the whole procedure is repeated [36]. This detection algorithm is in fact optimum [37]; it is merely a faster way, on average, of implementing ML detection. While its worst case complexity remains exponential in the number of bits transmitted per channel use [41], the computational advantage over direct application of ML detection is often substantial for small sized systems [37].

If an appropriate value of C_0 is available at the receiver, application of the sphere detector principle can offer computational advantages over direct ML detection [38]. However, it is possible to achieve considerable complexity gains if the sphere detection principle is applied to a linearly preprocessed version of the received signal [42]. That is, for some matrix G, the sphere detector is applied to the new system model

$$y' = Gy = G\mathcal{H}s + Gv. \tag{2.20}$$

Notice that because G is not necessarily orthonormal, the noise Gv is not white in general and applying the sphere detector to find

$$\breve{s} = \arg\min_{s\in\Lambda_0} \|y' - G\mathcal{H}s\|.$$

is suboptimum. While the matrix G is typically chosen to correspond to a zero-forcing or a minimum mean squared error equalizer, other choices of F were also shown to

[5]Other search techniques that are based on the branch and bound algorithm can be found in [42]and [43].

yield significant computational advantages over direct sphere detection [38, 40, 42].

2.5 Summary

In this chapter we have described the fundamental principles of space-time communication systems. We have considered the capacity limits and the pairwise error probability for both coherent and non-coherent communication scenarios. For the coherent scenario, we have presented the basic elements of space-time signalling and detection strategies. In the next chapter we will consider a general signalling scheme for coherent space-time systems that encompasses the signalling schemes presented in this chapter. The design method that we propose suits any antenna configuration and becomes asymptotically optimum from several design perspectives as the number of transmit antennas grows.

Chapter 3

Design of Linear Dispersion Codes: Asymptotic Guidelines and Their Implementation

The previous chapter provided a broad view on the fundamental principles of wireless MIMO systems. These systems were classified according to the amount of channel information available at the communicating terminals. In particular, when full channel knowledge is available at the receiver but not at the transmitter the system is called coherent and when no channel knowledge is available at either the transmitter or the receiver the system is called non-coherent. For coherent systems we summarized the characteristic features of two important classes of space-time signalling designs; orthogonal and layered designs. In this chapter we develop a design method for a diverse class of space-time codes known as linear dispersion (LD) codes [14]. This class subsumes several standard designs, including the orthogonal and the layered designs described in Chapter 2. We begin by showing that for systems that employ a

large number of transmit antennas, LD codes constructed from unitary coding matrices [1] are asymptotically optimum from different design perspectives, viz., Minimum Mean Square Error (MMSE), mutual information and average Pairwise Error Probability (PEP). As mentioned in Chapter 2, those measures have a direct impact on the detection complexity, data rate and error performance that a space-time code can achieve. Using the insight generated by the asymptotic result, we provide a structured design technique for the LD coding matrices that suits a broad class of configurations. The resulting codes can support high data rates and provide performance advantages over current designs when decoded with a standard sphere detector. Based on the asymptotic results, we also propose a row interleaving scheme which is shown to result in significant performance enhancement at high SNR.

3.1 Introduction

In Chapter 2 we mentioned that wireless communication systems with multiple antennas at both the transmitter and the receiver have the potential to provide reliable transmission at high data rates [2]. In particular, for a sufficiently rich scattering environment, the capacity of a coherent communication channel employing M transmit and N receive antennas was shown to grow linearly as $\min(M, N)$, [2, 6, 15]. The design of coding schemes for multiple antenna systems operating at high SNRs involves a trade-off between the achievable rate (normalized by log(SNR)) at which the system capacity grows and the normalized rate at which the error probability decays [6]. This inherent trade-off provides a distinction between schemes like the Orthogonal Space-Time Block Codes (OSTBCs) [26] that sacrifice achievable rate for maximum reliability, and the BLAST schemes [31] that can support rates close to channel capacity, but do so without benefiting from the diversity of the channel. Since OSTBCs

[1] Following the lead of [44] and [19], in this as well as the following chapters, both "square" and "tall" matrices X that satisfy $X^\dagger X = I$ will be referred to as being unitary.

and BLAST achieve the extremes of the trade-off, there is considerable interest in developing design methods for schemes that provide intermediate performance in terms of achievable rate and error probability, and are applicable for a broad range of antenna configurations. The set of linear dispersion (LD) codes [14] is a diverse class of space-time codes that subsumes many existing schemes, including the OSTBC and BLAST schemes, and hence is a natural framework in which such design problems can be posed. While some recently developed codes, such as the Threaded Algebraic Space Time (TAST) codes [45] and those in [27], possess many desirable performance features, they remain proper subsets of the LD framework. Given the generality of the LD coding framework and the abundance of degrees of design freedom it possesses, the focus of this chapter is on the development and implementation of guidelines for the design of LD codes through the study of their asymptotic properties.

The original LD codes in [14] were designed to maximize the ergodic capacity of the system. However, it has recently been pointed out that such capacity optimal LD codes do not necessarily perform well in practice [46]. Moreover, the maximization of the ergodic capacity is performed under an implicit assumption that maximum likelihood (ML) detection will be performed at the receiver—a task which requires an exhaustive search that is often computationally infeasible. These observations prompt the search for codes that jointly achieve high data rates and perform well when only a suboptimal detector is available at the receiver. In the present chapter, we identify a class of LD codes that approach optimality from both performance and rate perspectives as the number of transmit antennas M grows. In particular, the class of codes presented herein asymptotically ensures minimum output mean square error without incurring any information loss. Minimizing the mean square error is a desirable feature for the class of suboptimum sphere detectors that employ a linear front end [36]. In addition to this property, we show that this class of codes asymptotically minimizes the high SNR average pairwise error probability.

Since we consider both capacity and performance in our designs, the underlying philosophy of our approach is similar to that followed in the concurrent development of frame-based LD codes [46]. A more recent design of LD codes that also takes into account both rate and performance was given in [47] and [33]. However, our methodology is substantially different from these designs. In particular, we derive a different objective function for the code design problem, and the set of feasible codes in [46] and [33] intersects that of the codes proposed herein, but neither is a proper subset of the other. As we will show in Section 3.6, our design method can generate codes that provide slightly better performance than those in [46]. Furthermore, our codes possess a structure that enables us to search the space of feasible codes efficiently without the need to perform the random search techniques employed in [46]. In comparison with the codes in [47] and [33], our codes become asymptotically information lossless for any number of receive antennas as the number of transmit antennas grows, whereas the design in [47] and [33] requires the number of receive antennas to be greater than or equal to the number of transmit antennas to guarantee information losslessness.

The design criteria for our LD codes are based on several observations. First, we show that LD codes with a certain unitary structure simultaneously (i) minimize a lower bound on the mean square error at the output of a linear preprocessing stage in the receiver; (ii) minimize a lower bound on the high SNR average pairwise error probability; and (iii) maximize an upper bound on the mutual information that an LD code can achieve. We then show that as the number of transmit antennas grows, these optimized bounds are achieved. Guided by this asymptotic result, we impose this unitary structure on finite-sized LD codes and show how the resulting equivalent channel matrix can be optimized. Imposing this unitary structure dramatically reduces the number of design parameters, which subsequently reduces the computational cost of determining the codes. In particular, our design procedure is

substantially simpler than that in [14] and does not require the additional manipulations employed therein. We will demonstrate via simulation that even for systems with a small number of antennas, our codes perform better than many existing codes, including the standard LD codes [14], the TAST codes [45] and the codes in [27].

The high SNR performance of a communication system is dominated by the outage probability [6], which is the probability that a specific channel realization fails to support the required data rate. In order to reduce the outage probability we propose a row interleaving procedure which improves the high SNR performance of the code by transmitting the rows of the code matrix over different channel realizations. Asymptotic analysis and supporting simulations demonstrate how our unitarily structured LD codes can benefit from row interleaving. In fact, we provide simulation results that demonstrate that row interleaving can substantially increase the performance advantage of our codes over the original LD codes.

3.2 Linear Dispersion Codes

We consider a system with M transmit and N receive antennas by which one wishes to transmit Q data symbols, $s_1, \ldots, s_Q$, from a given constellation $\mathcal{C}$ over T time slots. If we represent the channel symbols transmitted from the antennas at each time slot as the rows of a $T \times M$ matrix S, then each linear dispersion codeword can be written in the form [14]

$$S = \sum_{q=1}^{Q} (\alpha_q A_{2q-1} + \imath \beta_q A_{2q}), \tag{3.1}$$

where α_q and β_q are the real and imaginary parts of s_q respectively. The matrices A_q are $T \times M$ fixed coding matrices that define the code. Typically, they are normalized so that the average power transmitted by each antenna is unity; i.e.,

$$\mathrm{E}\{\mathrm{Tr}(SS^{\dagger})\} = TM. \tag{3.2}$$

If r denotes the constellation size of the data symbols s_q, then the transmission rate of the code is $R = \frac{Q}{T}\log_2 r$ bits/channel use.

We will adopt the standard frequency-flat block fading model of the channel described in Chapter 1 [14,26], in which the slow fading of the propagation coefficients is approximated by coefficients which are constant over a given block of T time slots and then fade independently in the next block. This can be a model for many transmission strategies including frequency hopping, ideally interleaved time division multiple access (TDMA) or packet-based transmission in which each frame of data sees an independent realization of the channel but the channel is constant within each frame [19]. As mentioned in Chapter 2, the received symbol matrix Y can be written as

$$Y = \sqrt{\frac{\rho}{M}}\, SH + V, \tag{3.3}$$

where ρ is the signal to noise ratio per receive antenna, and H is the $M \times N$ channel matrix whose $(m,n)^{th}$ element is the complex gain between the m^{th} transmit and the n^{th} receive antennas. We will assume that the scattering is rich enough for the channel coefficients, $[H]_{mn}$, to be modeled as independent complex circular Gaussian random variables of unit variance. The matrix V in (3.3) denotes the additive white Gaussian noise. Its elements are also independent complex circular Gaussian random variables of unit variance. Since we have assumed that the channel changes slowly, we will assume that the receiver has been able to acquire accurate model of the channel. By rearranging the elements in the matrices in (3.3), we can rewrite that equation as [14],

$$\underbrace{\begin{bmatrix} y_{R,1} \\ y_{I,1} \\ \vdots \\ y_{R,N} \\ y_{I,N} \end{bmatrix}}_{y} = \sqrt{\frac{\rho}{M}}\,\mathcal{H} \underbrace{\begin{bmatrix} \alpha_1 \\ \beta_1 \\ \vdots \\ \alpha_Q \\ \beta_Q \end{bmatrix}}_{s} + \underbrace{\begin{bmatrix} v_{R,1} \\ v_{I,1} \\ \vdots \\ v_{R,N} \\ v_{I,N} \end{bmatrix}}_{v}, \tag{3.4}$$

where, the subscripts $(\cdot)_{R,i}$ and $(\cdot)_{I,i}$ denote the real and imaginary parts of the i^{th} column respectively. The $2NT \times 2Q$ equivalent channel matrix, $\mathcal{H}$, is given by,

$$\mathcal{H} = \left[\begin{array}{cccc} I_N \otimes \mathcal{A}_1 & I_N \otimes \mathcal{A}_2 & \cdots & I_N \otimes \mathcal{A}_{2Q} \end{array} \right] [I_{2Q} \otimes \underline{h}], \tag{3.5}$$

where $\otimes$ denotes the Kronecker product, and

$$\mathcal{A}_{2q-1} = \left[\begin{array}{cc} A_{R,2q-1} & -A_{I,2q-1} \\ A_{I,2q-1} & A_{R,2q-1} \end{array} \right], \qquad \mathcal{A}_{2q} = \left[\begin{array}{cc} -A_{I,2q} & -A_{R,2q} \\ A_{R,2q} & -A_{I,2q} \end{array} \right]. \tag{3.6}$$

In (3.5), $\underline{h} = [h_1^T, \ldots, h_N^T]^T$, where $h_n = [h_{R,n}^T, h_{I,n}^T]^T$, and $h_{R,n}$ and $h_{I,n}$ are, respectively, the real and imaginary component vectors of the n^{th} column of the physical channel matrix H.

It can be seen from (3.5) that the columns of $\mathcal{H}$ are linearly transformed versions of each other. Therefore, unless the coding matrices A_q are carefully chosen, it can be quite likely that the resulting $\mathcal{H}$ is "close" to being degenerate. In that event, the performance of most detectors deteriorates substantially. Hence, an effective design technique for the coding matrices ought to guard against these occurrences, in addition to optimizing other design criteria. A candidate technique for doing so is provided in Section 3.4.

3.3 Performance Bounds and Asymptotic Optimality

In this section we derive the design criteria for our LD codes, and demonstrate the asymptotic optimality of codes with a certain unitary structure. It was shown in the previous section that the structure of LD codes allows us to explicitly manipulate the equivalent channel matrix (3.5). A question that arises is how to choose the coding matrices A_q so that the equivalent channel matrix ensures good average receiver

performance at a given data rate. Obviously, this design problem depends on the receiver structure, the number of available antennas at each end of the communication link, the block length T and the choice of the number of symbols Q in a block.

Optimum signal detection involves maximization of the likelihood function over the discrete set of the code alphabet—an NP-hard integer least squares problem; e.g., [38]. For a Maximum Likelihood (ML) receiver to detect the transmitted symbols reliably at high SNR, it is sufficient for the singular values of the equivalent channel matrix to be bounded away from zero in order to avoid ambiguity errors produced by system degeneracy [6]. However, it is not immediately clear what desirable conditions the equivalent channel matrix has to meet should we choose to use a less computationally expensive receiver. For example, consider the version of the sphere detector described in Section 2.4.1 [38, 40] when applied to the vectorized model in (3.4). As mentioned in Section 2.4.1, this detector performs the QR decomposition of the equivalent channel matrix $\mathcal{H}$, rotates y and performs a tree-structured search over (a certain subset) of the space of all possible transmitted vectors $\mathcal{C}^Q$ to determine

$$\hat{s} = \arg \min_{s_q \in \mathcal{C}'_q \subseteq \mathcal{C}} \|\tilde{y} - \mathcal{R}s\|, \tag{3.7}$$

where $\mathcal{H} = \mathcal{Q}\mathcal{R}$ and $\tilde{y} = \mathcal{Q}^T y$. Similarly we have described in Section 2.4 an alternative to sphere detection, namely, the "nulling and cancellation" approach [15, 31, 35]. In this approach decisions on the elements of s in (3.7) are made sequentially and are fed back to remove interference from subsequent decisions. Some interesting insight into our design approach (described below) can be gained by observing from (3.7) that if the columns of $\mathcal{H}$ can be made orthogonal, both the search in (3.7) and the "nulling and cancellation" approach reduce to simple detection of the individual entries of $\tilde{y}$; i.e., the entries of $\tilde{y}$ are decoupled. Having such a column-orthogonal $\mathcal{H}$ dramatically reduces the search space of the sphere detector and avoids the potential for error propagation in the nulling and cancellation approach. While we do not

deal with the column-orthogonality of $\mathcal{H}$ directly, our design approach (implicitly) generates equivalent channel matrices $\mathcal{H}$ with "increasingly" orthogonal columns as the size of the system grows. More precisely, $\mathcal{H}\mathcal{H}^T$ approaches a scaled identity for almost every channel realization.

3.3.1 Linear preprocessing and mean square error

Another approach used in sphere detection linearly processes y to form $\tilde{s} = Gy$, and then performs an ML search in the neighbourhood of $\tilde{s}$ [36]. Typically, G is chosen as the "zero-forcing" equalizer[2], $G_{\text{ZF}} = \mathcal{H}^{\#}$, or the linear minimum mean square error (MMSE) equalizer, $G_{\text{MMSE}} = \sqrt{\frac{\rho}{M}}\mathcal{H}^T(\frac{\rho}{M}\mathcal{H}\mathcal{H}^T + I_{2NT})^{-1}$. To ensure good performance at reasonable complexity from this type of sphere detector, one should design the coding matrices A_q in (3.1) to ensure that $\tilde{s}$ is, on the average, "close" to s. For a given channel H, the distance between $\tilde{s}$ and s can be measured in terms of the MSE. For the case where $G = G_{\text{MMSE}}$,

$$\begin{aligned}\text{MSE} &= \text{E}_{s,v}\{\text{Tr}\big((s-\tilde{s})(s-\tilde{s})^T\big)\} \\ &= Q - NT + \tfrac{1}{2}\,\text{Tr}\Big(\big(I_{2NT} + \tfrac{\rho}{M}\mathcal{H}\mathcal{H}^T\big)^{-1}\Big) \qquad (3.8)\\ &= \tfrac{1}{2}\,\text{Tr}\Big(\big(I_{2Q} + \tfrac{\rho}{M}\mathcal{H}^T\mathcal{H}\big)^{-1}\Big), \qquad (3.9)\end{aligned}$$

where (3.9) follows from (3.8) by using the matrix inversion lemma [48].

We will show later (in Section 3.3.4) that it is desirable to have Q as large as possible (from both symbol rate and asymptotic performance perspectives). However, the MSE expression (3.8) reinforces the standard practice that Q should be chosen to be no greater than NT [14].

Since we have assumed that the transmitter does not know the channel matrix H, for fixed values of Q and NT, an appropriate design strategy would be to choose the

[2]Here $(.)^{\#}$ denotes the Moore Penrose pseudo inverse.

coding matrices A_q embedded in $\mathcal{H}$ in order to minimize the expected MSE over the distribution of H. That is,

$$\min_{A_q} \quad \mathrm{E}_H\big\{\mathrm{Tr}\big(\big(I_{2NT}+\tfrac{\rho}{M}\mathcal{H}\mathcal{H}^T\big)^{-1}\big)\big\} \tag{3.10a}$$

$$\text{subject to} \quad \mathrm{Tr}(A_qA_q^\dagger)\leq TM/Q. \tag{3.10b}$$

The constraint in (3.10b) not only ensures that the coding matrices meet the overall power constraint in (3.2), it also guarantees that each data symbol satisfies the same bound on its transmitted power. The set of matrices $\{A_q\}$ satisfying (3.10b) is smaller than that satisfying (3.2), and hence enforcing (3.2) rather than (3.10b) may result in improved performance (e.g., [49]). However, we will show in Section 3.3.4 and Appendix A that any performance loss due to (3.10b) vanishes as M increases. In fact, satisfaction of (3.10b) is a necessary condition for the optimized bounds derived below to be asymptotically achieved. The problem in (3.10) can be quite awkward to solve directly because the objective involves an expectation and the design parameters enter $\mathcal{H}$ in a highly structured fashion. Rather than attempting to solve (3.10) directly, we now develop bounds on the objective function and show that, by exploiting the asymptotic properties of the bounds, we can obtain "good" LD codes in a relatively straightforward manner. The key to this development is Jensen's inequality [21]:

Lemma 3.1 *If f is a strictly convex function and X is a random variable, then* $\mathrm{E}\{f(X)\}\geq f(\mathrm{E}\{X\})$ *with equality iff* $X=\mathrm{E}\{X\}$ *with probability* 1.

The function $\mathrm{Tr}\big((I+X)^{-1}\big)$ is strictly convex in X over $\{X|X=X^T\succeq 0\}$. Therefore, using Jensen's inequality,

$$\mathrm{E}_H\big\{\mathrm{Tr}\big((I_{2NT}+\tfrac{\rho}{M}\mathcal{H}\mathcal{H}^T)^{-1}\big)\big\}\geq \mathrm{Tr}\big(\big(I_{2NT}+\tfrac{\rho}{M}\,\mathrm{E}_H\{\mathcal{H}\mathcal{H}^T\}\big)^{-1}\big). \tag{3.11}$$

We now attempt to find coding matrices A_q that minimize the lower bound in (3.11). We will show in Section 3.3.4 that the minimized lower bound is asymptotically achieved.

Observe that

$$\tfrac{1}{M}\mathcal{H}\mathcal{H}^T = \tfrac{1}{M}\sum_{q=1}^{2Q}(I_N \otimes \mathcal{A}_q)\underline{h}\ \underline{h}^T(I_N \otimes \mathcal{A}_q^T), \tag{3.12}$$

where $\mathcal{A}_q$ is defined in (3.6), and $\underline{h}$ in (3.5). Using (3.12), we have

$$\mathrm{E}_H\{\mathcal{H}\mathcal{H}^T\} = \tfrac{1}{2}(I_N \otimes \textstyle\sum_q \mathcal{A}_q\mathcal{A}_q^T) \tag{3.13}$$

and hence the lower bound in (3.11) can be written as

$$\mathrm{Tr}\big(\big(I_{2NT} + \tfrac{\rho}{2M}(I_N \otimes \textstyle\sum_q \mathcal{A}_q\mathcal{A}_q^T)\big)^{-1}\big). \tag{3.14}$$

For any positive definite matrix X, we have that [50]

$$\mathrm{Tr}(X^{-1}) \geq \textstyle\sum_i 1/[X]_{ii},$$

with equality holding if and only if X is diagonal. Therefore, when minimizing the lower bound in (3.14) we can restrict our attention to the case where $\sum_q \mathcal{A}_q\mathcal{A}_q^T$ is diagonal. In order to find the matrices $\mathcal{A}_q$ which minimize the right hand side of (3.11), we solve the following problem:

$$\min_{\mathcal{A}_q} \quad \sum_i \frac{1}{1 + \frac{\rho}{2M}\big[\sum_q \mathcal{A}_q\mathcal{A}_q^T\big]_{ii}} \tag{3.15a}$$

$$\text{subject to} \quad \mathrm{Tr}(\mathcal{A}_q\mathcal{A}_q^T) \leq 2TM/Q. \tag{3.15b}$$

By differentiating the Lagrangian function of (3.15) and setting it to zero we find that the optimal $\mathcal{A}_q$'s satisfy

$$\big[\sum_q \mathcal{A}_q\mathcal{A}_q^T\big]_{ii} = 2M, \qquad \forall i. \tag{3.16}$$

Hence, the optimal choice of $\{\mathcal{A}_q\}$ is one for which

$$\sum_q \mathcal{A}_q\mathcal{A}_q^T = 2MI_{2T}. \tag{3.17}$$

With this choice of $\mathcal{A}_q$, the inequality in (3.11) becomes

$$\mathrm{E}_H\big\{\mathrm{Tr}\big((I_{2NT}+\tfrac{\rho}{M}\mathcal{H}\mathcal{H}^T)^{-1}\big)\big\}\geq 2NT/(1+\rho). \tag{3.18}$$

In the case when we have $M\geq T$, the matrices $\mathcal{A}_q$ are square or "fat", and a simple choice that satisfies (3.17) and the power constraint on each transmitted symbol is given by

$$\mathcal{A}_q\mathcal{A}_q^T=\tfrac{M}{Q}I_{2T}. \tag{3.19}$$

In order to satisfy (3.19), the matrices A_q have to be unitary. That is, $A_qA_q^\dagger=\frac{M}{Q}I_T$ for $1\leq q\leq Q$. When we have $M<T$, we cannot satisfy the restricted optimality condition in (3.19) but if $T\leq 2MQ$, it is possible to satisfy the general optimality condition in (3.17), as we will show in Example 3.2 in Section 3.6.

3.3.2 Mutual Information

In the previous section, we considered code design from a performance perspective with a certain class of suboptimum detectors in mind, and we argued that coding matrices with unitary structure minimize a lower bound on the MSE. In this section we discuss the status of these codes from a mutual information perspective.

If s assumes the capacity-achieving standard circular Gaussian distribution, the model in (3.4) implies that the mutual information between transmitted and received signals is given by [2, 14],

$$I(s;y)=\frac{1}{2T}\,\mathrm{E}_H\big\{\log\det(I_{2NT}+\tfrac{\rho}{M}\mathcal{H}\mathcal{H}^T)\big\}. \tag{3.20}$$

Since $\log\det(I+X)$ is strictly concave in X over $\{X|X=X^T\succeq 0\}$, it follows from Jensen's inequality (Lemma 3.1) that

$$\frac{1}{2T}\,\mathrm{E}_H\big\{\log\det(I_{2NT}+\tfrac{\rho}{M}\mathcal{H}\mathcal{H}^T)\big\}\leq\frac{1}{2T}\log\det\big(I_{2NT}+\tfrac{\rho}{M}\,\mathrm{E}_H\{\mathcal{H}\mathcal{H}^T\}\big). \tag{3.21}$$

We will now show that the coding matrices A_q which maximize this upper bound possess the same unitary structure as those which minimized the lower bound on the MSE. In Section 3.3.4 will we will show that such coding matrices asymptotically achieve the maximized upper bound.[3]

Using the expression in (3.13), to maximize the upper bound in (3.21) we need to solve the following optimization problem:

$$\max \quad \log\det\big(I_{2NT} + \tfrac{\rho}{2M}(I_N \otimes \textstyle\sum_q \mathcal{A}_q\mathcal{A}_q^T)\big) \tag{3.22a}$$

$$\text{subject to} \qquad \mathrm{Tr}(\mathcal{A}_q\mathcal{A}_q^T) \leq 2TM/Q. \tag{3.22b}$$

Using Hadamard's inequality, we have that for any positive definite matrix X,

$$\det(X) \leq \prod_i X_{ii} \tag{3.23}$$

with equality if and only if X is diagonal. By restricting our attention to the set of matrices $\{\mathcal{A}_q\}$ for which $\sum_q \mathcal{A}_q\mathcal{A}_q^T$ is diagonal, and setting the derivative of the Lagrangian of (3.22) equal to zero we find that the optimal $\mathcal{A}_q$'s must satisfy,

$$\big[\sum_q \mathcal{A}_q\mathcal{A}_q^T\big]_{ii} = 2M.$$

Hence, the optimal choice of the set $\{\mathcal{A}_q\}$ is one for which

$$\sum_q \mathcal{A}_q\mathcal{A}_q^T = 2MI_{2T}. \tag{3.24}$$

It is clear from (3.24) that the coding matrices that minimize the lower bound of the mean square error also maximize the upper bound on the mutual information that can be achieved by an LD code. Using (3.24) and (3.21), we can write the maximized bound on the mutual information as,

$$I(s;y) \leq N\log(1+\rho). \tag{3.25}$$

[3]The upper bound in (3.21) and the observation that it is maximized by unitary coding matrices appeared independently in [51]. In Section 3.3.4, we will enhance that result by showing that unitary coding matrices not only maximize the upper bound, but also asymptotically achieve it.

In Appendix B, we show that the right hand side of (3.25) is not only a bound on the maximum mutual information that an LD code can achieve, but is also an upper bound on the ergodic channel capacity. Furthermore, we show that as the number of transmit antennas grows, the ergodic channel capacity approaches the right hand side of (3.25). In Section 3.3.4, we will show that as M (and T) grow, the actual mutual information achieved by an LD code that satisfies (3.24) also approaches the bound in (3.25), and hence approaches the ergodic capacity of the channel.

3.3.3 Pairwise error probability

In this section, we point out that the codes which simultaneously optimize the bounds on the MSE and mutual information derived in Sections 3.3.1 and 3.3.2, respectively, also have desirable properties in terms of a measure of the pairwise error probability (PEP). The measure that we use is the average PEP for the case where the symbol vectors s are drawn from a Gaussian codebook (c.f., [14]), where the average is taken over the channel realizations and all possible codeword pairs of the codebook. More specifically, if $P(s \to s'|\mathcal{H})$ denotes the probability that, conditioned on a specific equivalent channel realization $\mathcal{H}$, the receiver selects the codeword s' given that s was sent, then the average PEP is defined to be [14]

$$\mathrm{PEP}_{av} = \mathrm{E}_H\big\{\mathrm{E}_{s,s'}\{P(s \to s'|\mathcal{H})\}\big\}, \tag{3.26}$$

where s and s' are drawn from a Gaussian codebook.[4] For the model in Section 3.2, it has been shown that [14],

$$\mathrm{E}_{s,s'}\{P(s \to s'|\mathcal{H})\} = \frac{1}{4\pi}\int_{-\infty}^{\infty}\frac{d\omega}{\omega^2+1/4}\prod_{q=1}^{2Q}\frac{1}{\sqrt{1+2\rho\sigma_q(\omega^2+1/4)/M}}, \tag{3.27}$$

[4] Although this average PEP measure [14] is significantly different from the conventional PEP [26], it does provide similar insight, as we now show.

where $\sigma_q \geq \sigma_{q+1}$ denote the eigenvalues of $\mathcal{H}\mathcal{H}^T$.

If we define $r = \text{Rank}(\mathcal{H})$, then when the SNR is sufficiently high, we have $\rho\sigma_r/M \gg 2$. In that case, the unity term under the square root in (3.27) can be neglected and the integral can be evaluated analytically [52, p. 377, p. 441] to obtain

$$\text{E}_{s,s'}\{P(s \to s'|\mathcal{H})\} \leq \eta_r \big(\frac{\rho}{M}\big)^{-r/2} \prod_{q=1}^{r} \sigma_q^{-1/2}, \tag{3.28}$$

where

$$\eta_r = \frac{1}{4\pi}\int_{-\infty}^{\infty} \frac{d\omega}{(\omega^2+1/4)^{1+r/2}} = \begin{cases} 2^{r/2-1}\Big(\frac{(r-1)(r-3)\cdots(1)}{(r/2)!}\Big) & r \text{ even}, \\ \frac{2^r}{2\pi}\sum_{m=0}^{r-1/2}\binom{\frac{r-1}{2}}{m}\frac{(-1)^m}{2m+1} & r \text{ odd}. \end{cases}$$

If $r = \text{Rank}(\mathcal{H}) = \min\{2Q, 2NT\}$, then the product term in (3.28) can be expressed as

$$\prod_{q=1}^{r} \sigma_q^{-1/2} = \begin{cases} \det(\mathcal{H}\mathcal{H}^T)^{-1/2} & Q \geq NT, \\ \det(\mathcal{H}^T\mathcal{H})^{-1/2} & Q \leq NT, \end{cases} \tag{3.29}$$

where we have used the fact that for $1 \leq q \leq r$, $\sigma_q(\mathcal{H}\mathcal{H}^T) = \sigma_q(\mathcal{H}^T\mathcal{H})$ and the fact that $\det(I_{2NT} + \mathcal{H}\mathcal{H}^T) = \det(I_{2Q} + \mathcal{H}^T\mathcal{H})$. Combining (3.26), (3.28) and (3.29), we obtain

$$\text{PEP}_{av} \leq \begin{cases} \eta_{2NT}\big(\frac{\rho}{M}\big)^{-NT}\,\text{E}_H\big\{\det(\mathcal{H}\mathcal{H}^T)^{-1/2}\big\} & Q \geq NT, \\ \eta_{2Q}\big(\frac{\rho}{M}\big)^{-Q}\,\text{E}_H\big\{\det(\mathcal{H}^T\mathcal{H})^{-1/2}\big\} & Q \leq NT. \end{cases} \tag{3.30}$$

The bound in (3.30) is tight if $r = \text{Rank}(\mathcal{H}) = \min\{2Q, 2NT\}$ with probability 1, and is trivial otherwise.

Our goal in this section is to minimize PEP_{av} or alternatively to minimize the upper bound in (3.30) provided that the latter is tight. As in Sections 3.3.1 and 3.3.2, we will not minimize the upper bound in (3.30) directly, but we seek a lower bound on $\text{E}_H\{\det(\mathcal{H}\mathcal{H}^T)^{-1/2}\}$ when $Q \geq NT$, and a lower bound on $\text{E}_H\{\det(\mathcal{H}^T\mathcal{H})^{-1/2}\}$ when $Q < NT$. To that end, we observe that the function $f(X) = \det(X)^{-1/2}$ is

strictly convex over $\{X|X = X^T \succ 0\}$.[5] Thus we can employ Jensen's inequality (Lemma 3.1), to show that

$$\mathrm{E}\{\det(X)^{-1/2}\} \geq \det(\mathrm{E}\{X\})^{-1/2}, \tag{3.31}$$

where X is defined as

$$X = \begin{cases} \mathcal{H}\mathcal{H}^T & Q \geq NT, \\ \mathcal{H}^T\mathcal{H} & Q \leq NT. \end{cases}$$

As in the previous subsections, this bound is optimized if $\mathrm{E}\{\mathcal{H}\mathcal{H}^T\} \rightarrow MI_{2NT}$ for $Q \geq NT$ and $\mathrm{E}\{\mathcal{H}^T\mathcal{H}\} \rightarrow \frac{MNT}{Q} I_{2Q}$ for $Q < NT$. In the next section, we will show that when the number of symbols per block, Q, is appropriately chosen, coding matrices A_q with a unitary structure asymptotically achieve the minimized lower bound of the high-SNR average PEP in (3.30).

3.3.4 Asymptotic Optimality of Unitary Coding Matrices

In this subsection we will show that unitary coding matrices A_q not only minimize the lower bound on the MSE in (3.11) and the PEP bound in (3.30), as well as maximize the upper bound on the mutual information that can be achieved by an LD code in (3.21). For any given N, they also asymptotically attain these bounds as T, M and Q grow, so long as the scattering environment remains sufficiently rich to provide independence between the entries of the channel matrix.

The justification of the claim of asymptotic optimality of the unitary coding matrices, is based on the following lemma [53].

Lemma 3.2 *Let C and $D \in \mathbb{R}^{n\times n}$ be diagonal matrices with $C = \mathrm{Diag}(c_1, \ldots, c_n)$ and $D = \mathrm{Diag}(d_1, \ldots, d_n)$ where $c_1 \geq c_2 \geq \ldots \geq c_n \geq 0$, $d_1 \geq d_2 \geq \ldots \geq d_n \geq 0$ and $\|C\| = \|D\| = n$. Let $\Delta = \Gamma + j\Lambda$ be a unitary matrix uniformly distributed*

[5] In fact, $f(X)$ is log-convex over $\{X|X = X^T \succ 0\}$ and hence convex over this set.

according to the Haar measure[6]*. Then as* n *increases,* $\big(\mathrm{Tr}(C\Gamma), \mathrm{Tr}(D\Lambda)\big)$ *converges in distribution to* $\frac{1}{\sqrt{2}}(Z_1, Z_2)$*, where* Z_1 *and* Z_2 *are independent and identically distributed standard normal random variables. That is,* $\mathrm{Tr}(C\Gamma + jD\Lambda)$ *converges to a complex standard circular normal distribution.*

In order to enable the asymptotic analysis, we assume that the coding matrices A_q are randomly chosen from the uniform distribution (in the Haar measure) on the group of unitary matrices. Using the result in Lemma 3.2, we prove the following proposition in Appendix A.

Proposition 3.1 *Let* $\mathcal{H} \in \mathbb{R}^{2NT\times 2Q}$ *(c.f.,* (3.5)*) be given by*

$$\mathcal{H} = \Big[\begin{array}{cccc} I_N \otimes \mathcal{A}_1 & I_N \otimes \mathcal{A}_2 & \cdots & I_N \otimes \mathcal{A}_{2Q} \end{array}\Big] [I_{2Q} \otimes \underline{h}],$$

where the entries of $\underline{h} \in \mathbb{R}^{2MN}$ *are independent identically distributed (i.i.d.) zero mean Gaussian random variables with variance of one half and* $\forall q \in [1, 2Q]$*,* $\mathcal{A}_q$ *is given by* (3.6)*, where* $\{A_q\}$ *are i.i.d. random unitary matrices that are uniformly distributed with respect to the Haar measure. Then, for any* $N \geq 1$*,* $Q \geq M$ *and with the ratio* $\frac{T}{M} \leq 2Q$ *held constant,*

$$\mathcal{H}\mathcal{H}^T \xrightarrow{a.s.} \mathrm{E}\{\mathcal{H}\mathcal{H}^T\}, \tag{3.32}$$

as $M \to \infty$*, where* $\xrightarrow{a.s.}$ *denotes almost sure convergence.*

The condition in (3.32) is sufficient for the bounds derived in Sections 3.3-A–C to be approached, and hence randomly selecting unitary coding matrices is asymptotically optimal as M and T grow.

[6]The Haar measure [54] is the unique rotationally invariant measure (up to scalars) associated with compact measurable sets of unitary matrices. Thus, if $\mathcal{S}$ is a measurable subset of the set of unitary $p \times q$ matrices, then the Haar measure associated with this subset, $\mu(\mathcal{S}) = \mu(P\mathcal{S})$ for any $p \times p$ unitary matrix P. For example, in $\mathbb{R}^2$, the Haar measure $\mu(\mathcal{S})$ associated with a measurable set of unit vectors $\mathcal{S}$ is given by the length of the arc of the unit circle spanned by the unit vectors contained in $\mathcal{S}$. A general $M \times N$ unitary matrix is said to be isotropically distributed if it is uniformly distributed with respect to the Haar measure [19].

It is to be noted here that although we have considered complex coding matrices A_q, the above asymptotic analysis is valid for real orthogonal matrices as well. An advantage of constraining the coding matrices to be real is that it reduces the number of parameters to be optimized in designing the code. However, this reduction in design complexity comes at the possible risk of a reduction in performance.

It is interesting to compare the result in Proposition 3.1 with a related result that appeared recently in [55]. There, it was shown that using orthogonal coding matrices is asymptotically information lossless as the SNR$\rightarrow$ 0. It was conjectured therein that that result carries over to the high SNR realm. Using Proposition 3.1, we can obtain a complementary result that states that for any SNR, unitary coding matrices are asymptotically information lossless as the number of transmit antennas grows.

3.4 Design Procedure

In the previous section it was argued that for large systems (with T/M held constant) picking unitary coding matrices A_q randomly is optimal in the sense that it enables $\mathcal{H}\mathcal{H}^T$ to approach $E\{\mathcal{H}\mathcal{H}^T\}$ as the dimensions of $\mathcal{H}$ grow, i.e., $\mathcal{H}\mathcal{H}^T$ concentrates around its mean. However, when the dimension of the coding matrices is not large enough to obtain statistical independence between the entries, picking the coding matrices at random may result in a nearly singular equivalent channel matrix $\mathcal{H}$ for many channel realizations, and hence poor performance. In order to obtain "good" unitary coding matrices for such practical systems, we need a selection criterion. In this section we exploit insight from the proof of Proposition 3.1 to develop a candidate design procedure. In Section 3.6 we will demonstrate that our design procedure can provide codes which perform well in practice.

The first step in the design procedure is to determine the number of symbols Q to be transmitted over the channel in each block of T channel uses. The fact

that $\mathcal{H}$ has dimensions $2NT \times 2Q$, immediately suggests choosing $Q \leq NT$, [14]. This choice of Q is also supported by the MSE expression in (3.8). However, the proof of Proposition 3.1 suggests that in order to approach the optimized bounds in Section 3.3, one should choose Q to be as large as possible in order to provide averaging over the largest possible set of coding matrices. Based on these observations, we do not restrict Q to be equal to $\min\{NT, MT\}$ as in [14]. Instead, we propose choosing $Q = NT$ which yields a square equivalent channel matrix $\mathcal{H}$.

We also require a selection criterion for designing the unitary coding matrices, A_q. To develop an appropriate criterion, we assess the analysis of Section 3.3. The PEP bound in (3.28), suggests that we need to ensure that the minimum eigenvalue of $\mathcal{H}\mathcal{H}^T$ is bounded away from zero for "as many channel realizations as possible". In a complementary way, the MSE and mutual information analyses show that lower and upper bounds on these quantities, respectively, are achieved at their optimized values when $\mathcal{H}\mathcal{H}^T$ approaches scaled identity for every channel realization. Therefore, we expect good performance from the coding scheme if the equivalent channel matrix $\mathcal{H}$ is "close" to being orthogonal for as many realizations as possible. We will use a statistical measure of the proximity of $\mathcal{H}$ to a scaled identity so that a standard stochastic optimization technique can be employed. The measure is based on the observation that for any $n \times n$ positive definite matrix X,

$$\arg \max_{\mathrm{Tr}(X) \leq cn} \det(X) = cI. \tag{3.33}$$

Hence, the expected determinant of $\mathcal{H}\mathcal{H}^T$ is an appropriate measure of the proximity of $\mathcal{H}\mathcal{H}^T$ to a scaled identity. Although it is possible to develop other measures that promote the same goal, this measure is consistent with the performance criteria discussed in Section 3.3. Our proximity measure has the advantage that it is a smooth continuous function of the parameters that characterize the unitary coding matrices and, as we will see in Section 3.6, it results in an effective design algorithm for all

configurations that satisfy[7] $\frac{T}{M} \leq 2Q$. Therefore, we will design finite codes which come close to achieving the asymptotically achievable optimized bounds by solving the following stochastic optimization problem[8]:

$$\max_{A_q} \quad \mathrm{E}_H\{\det(\mathcal{H}\mathcal{H}^T)\} \tag{3.34a}$$

$$\text{subject to } A_q A_q^\dagger = \tfrac{M}{Q} I. \tag{3.34b}$$

The optimization problem (3.34) looks rather similar to a high SNR instance of the capacity maximization problem presented in [14] with coding matrices restricted to the unitary group (c.f., (3.34b), [14, eq. (28)]). However, the fact that we do not have the offset provided by the identity matrix in the mutual information expression (3.20) means that our formulation (3.34) strongly penalizes bad equivalent channel events. That is, the expression in (3.20) will be quite insensitive to slight variations in the minimum eigenvalue of $\mathcal{H}\mathcal{H}^T$ when the latter approaches zero, whereas our formulation explicitly incorporates these variations. In Section 3.3.3 we have discussed the impact of the minimum eigenvalue on the PEP; c.f., (3.28).

In order to explore the relationship between our design approach and the conventional diversity gain in more detail, we recall that the diversity gain of a multiple antenna system is quantified through the rank criterion defined in [20]. For an LD code (c.f., (3.1)), the transmitted codewords take the form $S = \sum_q \alpha_q A_{2q-1} + \beta_q A_{2q}$, and the diversity gain is given by,

$$\min_{\alpha+j\beta,\alpha'+j\beta' \in \mathcal{C}} \Big\{ \mathrm{Rank}\big[\sum_q (\alpha_q - \alpha'_q) A_{2q-1} + (\beta_q - \beta'_q) A_{2q}\big] \Big\}.$$

Now, consider our design problem (3.34). By maximizing $\det(\mathcal{H}\mathcal{H}^T)$ we implicitly attempt to reduce the linear dependence of the different columns of $\mathcal{H}$. Columns

[7] Since we have chosen $Q = NT$, this condition is always satisfied.

[8] In relation to (3.33), the trace constraint in (3.33) is captured by the power constraint on the coding matrices (c.f., (3.34b)) and the norm of the given channel realization.

of $\mathcal{H}$ are linearly independent if and only if $\gamma_1 \breve{h}_j + \gamma_2 \breve{h}_k \neq 0$ for all $\gamma_1, \gamma_2 \neq 0$, $\|\breve{h}_j\|, \|\breve{h}_k\| \neq 0$, where $\breve{h}_r$ denotes the rth column of $\mathcal{H}$. That is, if and only if

$$\big(\gamma_1(I_N \otimes \mathcal{A}_j) + \gamma_2(I_N \otimes \mathcal{A}_k)\big)\underline{h} \neq 0, \qquad \forall \underline{h} \neq 0,\ 1 \leq j,k \leq 2Q.$$

However, if $B = \gamma_1(I_N \otimes \mathcal{A}_j) + \gamma_2(I_N \otimes \mathcal{A}_k)$ is rank deficient, then there is always an $\underline{h}$ that lies in the null space of B for which the determinant will be zero and hence the columns will be linearly dependent. Hence, by maximizing $\mathrm{E}_H\{\det(\mathcal{H}\mathcal{H}^T)\}$, we penalize rank deficiency of B and indirectly attempt to maximize diversity gain.

An advantage of our formulation is that the objective is independent of the constellation $\mathcal{C}$, and hence we can apply standard (stochastic) optimization techniques based on analytic expressions for the gradient of the objective (see Section 3.6 and Appendix C). This is in contrast to an alternative performance orientated design [46] which uses a constellation dependent PEP criterion and hence as the constellation size increases, considerable computational effort is required to merely compute the objective. Actually, our constraint in (3.34b) that the code matrices be unitary is also slightly different from the constraint that was imposed in [46]. In our notation, the constraint in [46] corresponds to

$$\mathrm{Tr}(A_q^\dagger A_p) = \tfrac{TM}{Q}\delta_{pq}, \tag{3.35}$$

where δ_{pq} is the Kronecker delta. The set of matrices which satisfy (3.35) intersects the set of unitary matrices, but neither is a proper subset of the other. However, if $\{A_q\}$ are i.i.d. and uniformly distributed then $\mathrm{E}\{\mathrm{Tr}\big(A_q^\dagger A_p\big)\} = \frac{TM}{Q}\delta_{pq}$. Furthermore, for such $\{A_q\}$, Lemma 3.2 suggests that for sufficiently large matrices for which the conditions of Proposition 3.1 hold, $A_q^\dagger A_p \overset{a.s.}{\to} \mathrm{E}\{A_q^\dagger A_p\} = \frac{T}{Q} I_M \delta_{pq}$. This implies that in the limit as the dimension of the coding matrices increases, these matrices will satisfy (3.35). While coding matrices that satisfy (3.35) only are capacity optimal when $Q \geq MT$, they do not necessarily provide good performance. Moreover, if

$N < M$ effective detection for systems with $Q \geq MT > NT$ may incur considerable computational cost and performance degradation; c.f., (3.8). In contrast, by only constraining A_q to be unitary, we almost surely obtain optimality from both mutual information and performance perspectives for any number of receive antennas as the size of the system grows.

3.5 Row Interleaving

At high SNR, the error rate performance of a space-time code is dominated by the outage probability—the probability that the channel is unable to support the required data rate. Outage is associated with the event of the channel matrix dropping rank [6]. In order to reduce the probability of outage, one can employ interleaving. The general philosophy of interleaving in communication over fading channels is to first impose structure on the data sequence to be transmitted, and then to interleave the structured sequence so that related components are transmitted over independent channel realizations. The standard implementation of this strategy in the space-time coding literature is to impose the structure on the data sequence using an outer (scalar) code, then interleave the coded stream and pass it to a standard space-time mapper (e.g., BLAST or OSTBC). The alternative approach that we propose in this section is to exploit the structure imposed by the LD code itself. We will show in Section 3.6 that the structure of our codes enables them to significantly outperform the standard LD codes [14] when the interleaving scheme we describe below is employed.

A disadvantage of the standard LD coding framework that we have considered in this chapter is that each row of the codeword S is transmitted over the same channel. While maximizing $\mathrm{E}\big\{\det(\mathcal{H}\mathcal{H}^T)\big\}$ penalizes the occurrence of an outage, it may be insufficient to protect the transmitted codeword if $\|\underline{h}\|$ drops below a certain

level. However, by augmenting the LD code framework by grouping successive codeword matrices together and interleaving their rows, we can benefit from the temporal diversity provided by different channel realizations. If the codewords are carefully structured, this scheme can be used to reduce the outage probability and hence to improve the high-SNR performance. (Recall that we have assumed an independent block fading model for the channel.) In particular, given the codewords $S_1, S_2, \ldots, S_J$, (c.f. (3.1)) we construct the row-interleaved codewords $\tilde{S}_1, \tilde{S}_2, \ldots, \tilde{S}_J$ such that,

$$\begin{bmatrix} \tilde{S}_1 \\ \vdots \\ \tilde{S}_J \end{bmatrix} = P \begin{bmatrix} S_1 \\ \vdots \\ S_J \end{bmatrix}, \tag{3.36}$$

where J is called the interleaving depth and P is some $JT \times JT$ permutation matrix. Since the channel is assumed to change to an independent realization after a block of T channel uses, the fact that each codeword constitutes T rows, implies that J should be chosen so that $J \leq T$. Otherwise, row interleaving will lead to further processing delay without extracting additional temporal diversity. In this chapter, we will choose $J = T$. This choice ensures that each codeword can be symmetrically dispersed over the same number of channel realizations, i.e., there exists (at least) one permutation matrix P that shuffles the T^2 rows in such a way that rows are interleaved across (rather than within) blocks. In order to gain some insight into the proposed interleaving scheme we will choose such a P, namely the one whose (i,j)th entry is given by $P(i,j) = 1$ for all $j = \lceil \frac{i}{T} \rceil + T\big((i-1) \bmod T\big)$, $i \in [1, T^2]$ and zero otherwise. The row-interleaved codewords $\tilde{S}_t$ are then transmitted over the respective channel realizations $H^{(t)}$, $t \in [1, T]$. This model can be considered as a special case of the general block fading model of [56]. However, unlike [56], our interleaving scheme does not incur extra detection complexity due to augmentation of the equivalent channel matrix. This fact will become clear as we discuss our proposed scheme in more detail. While we do not claim optimality of the proposed interleaving scheme,

we will discuss below the intuition that led to its development and in Section 3.6 we will demonstrate its effectiveness.

With the row interleaving scheme in (3.36), the vectorized received symbol matrix can be written in a form similar to (3.4) as

$$y = \sqrt{\frac{\rho}{M}}\,\tilde{\mathcal{H}}s + v,$$

where

$$\tilde{\mathcal{H}} = \left[\begin{array}{cccc} I_N \otimes \tilde{\mathcal{A}}_1 & I_N \otimes \tilde{\mathcal{A}}_2 & \cdots & I_N \otimes \tilde{\mathcal{A}}_{2Q} \end{array}\right] \left[I_{2Q} \otimes \underline{\tilde{h}}\right]. \tag{3.37}$$

If $\mathcal{A}_q(i,:)$ denotes the i^{th} row of $\mathcal{A}_q$, and if we define the matrix E_{ij} to be the all zero $2T \times T$ matrix with unity in the (i,j)th position [57], then our particular choice of the permutation matrix P will result in,

$$\tilde{\mathcal{A}}_q = \sum_{i=1}^{2T} E_{i,\kappa(i)} \otimes \mathcal{A}_q(i,:),$$

where

$$\kappa(i) = 1 + (i-1) \bmod (T), \tag{3.38}$$

and $\underline{\tilde{h}} = \left[h_1^{(1)^T}, \cdots, h_1^{(T)^T}, \cdots, h_N^{(1)^T}, \cdots, h_N^{(T)^T}\right]^T$, where $h_n^{(t)}$ is the vector h_n in (3.5) at the t^{th} realization of the channel matrix, $1 \leq t \leq T$. Notice that the size of $\tilde{\mathcal{H}}$ is the same as the size of $\mathcal{H}$. This fact guarantees that the complexity of the detector used at the receiver remains the same as for the non-interleaved codes. That is, while the proposed interleaving scheme incurs the standard latency penalty of transmission schemes which code over independent realizations, the complexity of the detection problem is unchanged.

As we show in Appendix D, using unitary coding matrices along with row interleaving enhances diagonal dominance of $\tilde{\mathcal{H}}\tilde{\mathcal{H}}^T$ over that of $\mathcal{H}\mathcal{H}^T$ and hence makes $\tilde{\mathcal{H}}$ "closer" to being orthogonal than $\mathcal{H}$, even for systems of finite size. The arguments that led to the design problem in (3.34) suggest that row interleaving will improve

the high SNR performance of our LD codes. As we will show in the next section, these performance improvements can be substantial.

3.6 Numerical Results

In this section, we provide some numerical examples that illustrate the potential of the proposed designs. We have chosen scenarios from Hassibi and Hochwald's work [14] in which their codes (which will be referred to as HHLD codes) were shown to outperform OSTBCs and BLAST. Given that the LD codes framework subsumes other recent designs, we have also chosen scenarios from [46], [45] and [27]. Before we begin, a few remarks regarding the practical implementation of our design approach are provided below:

1. The optimization problem in (3.34) can be solved by combining the principles of stochastic optimization [58] to deal with the expectation in the objective, with the principles of optimization over the Stiefel manifold [44, 59, 60] to deal with the orthogonality constraints. In the examples below we have chosen to constrain the coding matrices to the manifold in (3.34b) by parameterizing A_q via Givens rotations [61]. We then applied stochastic quasi-gradient methods [58] to solve (3.34). Note that by parameterizing A_q via Givens rotations the optimization problem (3.34) becomes unconstrained and hence more straightforward to solve. Furthermore, the gradient and (the Hessian matrix) of the stochastic optimization objective with respect to the Givens rotations can be found analytically. For convenience, in Appendix C we have provided the expression for the gradient along with a brief description of the Givens parameterization.

2. For the case where $T = M$, the restriction of our search to the group of unitary matrices reduces the number of parameters to be optimized from $4QM^2$ real

parameters to $2QM^2$ real parameters. This is a significant reduction in complexity. Further reduction can be achieved by restricting our attention to real orthonormal matrices. In that case, the number of parameters is $QM(M-1)$.

3. When $T \neq M$, we embed the matrices A_q in square unitary matrices of dimension $\max(T, M)$ and parameterize the square matrices. The resulting coding matrices will be a subset of the columns or rows of the square matrices. In the case when we choose $M > T$, this parameterization guarantees that condition (3.19) holds, and in the case where $M < T \leq 2MQ$, we can structure the embedding so that unitarity of the square matrix implies that (3.17) holds.

4. In each of the considered examples, row interleaving was implemented using the permutation matrix P given in Section 3.5.

5. The coding matrices used in the following examples were obtained using the procedure outlined in Section 3.4 and are available at `http://www.ece.mcmaster.ca/%7Edavidson/pubs/RamyLD.html`.

6. In all comparisons, the simulation programs were run until hundred errors were generated. Under a Gaussian approximation of the error in the estimation of the probability of error [62], this choice of the number of errors means that the 95% confidence interval lies within $[8 \times 10^{-(\nu+1)}, 2 \times 10^{-\nu}]$, where ν is the error probability. For target error probabilities below 10^{-7}, parallel simulations were run on different machines with distinct sets of pseudorandom channel, noise and data realizations. The output of these simulation runs were averaged to produce the reported results.

Example 3.1 We begin with a comparison with the HHLD codes [14] and the full-rate full-diversity layered code of Ma and Giannakis [27] (denoted MG) in the simple

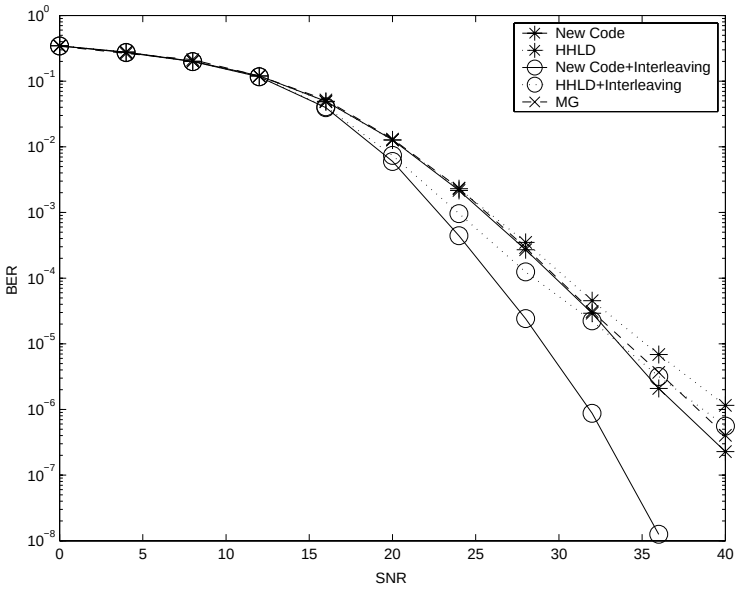

Figure 3.1: A comparison between an LD code designed using (3.34), and the corresponding HHLD [14] and MG [27] codes when $M = N = T = 2$, $Q = NT = 4$ and 16-QAM symbols are transmitted.

case in which $M = N = T = 2$, $Q = NT = 4$ and the symbols are drawn from a Gray-coded 16-QAM constellation.

The resulting transmission rate is $R = 8$ bits per channel use. Figure 3.1 shows the bit error rate (BER) performance, for the HHLD code [14], the MG [27] code and a code we designed using (3.34). When no row interleaving is used, our code provides a slight improvement in performance over the HHLD and the MG codes. When row interleaving is employed, our code provides substantially better performance than the HHLD code. For example, the SNR gain of our code over the HHLD code is about 8 dB at a BER of around 10^{-6}. □

Example 3.2 In this example, we choose $M = 3$, $N = 1$, $T = 3$ and $T = 6$. When $T = 3$ we provide comparisons with the corresponding TAST code [45] and when $T = 6$ we provide comparisons with the corresponding HHLD code [14]. In all cases, the number of symbols per block, Q, was chosen to be $Q = NT$. Therefore, the data

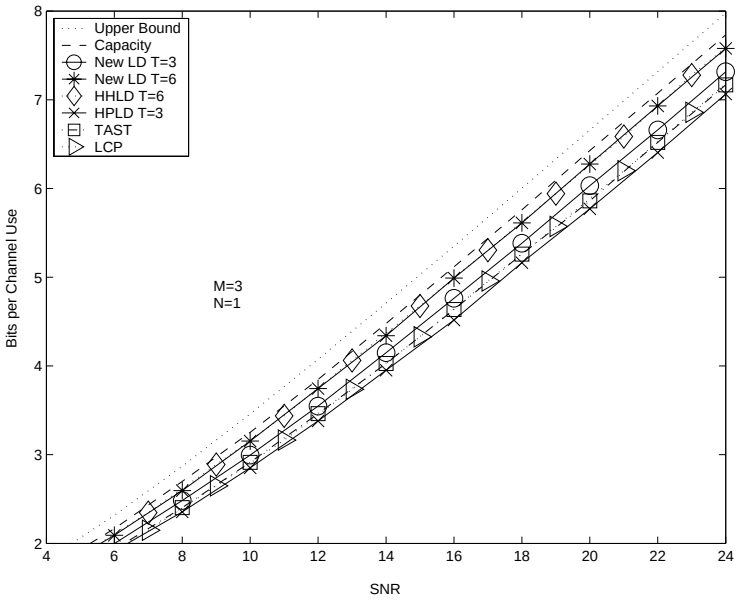

Figure 3.2: The actual channel capacity, the upper bound in (3.25) and the information rate achieved by our LD code, the HHLD code [14] and the TAST code [45] in Example 3.2, the HPLD code [46] in Example 3.3 and the LCP code [63] in Example 3.4.

rate is maintained the same for all cases.

The mutual information achieved by each code is illustrated in Figure 3.2, along with the ergodic channel capacity and the bound derived in Section 3.3.2; c.f., (3.25). We observe that for $T = 3$ our code provides larger mutual information than the TAST code. (The SNR gap to the ergodic capacity is around 1.2 dB for our code and around 1.6 dB for the TAST code.) However, unlike TAST codes, LD codes naturally allow the exploitation of channel coherence intervals that are longer than the number of transmit antennas. In particular, when $T = 6$ the mutual information achieved by our code and the HHLD code is substantially closer to the channel capacity. (The SNR gap has been reduced to 0.4 dB). This reduction in the SNR gap is in agreement with the result in Proposition 3.1, where it was shown that increasing the size of the (unitary) coding matrices reduces the statistical dependence between the

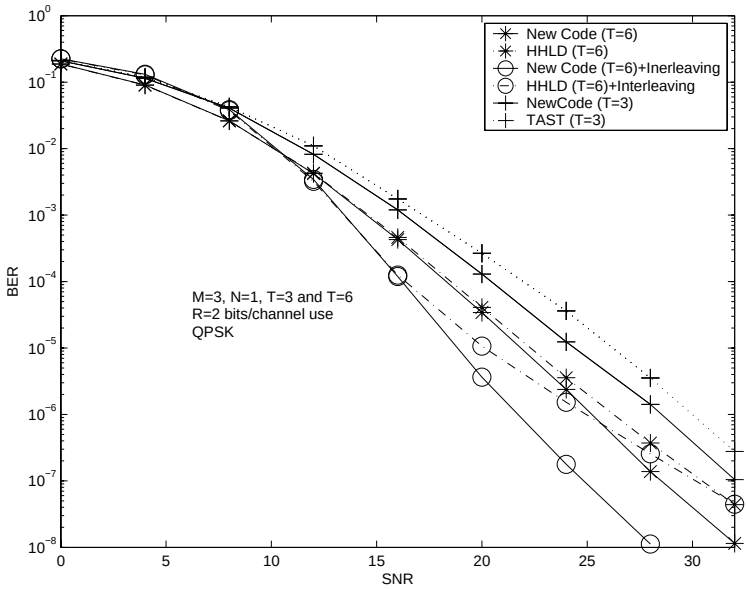

Figure 3.3: A comparison between an LD code designed using (3.34) and codes presented in [14] (HHLD) and [45] (TAST) when $M = 3,\ N = 1,\ T = 6$, $Q = NT = 6$ and QPSK symbols are transmitted.

entries. Moreover, since the number of symbols, Q, is chosen to be equal to NT, by increasing T we allow more averaging over the coding matrices (c.f., (3.24)) which also contributes to the reduction of the SNR gap between the ergodic channel capacity and the mutual information achieved by the code. To examine the performance of these systems, we consider the case in which the symbols are drawn from the QPSK constellation and hence the rate is $R = 2$ bits per channel use. For the case when $T = 3$, our design provides a considerable BER performance gain over the TAST code, as can be seen from Figure 3.3. For the case of $T = 6$, our design provides appreciable BER performance gain over the HHLD design at high SNR in the absence of row interleaving, and substantial performance gain when row interleaving is used. (An SNR gain of around 5 dB of is achieved at a BER of 10^{-6}.) There is a detectable deterioration in performance of the interleaved scheme at low SNRs. This is due to the fact that the proposed interleaving scheme does not control the conditioning of $\tilde{\mathcal{H}}\tilde{\mathcal{H}}^T$,

and the weaker dimensions are more vulnerable to noise. However, the interleaved codes perform better than the non-interleaved codes at typical operating SNRs. □

Example 3.3 In this example, we compare our codes with the $M = T = 3$, $N = 1$ and $Q = NT = 3$ code presented in [46] which we will denote by HPLD. The mutual information achieved by this code is shown in Figure 3.2. At a data rate of 3 bits/channel use, the SNR gap to the ergodic capacity of this code is about 1.9 dB, which is larger than the SNR gaps of both the proposed LD code and the TAST code. In order to examine the performance of our codes in comparison with that of the HPLD code, we consider the case in which the transmitted symbols are drawn from a 16-QAM constellation, yielding a transmission rate $R = 4$ bits per channel use. We have designed two LD codes in this case; one each for the schemes with and without row interleaving. For the case when row interleaving is employed, we restricted our attention, as in [46], to coding matrices that satisfy $A_{2q-1} = A_{2q}$ for $q = 1, \ldots, Q$. Notice that this choice of A_q results in the $(2q-1)$th and the $(2q)$th columns of $\mathcal{H}$ to be orthogonal to each other.

We observe from Figure 3.4 that, at high SNR, row interleaving provides significant improvement in performance for both codes. However, our codes perform slightly better than those designed in [46], and are much easier to design. □

Example 3.4 As a final example, we compare our designs with the full-rate full-diversity layered code of Ma and Giannakis [27] (denoted MG) and the linear constellation precoding scheme developed in [63] (denoted LCP). We will also provide comparisons with the HPLD codes [46] and TAST [45] codes. We choose $T = M = 3$ and $N = 1$. For our codes, the number of transmitted symbols, Q is chosen to be $Q = NT = 3$, which is the same as the value of Q chosen for the corresponding LCP, HPLD and TAST codes. The MG codes are a full symbol rate design, and hence $Q_{\text{MG}} = MT = 9$. One of the advantages of the MG codes in this scenario

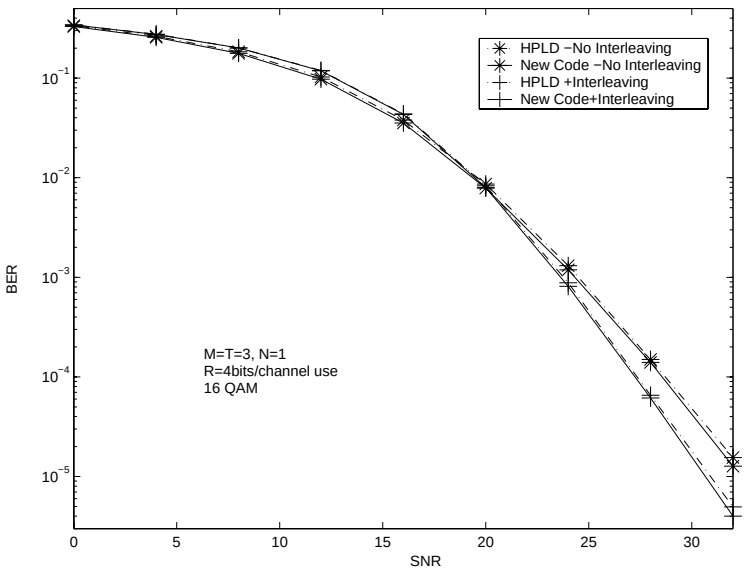

Figure 3.4: A comparison between the new LD codes and the HPLD code [46] when $M = T = 3$, $N = 1$, $Q = NT = 3$ and 16-QAM symbols are transmitted.

is that they are "information lossless". That is, the mutual information achieved by the MG codes coincides with the dashed line representing the ergodic capacity in Figure 3.2. In addition, the MG, LCP and TAST codes generically achieve full diversity and the HPLD code for this scenario also achieves full diversity. Therefore, there is considerable interest in comparing the block error rate performance of these codes with that of our code. (Recall that diversity is defined in terms of the rate of decay of the block error rate with log(SNR) at high SNR.) Since $Q_{\mathrm{MG}} = 9$ and $T = 3$, the smallest uncoded data rate that we can consider is 3 bits per channel use, which corresponds to using BPSK symbols in the MG code. Since $Q = 3$ for the other codes, they must employ an octal constellation to achieve the same data rate, and we will choose Gray-coded 8-PSK. The block error rate curves for these systems are provided in Figure 3.5. At high SNRs, the slopes of these curves are (essentially) the same, and hence all five schemes (essentially) achieve full diversity. However, our code has

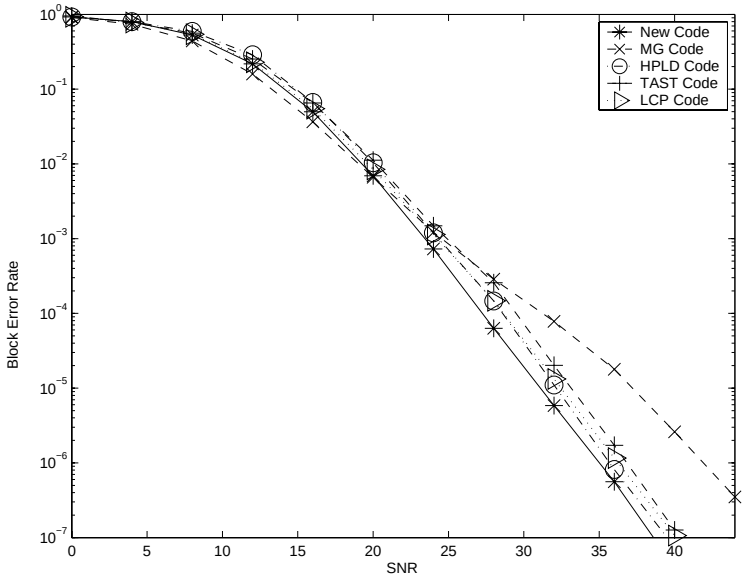

Figure 3.5: A comparison between the new LD code and the codes presented in [27] (MG), [63] (LCP), [46] (HPLD) and [45] (TAST) when $M = T = 3$, $N = 1$. For the MG code $Q = 9$ and the underlying constellation is BPSK, and for the other codes $Q = 3$ and the underlying constellation is 8-PSK.

a significant performance advantage over the HPLD, LCP and TAST codes (approximately 1, 1.2 and 2 dB, respectively at a block error rate of 10^{-5}), and a substantial advantage over the MG codes (approximately 6 dB at a block error rate of 10^{-5}). The performance advantage of our codes is due, in part, to the fact that our design (implicitly) considers the overall average pairwise error probability (see Sections 3.3 and 3.4), rather than just the diversity component. The slow rate of decay of the block error rate of the MG code at moderate SNRs is worthy of some discussion. We suspect that this is due to the fact that in this example the MG code results in a "fat" equivalent channel matrix (of dimension[9] 6×9), whereas the equivalent channel matrices of the other codes are square (6×6). In addition to this performance issue, the "fat" equivalent channel matrix of the MG code requires the use of computationally

[9]The equivalent channel matrix $\mathcal{H}$ is nominally $2NT \times 2Q = 6 \times 18$, but since BPSK signaling is employed, only Q columns of $\mathcal{H}$ are active.

expensive detection techniques [39]. These difficulties are alleviated by the flexibility of the LD framework, which allows the designer to manipulate the signaling strategy so that the equivalent channel matrix is square (or tall).

3.7 Conclusion

In this chapter, we demonstrated that coding matrices drawn at random from the group of unitary matrices are asymptotically optimal from several design perspectives, including mean square error, mutual information and average pairwise error probability. We then provided a systematic, versatile, and efficient constellation-independent design technique for finding "good" unitary coding matrices for practical systems. In our examples, these codes performed better than those currently available. The properties of a unitary coded system prompted us to propose a row interleaving scheme for LD codes that was shown to significantly improve the system performance at high SNR without increasing the complexity of the detector.

Chapter 4

Non-Coherent MIMO Communication using Grassmannian Constellations

The previous chapter developed a generic procedure for designing space-time codes for systems operating over coherent communication channels. It was shown that this design procedure yields asymptotically optimum codes from different design perspectives as the number of transmit antennas grows. In this chapter, we will focus on the design of space-time codes for systems communicating at moderate-to-high SNRs over non-coherent channels. In particular, we consider communication over a frequency-flat MIMO Rayleigh block-fading channel when neither the transmitter nor the receiver has access to the channel fading coefficients. At high SNRs, the capacity-achieving distribution for this channel corresponds to the isotropic distribution on a Grassmann manifold. Using a subspace perturbation analysis, an appropriate metric for the distance between Grassmannian constellation points is determined, and a greedy technique for designing constellations that mimic the isotropic distribution is then proposed. We will show that our choice of the metric yields constellations that

provide better performance than other designs as the data rate approaches the high SNR non-coherent capacity limit.

4.1 Introduction

In this chapter we consider communication over a frequency-flat MIMO Rayleigh block-fading channel with block size T when neither the transmitter nor the receiver has any *a priori* knowledge of the channel realization (i.e., no channel state information, CSI, is available.) As mentioned in Chapter 2, this model is usually referred to as being non-coherent [16, 19, 23]. While the coherent framework, in which the receiver has complete *a priori* CSI, facilitates the application of conventional transmission and reception principles [16], the non-coherent framework has the advantage that it accounts for the communication resources that would have to be expended to obtain CSI at the receiver. This is important in several scenarios, including certain time division duplex (TDD) schemes and frequency hopping schemes [19]. Despite the absence of *a priori* CSI at the receiver, non-coherent communication systems with multiple antennas can provide reliable transmission at high data rates. Indeed, it was shown in [16] and [19] that these multiple-input multiple-output (MIMO) non-coherent systems can achieve a significant fraction of the ergodic channel capacity [2] associated with their coherent counterparts.

For a MIMO communication system with M transmitter antennas and N receiver antennas operating non-coherently over a richly-scattered, frequency-flat, block-fading channel with block length T, the generic form of the input signals that enable communication at rates approaching the non-coherent ergodic capacity can be expressed as the product of an isotropically distributed $T \times M$ random unitary matrix and a diagonal $M \times M$ matrix D with real nonnegative entries [16]. While this structure of the input signals is capacity-achieving irrespective of the values of the received

SNR and the channel coherence time T, the distribution of the entries of the diagonal matrix D depends on these two factors. For example, it was shown in [64] that at low SNR only one entry of D is non-zero when the transmitter is active. In contrast, achieving capacity for high SNR scenarios requires the input signals to be in the form of isotropically distributed unitary matrices [19, 23], provided that T satisfies

$$T \geq \min\{M, N\} + N. \tag{4.1}$$

That is, when T satisfies (4.1), setting D equal to the identity achieves the high SNR ergodic capacity of the non-coherent channel. By comparing the degrees of freedom supported by the unitary component to those supported by the diagonal matrix, D, it was concluded in [65] that even at moderate SNRs most of the information will be carried by the unitary component.

By assuming that the communication system operates in the moderate-to-high SNR region, one can gain insight into the manner in which the coherence time, T, affects the achievable data rate. It was shown in [19] and [24] that for given M and N, the capacity of the non-coherent channel approaches that of the coherent one as T grows; from which one can conclude that if T is sufficiently long, the amount of time needed for the receiver to acquire a sufficiently accurate channel model becomes insignificant in comparison with the overall signalling interval. On the other hand, when T does not satisfy (4.1), non-coherent communication can be rather power inefficient. In particular, in the extreme case of $T = 1$, it was shown in [66] that capacity grows only double logarithmically with SNR. As mentioned in Chapter 2, the moderate-to-high SNR assumption also provides some insight into how the number of transmit antennas should be chosen for a given block length. In particular, given T and N for a system that satisfies (4.1), the number of transmit antennas, M, required to attain the maximum number of communication degrees of freedom is [19]

$$M = \min\{\lfloor \tfrac{T}{2} \rfloor, N\}. \tag{4.2}$$

In fact, increasing the number of transmit antennas beyond the value in (4.2) reduces the number of communication degrees of freedom. It is also interesting to note that choosing N to be greater than M does not increase the degrees of freedom [19]. However, choosing $N > M$ does result in an increase in the capacity by an additive term that is independent of the SNR.

In this chapter we will consider communication at moderate-to-high SNRs over a non-coherent MIMO block fading channel in which the block length T satisfies (4.1) and the number of transmit antennas M satisfies (4.2). Under these conditions unitary signalling is not only optimum from a capacity [19] perspective, it also possesses desirable performance characteristics [25]. Our approach will be based on the concept of coordinate change, which was identified in [19] with the non-coherent signalling model. The insight generated by the concept of coordinate change arises from the observation that the fading channel matrix does not change the subspace in which the transmitted signal resides. It merely rotates and scales the bases of this subspace. However, the combined effect of noise and fading results in the perturbation of the signal subspace in a specific manner. Based on this geometric insight, it was shown in [19] that, at high SNR, the information carrying object is a linear subspace. That is, information about the transmitted data is contained in the subspace of the received signal and the particular orientation of the received signal vector within the subspace is "informationless". These observations suggest that, for the non-coherent channel, spectrally efficient signalling at high SNR requires the design of the *bases* of a set of linear signal subspaces rather than the design of the actual signal values. Although the rotation of bases within the subspace is inconsequential, the scaling associated with those bases provides implicit information about the channel. In Chapter 5 we will use this fact to develop a reduced complexity detector.

In addition to unitary signalling [23, 67], a few alternative approaches to space-time coding for non-coherent MIMO channels are available. Differential schemes

which assume that the channel variation within two consecutive blocks is negligible were proposed in [60] and [23]. However, this assumption is not sufficiently accurate under the current block fading model, in which there is an independent channel realization for each block. In order to suit operation over independent block fading channels, signalling techniques that allow a portion of the coherence time to be used for training have been developed [19, 24, 68]. These schemes comprise two phases: a training phase and a coherent communication phase. During the training phase the transmitter sends pilot symbols which are used by the receiver to estimate the channel. In order for the receiver to acquire a reasonably accurate model of the channel, the training phase must occupy a number of channel uses that is at least as large as the number of transmit antennas; e.g., [24]. Assuming that the channel estimate obtained during the training phase is sufficiently accurate, the receiver then switches to a coherent mode of operation in which the remaining channel coherence time is used to detect the transmitted information coherently. Although training-based schemes were shown [19] to achieve the maximum number of degrees of freedom available for communication at high SNR, they are still short of attaining the full channel capacity which involves an SNR independent term. This term can be particularly significant when a large number of receive antennas is employed.

Guided by the results in [19] and [23], we consider communication over the non-coherent channel through the design of signal constellations that directly mimic the high SNR capacity-achieving isotropic distribution. A fundamental issue [69] that arises in constructing a signal constellation is the metric used to measure distances between different constellation points. The Asymptotic Union Bound (AUB) was proposed as a distance metric in [70], but this bound can be rather loose, and the weakness of that bound may be reflected in the resulting constellations. As an alternative, in [71] multilevel unitary signal constellations were designed using the Kullback-Leibler distance metric. This appears to be a sensible distance metric when

constellation points belong to hyperspheres of different radii; a signalling scheme that suits low-to-moderate SNR operation. Our approach to determine the appropriate distance metric for the constellation differs from related work in that it is based on subspace perturbation analysis. We begin by arguing that an appropriate distance measure is given by the chordal Frobenius norm rather than the commonly used chordal Frobenius distance [69]. We then introduce a practical greedy algorithm for constructing Grassmannian constellations. Our approach differs from the surrogate based approach in [67] in both the metric used to quantify the distance between constellation points as well as the formulation of the underlying optimization problem. In particular, we exploit the smooth geometry of the Grassmann manifold to synthesize an analytic cost function that jointly penalizes the chordal Frobenius norm between the new constellation point and the constellation points already designed. We then minimize this cost function by using a derivative-based optimization algorithm that automatically restricts the iterates to the surface of the Grassmann manifold [44]. As compared to the approach in [67], our approach is considerably simpler and better adapted to different rates and configurations.

Throughout this chapter we will denote the space of $p \times q$ unitary matrices, where $p \geq q$, by $\mathbb{V}_{p,q}$. That is, $\mathbb{V}_{p,q} = \{Z \in \mathbb{C}^{p\times q} | Z^\dagger Z = I_q\}$. We will also use $[Q]$ to denote the equivalence class represented by $Q \in \mathbb{V}_{T,M}$. That is, $[Q] = \{\Phi \in \mathbb{V}_{T,M} | \Phi = QP,\ P \in \mathbb{V}_{M,M}\}$. When $[\cdot]$ is implicit from the context, it will be dropped for simplicity.

4.2 System Model

We consider the scenario of moderate-to-high SNR non-coherent communication over a richly-scattered frequency-flat block-fading channel with block length T that satisfies (4.1), M transmit antennas and N receive antennas, where M and N satisfy (4.2).

The transmitter excites the channel in blocks of T channel uses with the rows of the $T \times M$ matrix Q_X. The $T \times N$ received signal matrix Y is given by[1]

$$Y = Q_X H + \sqrt{\frac{M}{\rho T}} V, \tag{4.3}$$

where H is an $M \times N$ channel matrix whose entries are drawn independently from the standard complex Gaussian distribution $\mathcal{CN}(0,1)$, and the $T \times N$ matrix V represents the additive noise whose entries are also drawn from $\mathcal{CN}(0,1)$. The signal to noise ratio is given by ρ and is independent of the number of transmit antennas M.

The capacity-achieving input signals at high SNR can be represented by isotropically distributed M-dimensional linear subspaces that reside in a larger ambient T-dimensional complex Euclidean space, $\mathbb{C}^T$. Since an M-dimensional linear subspace of $\mathbb{C}^T$ can be represented by a "tall" $T \times M$ unitary matrix whose columns form a basis for this subspace, we will henceforth assume the input signal matrix Q_X to be unitary; i.e., $Q_X^\dagger Q_X = I_M$. Each of these M-dimensional linear subspaces can be regarded as a single point on the compact Grassmann manifold $\mathbb{G}_M(\mathbb{C}^T)$. Since a linear subspace can be specified by an arbitrary basis, points on $\mathbb{G}_M(\mathbb{C}^T)$ are equivalence classes of $T \times M$ unitary matrices, where two matrices are equivalent if they span the same M-dimensional subspace. Therefore, the Grassmann manifold can be expressed as [44], $\mathbb{G}_M(\mathbb{C}^T) = \{[Q] | Q \in \mathbb{V}_{T,M}\}$.

When the signal matrix Q_X in (4.3) is right multiplied by the $M \times N$ channel matrix H, the basis vectors that span the M-dimensional subspace are rotated and scaled within the same subspace. With this observation [19], one concludes that when the receiver does not know the channel, the particular rotation of the subspace basis is not detectable while the M-dimensional linear subspace spanned by this basis is detectable. It follows that the transmitter design problem is to assign information bits

[1]Notice that this model is the transpose of the model in (2.2). This transposition bears no fundamental significance and is chosen for mathematical convenience.

to distant linear subspaces, where the distance should be measured in an appropriate sense. The corresponding role of the receiver is to decide on which subspace was transmitted irrespective of its basis. The received signal Y, spans an N-dimensional subspace. This subspace can be exposed by performing the QR decomposition (in the sense of [72]) on the received signal Y (see Section 4.3). In that case, one obtains $Y = Q_Y R_Y$, where Q_Y contains a basis of the N-dimensional subspace with some arbitrary orientation and R_Y specifies the scaling and rotation within the subspace. It will be shown in Chapter 5 that R_Y is statistically independent of Q_X. This indicates that the available information about the channel H appears in R_Y, whereas all the information about Q_X is captured by the unitary component Q_Y. That is, Q_Y represents the perturbed version of the transmitted subspace available at the receiver. Seeing as the receiver does not have a model for the channel, it attempts to detect the subspace spanned by the columns of Q_X from the subspace spanned by the columns of Q_Y using the implicit channel information contained in R_Y.

4.3 Metric Choice

In order to design a signal constellation, one needs to define a suitable metric to measure the distance between constellation points. The choice of an appropriate metric is crucial in determining the number of spheres of a given radius that can be packed in a manifold of a specific volume [69]. In the current setting, the manifold under investigation is a Grassmann manifold whose volume is a function of the system SNR. Unless an appropriate distance metric is specified, signal points can seem closer or further from each other than they actually are. This may result in system performance measures that do not scale with the increase in SNR in the right sense. In this section, we study the way in which the noise and the channel perturb the signal subspace. Based on this analysis, we will conclude that the chordal Frobenius norm is

an appropriate metric. We will then discuss a number of other distance metrics that have previously been employed in constellation design for the non-coherent MIMO channel.

4.3.1 The appropriate distance metric

Our approach to answering the question of the appropriate distance metric between signal subspaces is based on analysis of the received signal Y in (4.3). We have stated in Section 4.2 that in the absence of noise, the signal subspace is not affected by propagation through the channel [19]. However, when the received signal is contaminated by additive noise, the signal subspace is perturbed in a particular fashion that depends on both the channel and noise. Our goal in this subsection is to identify the effect of different components of the noise and their interaction with the signal subspace.

We begin our analysis by stating a result due to Stewart [72] which we have generalized to the case of $M \leq N$. This result allows us to understand the statistical dependencies between the transmitted and received signal subspaces. We will exploit these dependencies in Section 5.2 to develop an efficient detection scheme.

Lemma 4.1 *Let $A = QR$, where $A \in \mathbb{C}^{T\times N}$ and $R \in \mathbb{C}^{M\times N}$ have rank M with $M \leq N$, and let $Q \in \mathbb{V}_{T,M}$. Denote the orthogonal complement of Q by $Q^{\perp} = \left[\begin{array}{cc} Q_1^{\perp} & Q_2^{\perp} \end{array}\right]$, where $Q_1^{\perp} \in \mathbb{V}_{T,N-M}$ and $Q_2^{\perp} \in \mathbb{V}_{T,T-N}$. If $E \in \mathbb{C}^{T\times N}$, is such that*

$$\tilde{R} + \tilde{Q}^{\dagger}E \quad \textit{is non-singular}, \tag{4.4}$$

where $\tilde{Q} = \left[\begin{array}{cc} Q & Q_1^{\perp} \end{array}\right]$ and $\tilde{R} = \left[\begin{array}{cc} R^{\dagger} & 0_{N\times(N-M)} \end{array}\right]^{\dagger}$, then there exist matrices $W \in \mathbb{C}^{T\times N}$ and $F \in \mathbb{C}^{N\times N}$ that are unique up to right multiplication by $N \times N$ unitary

matrix, such that

$$A+E=(\tilde{Q}+W)(\tilde{R}+F) \qquad \textit{where } (\tilde{Q}+W)\in \mathbb{V}_{T,N}, \tag{4.5}$$

$$L=(Q_2^{\perp})^{\dagger}E(\tilde{R}+\tilde{Q}^{\dagger}E)^{-1}, \tag{4.6}$$

$$F=(I+L^{\dagger}L)^{1/2}(\tilde{R}+\tilde{Q}^{\dagger}E)-\tilde{R}, \tag{4.7}$$

$$W=(E-\tilde{Q}F)(\tilde{R}+F)^{-1}. \tag{4.8}$$

Observe that no structure is imposed on the R-matrix in the QR decomposition in Lemma 4.1, and hence the decomposition is not unique. That is, for any unitary $M\times M$ matrix P, QR and $Q'R'=(QP)(P^{\dagger}R)$ are equivalent QR decompositions of A in the sense of [72]. Equation (4.5) says that the additive perturbation E results in the augmentation of the M-dimensional subspace spanned by the columns of Q, namely $[Q]\in\mathbb{G}_M(\mathbb{C}^T)$, to the N-dimensional subspace spanned by the columns of $\tilde{Q}+W$, namely $[\tilde{Q}+W]\in\mathbb{G}_N(\mathbb{C}^T)$. Notice that when $N=M$, $\tilde{Q}$ will be equal to Q and the subspace represented by the point Q on $\mathbb{G}_M(\mathbb{C}^T)$ is perturbed to the subspace represented by $Q+W$ on the same manifold.

To apply Lemma 4.1 to the signal model in (4.3) we observe that the signal subspace represented by Q_X corresponds to Q, and the channel matrix H corresponds to R. That is, Q_XH in (4.3) corresponds to the QR decomposition of A in Lemma 4.1 and the additive Gaussian noise term $\sqrt{\frac{M}{\rho T}}V$ corresponds to the perturbation matrix E. Our goal is to analyze the properties of the perturbation W, but before we do so, we need to study the roles played by the different components of the noise term. This will enable us to bound the probability that the condition (4.4) for Lemma 4.1 to hold is violated. For the time being we assume that (4.4) is satisfied. Hence, based on Lemma 4.1 we can identify the following noise components:

$$G=Q_X^{\dagger}V \quad \text{and} \quad \hat{G}=\begin{bmatrix}\hat{G}_1^{\dagger} & \hat{G}_2^{\dagger}\end{bmatrix}^{\dagger}=(Q_X^{\perp})^{\dagger}V, \tag{4.9}$$

where $\hat{G}_1\in\mathbb{C}^{(N-M)\times N}$ and $\hat{G}_2\in\mathbb{C}^{(T-N)\times N}$. As will become clear in Section 5.2, each of those components affects the transmitted signal in a certain way. In particular, by

observing that $Q_X Q_X^\dagger + Q_{X_1}^\perp (Q_{X_1}^\perp)^\dagger + Q_{X_2}^\perp (Q_{X_2}^\perp)^\dagger = I_T$, where the partition of $Q_X^\perp$ is conformal with that in Lemma 4.1, one can rewrite the signal model in (4.3) as

$$\begin{aligned} Y &= Q_X H + \sqrt{\frac{M}{\rho T}}(Q_X G + Q_{X_1}^\perp \hat{G}_1 + Q_{X_2}^\perp \hat{G}_2), \\ &= \begin{bmatrix} Q_X & Q_{X_1}^\perp \end{bmatrix} \begin{bmatrix} H + \sqrt{\frac{M}{\rho T}} G \\ \sqrt{\frac{M}{\rho T}} \hat{G}_1 \end{bmatrix} + \sqrt{\frac{M}{\rho T}} Q_{X_2}^\perp \hat{G}_2. \end{aligned} \tag{4.10}$$

Using the decomposition of noise in (4.10), we observe that,

- $G = Q_X^\dagger V$ is a noise component that does not affect the signal subspace. In fact, this noise component contributes to the received signal power; c.f., (4.11) below.

- For $M < N$, the channel matrix is "fat". Hence the product of the $T \times M$ signal Q_X and the $M \times N$ channel matrix H results in the immersion of the M-dimensional signal subspace in an N-dimensional subspace. The noise component $\hat{G}_1$ spans the range space of $Q_{X_1}^\perp$. If we assume, for the moment, that the noise component $\hat{G}_2$ is zero, then the corresponding received signal Y will be given by the first term on the right hand side of (4.10). The subspace spanned by the columns of this signal is N-dimensional of which only M-dimensions are spanned by the signal (and the noise component G) and the remaining $(N-M)$ dimensions are spanned by the noise component $\hat{G}_1$. Hence, even in the absence of $\hat{G}_2$, for the receiver to detect the transmitted signal, it will have to decide on which subspace was transmitted from all possible M-dimensional subspaces which are spanned by the columns of Y. (There are $\binom{N}{M}$ of these M-dimensional subspaces.) That is, the noise component $\hat{G}_1$ will introduce ambiguity in distinguishing the signal subspace from the noise subspace. However, it does not change the orientation of the original signal subspace.

The above observations suggest that the perturbations in the signal subspace are due only to the noise component $\hat{G}_2$. We will use this fact later in this section.

We now investigate the applicability of Lemma 4.1 in the stochastic framework of (4.3). To that end, we consider the probability that (4.4) is violated. Let

$$B = \left[\begin{array}{cc} (H + \sqrt{\frac{M}{\rho T}} G)^\dagger & \sqrt{\frac{M}{\rho T}} \hat{G}_1^\dagger \end{array} \right]^\dagger, \tag{4.11}$$

which corresponds to $\tilde{R} + \tilde{Q}^\dagger E$ in Lemma 4.1. In order to bound the probability that (4.4) is violated, we need to bound the probability of the event that the minimum eigenvalue of $BB^\dagger$, $\lambda_{\min}(BB^\dagger)$, falls below some threshold $\epsilon > 0$. The following lemma, which is based on a result from [73], provides the required bound.

Lemma 4.2 *Let $P_v(\epsilon)$ denote the probability that $\lambda_{\min}(BB^\dagger)$ is smaller than some $\epsilon > 0$.*

- *For $N = M$, $P_v(\epsilon) = 1 - e^{-\rho T M \epsilon/(\rho T + M)} = o\big(\frac{\rho T M \epsilon}{\rho T + M}\big)$.*
- *For $N > M$, $P_v(\epsilon) \leq 1 - e^{-\rho T N \epsilon / M} = o\big(\frac{\rho T N \epsilon}{M}\big)$.*

Proof. See Appendix E.

This lemma confirms that one can use Lemma 4.1 to investigate signal subspace perturbation for any finite SNR, ρ. That is, for $\rho < \infty$, the probability that Lemma 4.1 does not hold approaches zero as $\epsilon \to 0$. Moreover, as $\rho \to \infty$, one can see that the perturbation due to the noise term will vanish and the signal will only undergo fading which does not affect the signal subspace.

Lemma 4.1 states that the subspace $\tilde{Q}$ is perturbed additively by W; c.f., (4.8). We now study the properties of W in more detail. We begin by showing that in the general case W belongs to neither the compact Grassmann manifold nor to its tangent space at Q. The following lemma exposes the inherent structure of W.

Lemma 4.3 *Let $U_L\Sigma_L V_L^\dagger$ be the singular value decomposition (SVD) of L defined in (4.6), and let $\tilde{Q}$ and $Q_2^\perp$ be defined as in Lemma 4.1. Define $\Xi = \arccos\big((I_N + \Sigma_L^2)^{-1/2}\big)$. Then W in (4.8) can be written as*

$$W = \begin{bmatrix} \tilde{Q} & Q_2^\perp \end{bmatrix} \begin{bmatrix} -2V_L \sin(\frac{1}{2}\Xi) \\ 2U_L \cos(\frac{1}{2}\Xi) \end{bmatrix} \sin(\tfrac{1}{2}\Xi) V_L^\dagger. \tag{4.12}$$

Proof. See Appendix F.

Using the form of the perturbation W in (4.12), one can verify that,

$$W^\dagger W = 4V_L \sin^2(\tfrac{1}{2}\Xi) V_L^\dagger. \tag{4.13}$$

Notice that because $\tilde{R} + F$ in Lemma 4.1 does not have a particular structure, W in Lemma 4.1 (and hence in Lemma 4.3) is unique up to right multiplication by some $N \times N$ unitary matrix . Thus for W to belong to the compact Grassmann manifold, $W^\dagger W$ must be equal to the identity. Simple computation shows that this is the same as requiring L to be equal to a particular multiple of a unitary matrix. Due to the random nature of

$$L = \hat{G}_2 B^{-1}, \tag{4.14}$$

this condition is generally not satisfied, indicating that generally W is not a point on the Grassmann manifold.

In order to check whether $W \in \mathbf{T}_Q \mathbb{G}_N(\mathbb{C}^T)$, where $\mathbf{T}_Q \mathbb{G}_{T,N}(\mathbb{C})$ is the tangent space of the Grassmann manifold at Q, we use the following fact from [44].

Lemma 4.4 *At any point $Q \in \mathbb{G}_N(\mathbb{C}^T)$, the tangent vectors $\Delta \in \mathbf{T}_Q \mathbb{G}_N(\mathbb{C}^T)$ satisfy,*

$$Q^\dagger \Delta = 0. \tag{4.15}$$

Using (4.12), one can verify that,

$$Q^\dagger W = -2V_L \sin^2(\tfrac{1}{2}\Xi) V_L^\dagger. \tag{4.16}$$

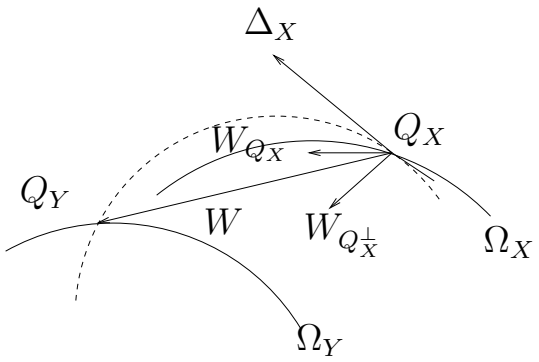

Figure 4.1: Subspace perturbation analysis: The dashed line shows the geodesic on the Grassmann manifold that passes through the two orbits Ω_X and Ω_Y. The vector Δ_X lies in $\mathbf{T}_{Q_X}\mathbb{G}_N(\mathbb{C}^T)$, the tangent space at Q_X.

Hence for W to belong to $\mathbf{T}_Q\mathbb{G}_N(\mathbb{C}^T)$, $\sin(\frac{1}{2}\Xi)$ must be equal to zero or equivalently $\Sigma_L = 0$, indicating that the component of noise in the range space of $Q_2^\perp$ is zero. The probability associated with this event is vanishingly small given the isotropic nature of noise.

In order to gain further insight into the nature of the perturbation in Lemma 4.1, we restrict ourselves to the case of $N = M$. In this case, the model can be simplified by observing that the noise component $\hat{G}_1$ does not exist, that $\tilde{Q} = Q$ and $Q_2^\perp = Q^\perp$, and that $W \in \mathbb{C}^{T\times M}$ that can be resolved (c.f., (4.12)) into one component that belongs to the range space of Q and another component that resides in the range space of $Q^\perp$. Figure 4.1 depicts this situation. The subspaces spanned by the columns of Q_X and $Q_Y = Q_X + W$ are represented by the orbits Ω_X and Ω_Y in the Euclidean space $\mathbb{C}^{T\times M}$. The geodesic that passes through the two orbits is also shown, with the vector Δ_X being tangent to the geodesic at Q_X. The message conveyed by Lemma 4.1 asserts that the perturbation of the orbits is additive in the Euclidean space, $\mathbb{C}^{T\times M}$. The following theorem formally states this result,

Theorem 4.1 *Let $Y = Q_Y R_Y = Q_X H + V$, where $Q_X, Q_Y \in \mathbb{V}_{T,M}$, $H \in \mathbb{C}^{M\times M}$ and $V \in \mathbb{C}^{T\times M}$. Let the subspace spanned by the columns of Q_Y be Ω_Y and that spanned*

by the columns of Q_X be Ω_X. Then the basis of Ω_Y is an additively perturbed version of the basis of Ω_X and the Frobenius norm of the perturbation vector is given by the chordal Frobenius norm between Ω_X and Ω_Y. Moreover, the tangential and normal components of the perturbation vector and hence the norm of the perturbation vector are statistically independent of Q_X.

Proof. See Appendix G.

Remark 4.1 Observe that while the tangential and normal components of W are independent of Q_X, W itself is not independent of Q_X. That is, W is not isotropically distributed. For W to be isotropically distributed, it is not sufficient that the tangential and normal components of W are independent of Q_X. It is also required that those components be independent of each other and identically distributed. In Appendix G we show that this is not the case. In particular, the component of W in the Q_X direction is given by a negative semidefinite matrix, whereas the component of W in the $Q_X^{\perp}$ direction has no specific structure. Further understanding of this remark can be obtained geometrically from Figure 4.2. Consider a translation along a geodesic that takes a point Q_X to a point $Q_{X'}$. Given the set of noise and channel realizations indexed by t, namely $\{(H_t, V_t)\}$, let $\{W_X(H_t, V_t)\}$ be the set of vectors that emanate from the point Q_X. If the directions of $W_X(H_t, V_t)$ were isotropically distributed (i.e., if they were independent of Q_X), then they would be determined solely by the channel and noise realizations. If that were the case, for the same channel and noise realizations $W_{X'}(H_t, V_t)$ would be equal to $W_X(H_t, V_t)$. However, we observe that each element of $\{W_X(H_t, V_t)\}$ is structured in such a way that it always points to a point on the Grassmann manifold; i.e., $Q_X + W_X(H_t, V_t) \in \mathbb{G}_M(\mathbb{C}^T)$.[2] If we were to parallel translate $\{W_X(H_t, V_t)\}$ to another point on the manifold, some directions will be no longer pointing to points on the manifold. That is, for some noise and

[2]More precisely, $[Q_X + W_X(H_t, V_t)] \in \mathbb{G}_M(\mathbb{C}^T)$, but we have dropped the brackets to simplify the notation.

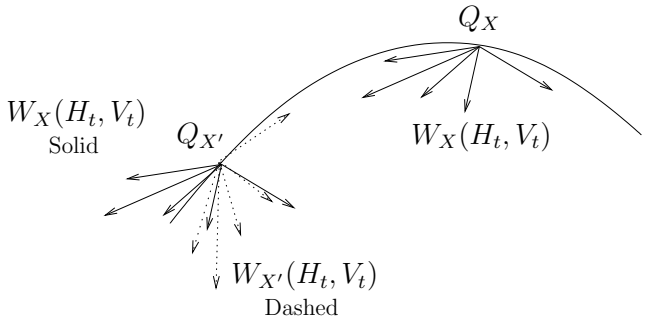

Figure 4.2: Dependence of W on Q_X: The curve joining Q_X and $Q_{X'}$ is a geodesic on the Grassmann manifold. The set of vectors $\{W_X(H_t, V_t)\}$ corresponding to a set of different channel and noise realizations $\{(H_t, V_t)\}$ are shown at the point Q_X. Those vectors are also parallel translated to the point $Q_{X'}$ (solid). The set of vectors $\{W_{X'}(H_t, V_t)\}$ corresponding to the same set of channel and noise realizations $\{(H_t, V_t)\}$ are also shown at the point $Q_{X'}$ (dashed). The parallel translated vectors $W_X(H_t, V_t)$ cannot displace a point $Q_{X'}$ on the Grassmann manifold to a point $Q_{X''}$.

channel realizations $Q_{X'} + W_X(H_t, V_t) \notin \mathbb{G}_M(\mathbb{C}^T)$. Therefore, we can conclude that $W_X(H_t, V_t)$ cannot be independent of Q_X and hence not isotropically distributed.

Having taken a closer look at the way in which the noise perturbs the signal subspace, we are now in a position to design signal constellations that are more resilient to perturbations caused by noise. In particular, we have shown that the combined effect of the channel and the noise gives rise to the perturbation vector W in (4.12) which takes the signal subspace spanned by the columns of Q_X to another subspace which is spanned by the columns of $Q_Y = \tilde{Q}_X + W \in \mathbb{G}_N(\mathbb{C}^T)$. For adverse channel and noise realizations the norm of the perturbation vector W may be large enough to cause the received signal subspace spanned by the columns of Q_Y to fall in the vicinity of a constellation subspace other than the transmitted one. In this case the receiver will decide in favour of this constellation point and produce an error. In order to reduce the probability of occurrence of such events, the constellation points should be spaced as far apart from each other as possible so that even under adverse conditions, the norm of W is rarely large enough to cause the received signal

subspace to settle in the neighbourhood of another constellation subspace. Based on this discussion and the result in Theorem 4.1 we propose the following design principle.

Design Principle: In order to design a signal constellation that is resilient to noise, constellation points ought to be well spaced in the sense of the chordal Frobenius norm. □

Before providing an expression for the chordal Frobenius norm, we state the following result from [61].

Lemma 4.5 *Let $A \in \mathbb{C}^{M\times M}$ and let $A = U_A \Sigma_A V_A^\dagger$ denote its SVD. Then*

$$\max_{Z\in\mathbb{C}^{M\times M},\, ZZ^\dagger = I} \operatorname{Tr}(Z^\dagger A^\dagger) = \max_{Z\in\mathbb{C}^{M\times M},\, ZZ^\dagger = I} \operatorname{Tr}(AZ) = \operatorname{Tr}(\Sigma_A), \tag{4.17}$$

and the optimal Z is given by $Z = V_A U_A^\dagger$.

The chordal Frobenius norm between the two subspaces that are spanned by the columns of Q_{Y_1} and Q_{Y_2} is defined [44] to be the square root of $d^2(Q_{Y_1}, Q_{Y_2})$, where

$$d^2(Q_{Y_1}, Q_{Y_2}) = \min_{Z\in\mathbb{C}^{M\times M},\, ZZ^\dagger = I} \|Q_{Y_1} - Q_{Y_2} Z\|^2 \tag{4.18a}$$

$$= 2M - \max_{Z\in\mathbb{C}^{M\times M},\, ZZ^\dagger = I} \big\{ \operatorname{Tr}(Z^\dagger Q_{Y_2}^\dagger Q_{Y_1}) + \operatorname{Tr}(Q_{Y_1}^\dagger Q_{Y_2} Z) \big\}, \tag{4.18b}$$

where $Q_{Y_1}^\dagger Q_{Y_2} = U_{Q_{Y_1}^\dagger Q_{Y_2}} \Sigma_{Q_{Y_1}^\dagger Q_{Y_2}} V_{Q_{Y_1}^\dagger Q_{Y_2}}^\dagger$ is the singular value decomposition (SVD) of $Q_{Y_1}^\dagger Q_{Y_2}$. Using Lemma 4.5, we have

$$d^2(Q_{Y_1}, Q_{Y_2}) = 2M - 2\operatorname{Tr}(\Sigma_{Q_{Y_1}^\dagger Q_{Y_2}}). \tag{4.19}$$

4.3.2 Other distance metrics

In the previous subsection we have used subspace perturbation analysis to conclude that the chordal Frobenius norm is an appropriate distance metric. In this subsection we will discuss the relationships between this metric and other distance metrics.

The discussion leading to Theorem 4.1 suggests that the combined effect of the channel and noise cannot perturb the signal subspace along a geodesic on the Grassmann manifold. Instead, it takes the signal along a more general path that resides in a higher dimensional space, namely $\mathbb{C}^{T\times M}$. (Note that $\mathbb{C}^{T\times M}$ has $2TM$ degrees of freedom whereas $\mathbb{G}_T(\mathbb{C}^M)$ has only $2M(T-M)$.) This observation suggests that the arc length (used in [74]) might not be the appropriate distance metric for constellation design and symbol detection. Another metric that has been used in [67, 75] for designing Grassmannian constellations and packings [75] is the projection Frobenius norm defined as,[3]

$$d_p^2(Q_{Y_1}, Q_{Y_2}) = \frac{1}{2}\|Q_{Y_1}Q_{Y_1}^\dagger - Q_{Y_2}Q_{Y_2}^\dagger\|^2 = M - \mathrm{Tr}(\Sigma^2_{Q_{Y_1}^\dagger Q_{Y_2}}). \tag{4.20}$$

This distance metric results from embedding the Grassmann manifold in the space of $T\times T$ projection matrices of rank M [44,69]. However, the norm defined through this embedding is strictly less than the norm defined through observing the Grassmann manifold, $\mathbb{G}_M(\mathbb{C}^T)$ as a subspace of the Euclidean space $\mathbb{C}^{T\times M}$. This is a consequence of the fact that the space of $T\times T$ projection matrices of rank M is of higher dimension than the Euclidean space $\mathbb{C}^{T\times M}$. By moving along higher dimensional paths, we may "cut corners" in measuring the distance between any two points [44]. However, the perturbation analysis in Lemma 4.1 shows that the noise perturbs the subspace by an additive term (W in (4.8)), and hence the perturbation path cannot lie in a space of higher dimension than the Euclidean space $\mathbb{C}^{T\times M}$.

A comprehensive discussion on other distance metrics and the corresponding embeddings can be found in [44] and [69]. It is worth mentioning that the impact of choosing the appropriate metric becomes less acute as the constellation becomes denser, because several metrics become equivalent in the limit as the angles between subspaces approach zero.

[3]This norm was called the chordal Frobenius distance in [75].

4.4 Constellation Design

Having determined the appropriate metric for measuring distances between constellation points on the Grassmann manifold in Section 4.3, we now develop a practical procedure for designing Grassmannian constellations that are well spaced with respect to the chordal Frobenius norm. Before we do so, we make the following remark: For unitary matrices $Q_Y \in \mathbb{V}_{T,M}$, a function $F(Q_Y)$ is said to be on the Grassmann manifold $\mathbb{G}_M(\mathbb{C}^T)$ if $F(Q_Y) = F(Q_Y P)$ for any $P \in \mathbb{V}_{M,M}$. Using Lemma 4.5, it is readily observed that for a given unitary Q_{Y_0}, $F(\cdot) = d(\cdot, Q_{Y_0})$ is a function on the Grassmann manifold.

Achieving the non-coherent ergodic channel capacity via isotropic unitary signalling was identified in [19] with packing spheres on the Grassmann manifold. That is, maximizing the number of spheres of a given radius that are contained in $\mathbb{G}_M(\mathbb{C}^T)$. (The dual form of sphere-packing in which the number of spheres is constant and the radius of spheres is maximized was considered in [67].) This connection between isotropically distributed unitary signals and sphere-packing implies that isotropically distributed unitary signals not only achieve capacity. They also ensure maximum distance between constellation points [25]. Using these observations and those in Section 4.3, the constellation design problem consists of finding unitary matrices Q_{X_i}, for $i = 1, \cdots, |\mathcal{C}|$, with maximum pairwise chordal Frobenius norm between the subspaces they span. That is, we seek to solve the following optimization problem.

$$\max_{\{Q_{X_r}\}_{r=1}^{|\mathcal{C}|}} \min_{1\leq i,j\leq|\mathcal{C}|} \quad d(Q_{X_i}, Q_{X_j}), \tag{4.21a}$$

$$\text{subject to} \quad Q_{X_i} \in \mathbb{G}_M(\mathbb{C}^T), \quad \forall i \in \{1, 2, \ldots, |\mathcal{C}|\}. \tag{4.21b}$$

Unfortunately, the computational cost of the direct solution of this problem increases rapidly with the data rate. However, for the special case when the block length T is an even number and the number of transmit antennas M is chosen to maximize the

number of degrees of freedom, that is $M = T/2$, we have the following proposition that can be used to reduce the computational complexity by a factor of two.

Proposition 4.1 *For $T = 2M$, if $|\mathcal{C}| = 2K$, for some integer K, and if $Q_{X_i} \in \mathcal{C}$ is generated by* (4.21) *then*

$$Q_{X_i}^{\perp} \in \mathcal{C}.$$

Proof. See Appendix H.

Remark 4.2 Observe that the statement of Proposition 4.1 also holds if the projection Frobenius norm (c.f., (4.20)) is used instead of the chordal Frobenius norm (c.f., (4.19)). This follows from the fact that through the definition of this norm, the Grassmann manifold $\mathbb{G}_M(\mathbb{C}^T)$ is isometrically embedded [69, 75] in a sphere in $\mathbb{C}^{(T^2-1)/2}$. This isometric embedding suggests that, for $|\mathcal{C}| = 2K$, the constellation points are mapped through this embedding to pairs of antipodal points that lie on the surface of the sphere in $\mathbb{C}^{(T^2-1)/2}$.

Given the complexity associated with the direct approach, we now propose a greedy algorithm to find an approximate solution to the constellation design problem. Starting from an arbitrary point on the Grassmann manifold, the essence of this algorithm is to augment the size of the codebook recursively by one constellation point[4] at a time. Since the isotropic distribution implies maximum distance between constellation points, given the set of current constellation points, we would like to choose the next constellation point to be the one that maximizes the minimum distance to all points in the set. That is, assume that $Q_{X_k}, k \in \{1, 2, \ldots, i-1\}$ are

[4]When $T = 2M$, we augment the size of the codebook by one pair of codewords at a time; c.f., Proposition 4.1.

already determined, then, for $i = 2, \ldots, |\mathcal{C}|$, we choose

$$\begin{aligned} Q_{X_i} &= \arg \max_{\{Q|Q^\dagger Q = I\}} \min_{1 \leq j \leq i-1} d(Q, Q_{X_j}) \\ &= \arg \min_{\{Q|Q^\dagger Q = I\}} \max_{1 \leq j \leq i-1} \mathrm{Tr}\big(\Sigma_{Q^\dagger Q_{X_j}}\big), \quad i = 2, \ldots, |\mathcal{C}|, \end{aligned} \tag{4.22}$$

where the SVD of $Q^\dagger Q_{X_j}$ is given by $U_{Q^\dagger Q_{X_j}} \Sigma_{Q^\dagger Q_{X_j}} V^\dagger_{Q^\dagger Q_{X_j}}$; see eq. (4.19). In order to solve (4.22), one needs to perform the inner maximization over the discrete set of $Q_{X_j},\ j \in \{1, i-1\}$. However, the discontinuity of the max function means that (4.22) is particularly difficult to solve. Instead of performing explicit maximization, we propose to exploit the "steepness" of the $\exp(\cdot)^2$ function to synthesize a smooth cost function that ensures that the distance to the nearest point in the set of all previously found constellation points dominates the distance to all other points in the set. In particular, we propose to choose the i-th constellation point to be the one that solves

$$Q_{X_i} = \arg \min_{\{Q|Q^\dagger Q = I\}} \sum_{j=1}^{i-1} \exp\Big(\mathrm{Tr}\big(\Sigma_{Q^\dagger Q_{X_j}}\big)\Big)^2. \tag{4.23}$$

We have noted in Section 4.3 that the squared chordal Frobenius norm $d(Q_Y, Q_{Y_0})$ and hence $\mathrm{Tr}\big(\Sigma_{Q_{Y^\dagger} Q_{Y_0}}\big)$ (c.f., (4.19)), is a function on the Grassmann manifold. Since the Grassmann manifold is a smooth topological space (by the definition of a manifold) and the objective function in (4.23) is also smooth, one can use efficient gradient-based optimization algorithms to solve the optimization problem in (4.23). A particular class of these algorithms is presented in [44]. In this class, the optimization algorithms start from an initial point on the manifold. Subsequent iterates are then generated by moving along geodesics of the manifold. This approach results in unconstrained optimization problems where the required orthogonality constraints are automatically satisfied at each iteration.

4.5 Numerical results

In this section we provide a few numerical results that illustrate the efficacy of our approaches to constellation design. The channel is assumed to be Rayleigh block-fading with coherence time $T = 4$. In order to achieve the maximum number of degrees of freedom of this channel (c.f., (4.1) and (4.2)), the numbers of transmit and receive antennas were chosen to be $M = N = T/2 = 2$. We consider data rates of 1, 2 and 2.5 bits per channel use (bpcu), which require 16-point, 256-point and 1024-point Grassmannian constellations respectively. These constellations were designed using the greedy algorithm in Section 4.4.

In Figure 4.3 we have plotted the distance spectrum of the 256-point and the 1024-point constellations, where the distance is measured in terms of the chordal Frobenius norm. Since the symbol error probability is dominated by the event of mistaking the transmitted symbol for one of its nearest neighbours, a constellation that is "good" from a performance perspective should maintain a small number of close neighbours while attempting to maximize the minimum distance between constellation points. From the distance spectrum of the two constellations, it is seen that the greedy algorithm attempts to aggregate the greater portion of the codewords away from the origin. The minimum chordal Frobenius distance for the 256-point constellation is about 0.7036, whereas that of the 1024-point constellation is about 0.5682.

In order to demonstrate the advantage of our constellation design over other non-coherent signalling techniques, in Figures 4.4 and 4.5 we compare the performance of our constellations with that of the constellations presented in [70] and the training-based scheme presented in [24] respectively. (Maximum likelihood detection was used in each case.) We refer to the constellations of [70] as MBV constellations.

The greedy approach used in our constellation design (c.f., Section 4.4) aims at maximizing the chordal Frobenius norm between constellation points, whereas the

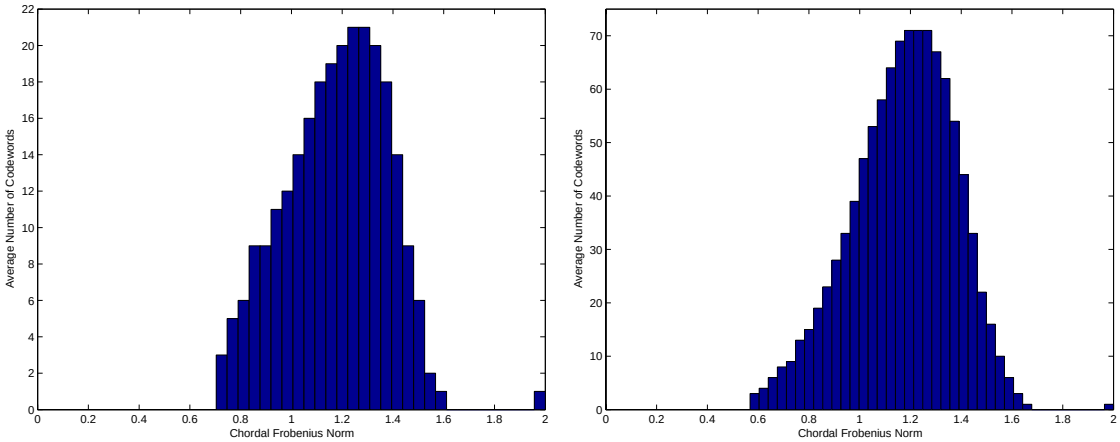

(a) 256-point Constellation (b) 1024-point Constellation

Figure 4.3: The distance spectrum of constellations designed using the greedy algorithm of Section 4.4.

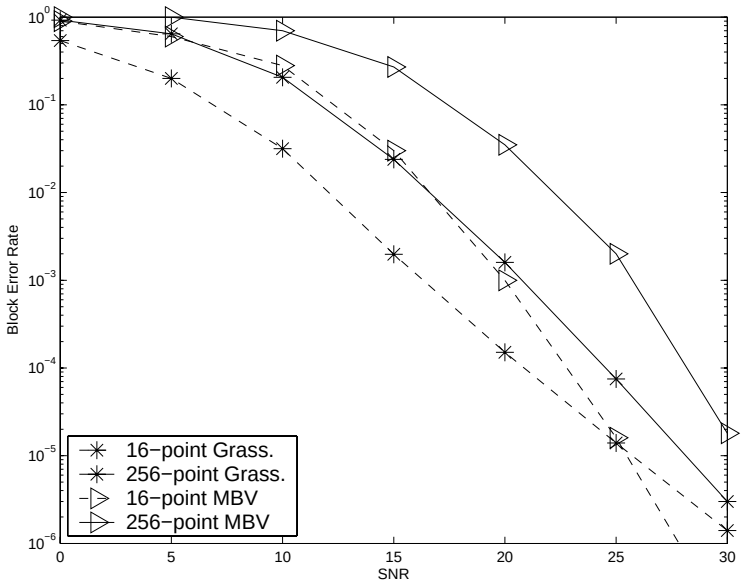

Figure 4.4: Performance comparison between the new constellations and the MBV constellations.

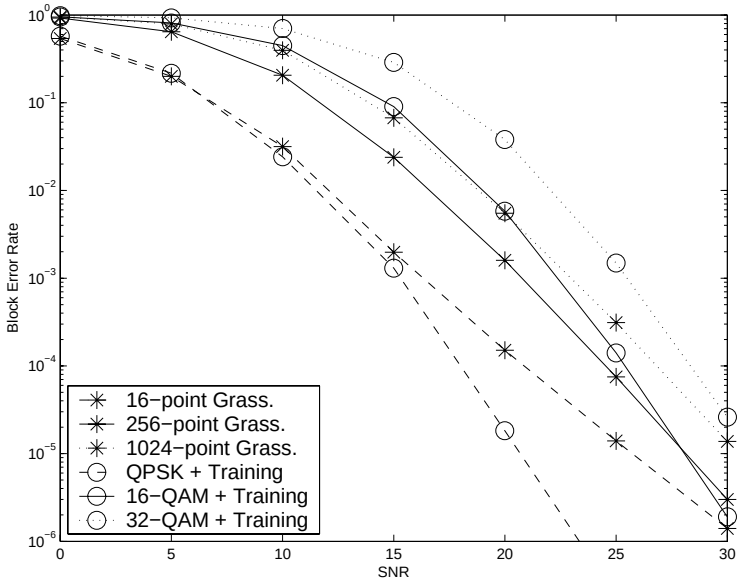

Figure 4.5: Performance comparison between signalling using new constellations and training-based signalling schemes.

design of the MBV constellations is based on minimizing the asymptotic union bound derived in [70]. Figure 4.4 shows that at a rate of 1 bpcu our constellation offers about a 4 dB advantage in performance over the corresponding MBV constellation at a block error probability of 10^{-3} (dashed curves). However, at a block error probability of about 10^{-5} the two curves intersect and the MBV constellation starts to outperform our constellation. When the data rate is increased to 2 bpcu, our 256-point constellation outperforms the corresponding MBV constellation by about 5.5 dB at a block error probability of 10^{-3} (solid curves). At this rate our constellation continues to exhibit performance advantage over the MBV constellation at lower error probabilities. This figure shows that when the system is operating close to the capacity limit our codes outperform the MBV codes. However, when the system is operating at data rates that are substantially lower than the capacity limit, it might be beneficial to use the MBV codes.

In order to gain further insight into the behaviour of our constellations, we recall

that in [19] it was shown that at high SNRs, every 3 dB increase in the SNR results in a capacity gain of $M(1 - M/T) = 1$ bpcu. However, as noted in [70], the MBV constellations require an increase of about 6 dB in SNR in order to gain 1 bpcu. That is, there is a 3 dB SNR gap between anticipated and actual performance. This discrepancy was reduced to less than 1 dB for our constellations; a consequence of choosing a distance metric that measures perturbation in an appropriate sense.

In [24] a training-based signalling scheme was presented. In the training phase of this scheme, the transmitter uses the channel M uses to send pilot symbols. The receiver uses these pilot symbols to generate a minimum mean square (MMSE) estimate of the channel. Assuming this estimate to be sufficiently accurate, the receiver then coherently detects the data sent by the transmitter during the remaining $T - M$ channel uses. This phase is known as the data communication phase. In order to compare the performance of this scheme with that of Grassmannian signalling, we have used an Alamouti signalling scheme [29] in the data communication phase. For the considered data rates the underlying constellations of the training scheme were chosen to be QPSK, 16-QAM and 32-QAM for effective data rates of 1, 2 and 2.5 bpcu respectively. From Figure 4.5, it can be seen that for rates much lower than the capacity limit, the training-based scheme outperforms Grassmannian signalling. However, as the data rate increases, Grassmannian signalling offers significant improvement over the training-based scheme. This advantage directly follows from the asymptotic optimality of Grassmannian signalling at high SNR.

4.6 Conclusion

In this chapter we have considered non-coherent MIMO communication over block Rayleigh fading channels using Grassmannian constellations. We began by studying the manner in which the channel and noise matrices perturb the subspace spanned by

the transmitted codeword matrix. This perturbation analysis was used to determine an appropriate distance metric for constellation design. The rationale behind choosing the distance metric was to quantify the perturbation that the signal subspace undergoes, in a sense that conforms with the communication model. This metric was found to be the chordal Frobenius norm rather than the commonly used chordal Frobenius distance. Having determined the appropriate distance metric, we then developed a greedy algorithm for designing Grassmannian constellations. As we illustrated, the choice of the appropriate metric is reflected through the performance of these constellations. In addition to offering substantial performance gain over constellations that were designed according to other distance metrics, these constellations exhibit performance characteristics that conform to established theoretical results.

Having developed a practical design procedure for non-coherent space-time codes in this chapter, in the next chapter we will focus on the detection of Grassmannian constellations. In particular, we will develop an efficient detection procedure that yields performance characteristics that closely approximate those of maximum likelihood detection but requires significantly less computational effort.

Chapter 5

Performance and Efficient non-coherent detection of Grassmannian constellations

Chapter 4 considered an efficient method for designing Grassmannian constellations that mimic the capacity-achieving isotropic distribution for non-coherent channels operating at high SNRs. In this chapter we will consider both optimum and suboptimum non-coherent detection of these constellations. In particular, given the computationally prohibitive cost of optimum ML detection, we seek a more economic way to obtain quasi ML decisions. In this chapter we will develop an efficient suboptimum detector. The performance of this detector is comparable to that of the maximum likelihood detector, but it requires considerably less computational effort.

In addition to developing an efficient suboptimum detector, in this chapter we derive an alternative expression for the pairwise error probability formula in (2.13). Our expression yields more insight into the key parameters that affect the high SNR performance of the non-coherent system.

5.1 Introduction

In Chapter 4 we demonstrated that using our constellations for non-coherent signalling can perform significantly better than other signalling techniques, including training schemes. This phenomenon becomes more pronounced as the data rate at which the non-coherent system operates approaches the high SNR capacity limit. The main advantage of training schemes follows from the fact that these schemes allow the non-coherent channel to inherit the well-established coding and detection techniques that have been originally designed for the coherent channel [68]. In particular, training schemes only require the data symbols to be linearly modulated in order to achieve the maximum data rate that these schemes can attain [24]. This feature not only facilitates data transmission but also makes the received signals amenable to quasi ML detection schemes such as sphere detectors; see Chapter 2. However, given that the data rate that can be supported by training schemes is less than the data rate that can be supported by properly designed Grassmannian constellations, it is desirable to seek a technique for non-coherent detection of Grassmannian constellations that, in principle, resembles sphere detection for coherent systems. That is, a non-coherent detection technique that is capable of producing quasi ML decisions without searching the entire constellation.

In this chapter we will re-use the subspace perturbation analysis of Chapter 4 to develop such a detector. This detector is based on exploiting an inherent property of Grassmannian constellations and on identifying the role of each component of the received signal matrix. The essence of this detector is to avoid the exhaustive search required for maximum likelihood (ML) detection. Specifically, this detector generates quasi ML decisions by examining a certain subset of codewords against the likelihood metric. We will demonstrate that, in comparison to maximum likelihood detection, this detection strategy results in no significant loss in performance and

that the cardinality of the subset of candidate codewords goes to one at least as fast as $1/\sqrt{\rho}$, where ρ denotes the SNR per receive antenna.

Seeing as the pairwise error probability (PEP) has typically been used (e.g., [23, 28, 70]) to assess the performance of space-time coding schemes at high SNR, in this chapter we will also seek a closed form expression for the PEP that can be used to provide further insight into the structure of different Grassmannian constellations. We show that the pairwise error probability corresponds to a specific point on the cumulative distribution function (cdf) of an indefinite quadratic form. As a by-product of our method, we obtain an analytic expression for the whole cdf. This expression can be useful in implementing detection strategies that are based on soft decisions. Our expression for the PEP will be in the form of an absolutely convergent series that does not involve the computation of residues required by those in [23] and [70], and hence can be used to study the key parameters that govern the performance of a given constellation; e.g., analyzing the impact of the distance spectrum of the constellation on performance.

5.2 Detection

In this chapter we will use the same signal model as the one described in Section 4.2. We will assume that the block length T satisfies (4.1) and that the number of transmit antennas, M, and the number of receiver antennas, N, satisfy (4.2). We will assume throughout this chapter that that the constellation points are isotropically distributed on the compact Grassmann manifold, $\mathbb{G}_M(\mathbb{C}^T)$. We will begin in this section by briefly discussing conventional non-coherent Maximum Likelihood (ML) detection [16]. We will then discuss the principles of the proposed reduced search detector.

5.2.1 Maximum Likelihood Detection

For ML detection, we observe from (4.3) that conditioned on Q_X, the received signal Y is a zero-mean isotropically distributed Gaussian random matrix. Hence,

$$\begin{aligned} p(Y|Q_X) &= \frac{\exp\Big(-\operatorname{Tr}\big(Y^\dagger(\frac{M}{\rho T}I_T + Q_X Q_X^\dagger)^{-1}Y\big)\Big)}{\pi^{TN}\det^N(\frac{M}{\rho T}I_T + Q_X Q_X^\dagger)} \\ &= \frac{\exp\Big(-\frac{\rho T}{M}\operatorname{Tr}\big(Y^\dagger(I_T - \frac{1}{1+M/\rho T}Q_X Q_X^\dagger)Y\big)\Big)}{(\pi M/\rho T)^{TN}(1+\rho T/M)^{MN}}, \end{aligned} \tag{5.1}$$

where the second equality follows from using the matrix inversion lemma [61] and the fact that for any two $p \times q$ matrices A and B,

$$\det(I_q + A^\dagger B) = \det(I_p + BA^\dagger).$$

A maximum likelihood detector tests the entire codebook, $\mathcal{C}$, in search for the codeword $\hat{Q}_X$ that maximizes $p(Y|Q_X)$ in (5.1). Equivalently,

$$\hat{Q}_X = \arg\max_{Q_X \in \mathcal{C}} \operatorname{Tr}\big(Y^\dagger Q_X Q_X^\dagger Y\big). \tag{5.2}$$

The main drawback associated with the ML detector is the computational cost of having to examine all possible codewords in the codebook. In order to increase the computational efficiency, the reduced search algorithm proposed below selects a particular set of candidate codewords to be examined against the maximum likelihood metric in (5.2).

5.2.2 Reduced Search Quasi-ML Detection

The reduced search algorithm is based on two concepts: the structure of Grassmannian constellations and the nature of the received signal. In order to visualize the structure of a Grassmannian constellation, it is instructive to consider a low-dimensional example. Consider the Grassmann manifold $\mathbb{G}_1(\mathbb{R}^3)$, which is the set of

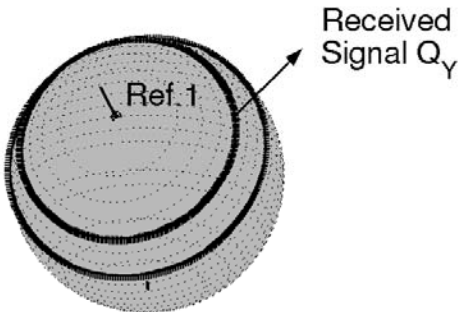

Figure 5.1: Reduced Search detection: The width of the band is determined by A_Y and B_Y.

all pairs of antipodal points that lie on (the surface of) the sphere S^2 in $\mathbb{R}^3$; see Figure 5.1. Consider a uniformly distributed constellation over the surface of the sphere and an arbitrary reference point on the constellation. Observing the constellation from $Q_{\text{ref},1}$, one can define a sequence of disjoint sets $\mathcal{C}_r(A_r, A_{r+1}, Q_{\text{ref},1})$ that cover the entire sphere. That is,

$$\mathbb{G}_1(\mathbb{R}^3) = \bigcup_r \mathcal{C}_r(A_r, A_{r+1}, Q_{\text{ref},1}),$$

where

$$\mathcal{C}_r(A_r, A_{r+1}, Q_{\text{ref},1}) = \{Q_X | A_r \leq d_D(Q_X, Q_{\text{ref},1}) < A_{r+1}\}, \tag{5.3}$$

and $d_D(\cdot,\cdot)$ is a distance metric (not necessarily the chordal Frobenius norm used in Section 4.4) and $\{A_r\}$ is a set of appropriate threshold values. For a perfect constellation, the elements of the set $\{A_{r+1} - A_r\}$ can be chosen sufficiently small for each $\mathcal{C}_r(A_r, A_{r+1}, Q_{\text{ref},1})$ to be either empty or to contain points that lie on a circle of a certain radius. For a practical constellation that is not perfectly uniform, the constellation points might be slightly perturbed and might not necessarily lie on the contour of a circle, but they will lie within a specific band.

In order to utilize the inherent structure of a Grassmannian constellation efficiently, the reduced search detector will employ a look-up table which contains the

distance between all possible constellation points $\{Q_{X_i}\}_{i=1}^{|\mathcal{C}|}$ and the reference point $Q_{\text{ref},1}$. This look-up table is only constructed once and is stored at the receiver.

In addition to the Grassmannian structure, the reduced search algorithm is also based on a specific feature of the received signal, Y. In particular, we have the following result.

Theorem 5.1 *Let $Y = Q_Y R_Y = Q_X H + V$, where $Q_Y R_Y$ is a non-unique QR decomposition of the received signal Y, Q_X is a $T \times M$ isotropically distributed random unitary matrix, $V \in \mathbb{C}^{T\times N}$ is an isotropically distributed random Gaussian matrix and $H \in \mathbb{C}^{M\times N}$. Then the mutual information between Q_X and R_Y is zero and the mutual information between Q_Y and H is zero. That is,*

$$I(Q_X; R_Y) = 0, \tag{5.4}$$

and

$$I(H; Q_Y) = 0. \tag{5.5}$$

Proof. See Appendix I.

Theorem 5.1 states that the perturbation in the signal subspace caused by the isotropically distributed additive noise does not couple the information about the signal subspace and the channel state. That is, all the information about the subspace spanned by the columns of Q_X is contained in the subspace spanned by the columns of Q_Y and all the channel state information is contained in R_Y.

In order to efficiently generate reliable decisions, the reduced search algorithm decomposes the ML detection in (5.2) into two steps. In the first step the detector uses the information contained in $Y = Q_Y R_Y$ and the look-up table to select a set of candidate codewords. In the second step the detector selects the codeword in that set with the largest likelihood; c.f., (5.2). Based on Theorem 5.1, the information

contained in R_Y and the information contained in Q_Y can be processed separately in the first step. In fact, we will show in the next section that, for each received signal matrix Y, the reduced search algorithm uses the information contained in R_Y to determine the size of the search region and the information contained in Q_Y to determine the location of the search region.

We now describe the detection procedure in more detail. The receiver initiates the detection process by computing the QR decomposition of Y. Since Theorem 5.1 states that all the information about Q_X is contained in Q_Y, the receiver attempts to localize the search by computing the distance between Q_Y and the reference point, $d_D(Q_Y, Q_{\text{ref},1})$. Using this distance, the receiver then consults the look-up table to select a certain set of candidate codewords. To determine the size of this set, the receiver uses the channel information contained in R_Y to generate two real values, A_Y and B_Y. Observing the constellation from $Q_{\text{ref},1}$, these values are used to define a band $\mathcal{C}'(A_Y, B_Y, Q_{\text{ref},1})$ that contains Q_Y. That is,

$$\mathcal{C}'(A_Y, B_Y, Q_{\text{ref},1}) = \{Q_X | A_Y \leq d(Q_X, Q_{\text{ref},1}) - d(Q_Y, Q_{\text{ref},1}) < B_Y\}. \tag{5.6}$$

Having determined $\mathcal{C}'(A_Y, B_Y, Q_{\text{ref},1})$, the second step of the detection process involves the examination of all the codewords that lie within this set against the maximum likelihood metric in (5.2). That is, the receiver decides in favour of

$$\breve{Q}_X = \arg \max_{Q_X \in \mathcal{C}'} \text{Tr}\big(Y^\dagger Q_X Q_X^\dagger Y\big). \tag{5.7}$$

Observe that $\mathcal{C}'$ is a subset of $\mathcal{C}$, and that the cardinality of $\mathcal{C}'$ depends on the width of the band in (5.6). If the width of the band is decreased, the number of likelihood computations is reduced but the probability of missing the correct codeword is increased. On the other hand, if the width of the band is increased, the probability of missing the correct codeword is reduced at the expense of computing redundant likelihoods. The trade-off between the cardinality of $\mathcal{C}'$ and performance can be

controlled through the choice of the threshold values A_Y and B_Y. In Section 4.5 we will show that by carefully choosing A_Y and B_Y, the cardinality of $\mathcal{C}'$ can be considerably reduced from that of $\mathcal{C}$ without significant loss in performance.

A further step in applying the reduced search detection strategy is to augment the look-up table by including distances from the constellation points to several other reference points. In particular, if distances from another reference point $Q_{\text{ref},2}$ are recorded in the look-up table, one can measure $d_D(Q_Y, Q_{\text{ref},1})$ and $d_D(Q_Y, Q_{\text{ref},2})$ and only consider the candidate points $Q_{\hat{X}_k}$ such that

$$Q_{\hat{X}_k} \in \bigcap_{i=1,2} \mathcal{C}'(A_Y, B_Y, Q_{\text{ref},i}).$$

From Figure 5.2, it is evident that the total area where the two bands intersect can be significantly less than the area of one band. However, this reduction in the search space must be properly accounted for in the computation of the values of A_Y and B_Y. In Section 4.5, the potential impact of using several reference points on reducing the search space is investigated.

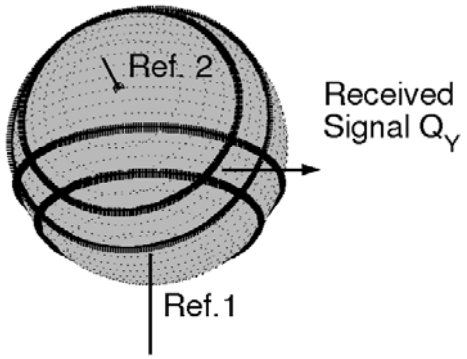

Figure 5.2: Pictorial view of the Reduced Search algorithm when two reference points are used.

An appropriate choice for the values of A_Y and B_Y in (5.6) would be one that yields the smallest value of the strap width $|A_Y - B_Y|$ that guarantees that the probability that the correct codeword does not lie inside $\mathcal{C}'$ is less than a small number, say $\delta \geq 0$.

That is,

$$(A_Y, B_Y) = \arg \inf_{\{(A,B)|P(Q_X \notin \mathcal{C}'|Y)<\delta\}} |A - B|, \tag{5.8}$$

where $\mathcal{C}'$ is defined in (5.6). Direct computation of the probability $P(Q_X \notin \mathcal{C}'|Y)$ is quite complicated and depends on the choice of the reference point. As an alternative, we propose to use Chebchev's inequality to bound this probability. Doing so, in Appendix J we obtain closed form expressions for A_Y and B_Y that can be used to generate some insight into the characteristics of the reduced search algorithm. As an indirect consequence of Theorem 5.1, we show that these threshold values are independent of both the transmitted signal subspace spanned by the columns of Q_X and the received signal subspace spanned by the columns of Q_Y. That is, we will show that the values of A_Y and B_Y depend only on R_Y. In fact, these values are dominated by the smaller singular values of the matrix R_Y. (In Appendix J we will show that R_Y is closely related to the channel matrix H.) By adjusting the values of A_Y and B_Y one can ensure that the correct codeword belongs to the set of candidate codewords with some prescribed high probability. For a channel matrix with small singular values, the width of the band, $|A_Y - B_Y|$, is typically large, which indicates that exhaustive search maximum likelihood detection is required, whereas for channel matrices with large singular values, the width of the band is small, which indicates that only a few constellation points need to be tested against the ML metric.

One drawback of the reduced search scheme is that it increases the memory requirement of the receiver. This is especially true if many reference points are used. This drawback can be reduced by quantizing distances from the reference points to the constellation points. For example, the look-up table can be organized such that the ij-th cell holds the index of the codewords that lie at distances between d_i and d_{i+1} from the j-th reference point. Using this approach we can obtain valuable reduction in the required memory.

5.3 Pairwise Error Probability

Since computing an exact expression for the probability of block error is usually infeasible in space-time signalling contexts, the pairwise error probability has often been employed to provide useful insight into the key features that govern the performance of a given space-time coding scheme [20, 23, 25, 28]. For unitary signalling in communication scenarios in which the channel is not known at the receiver, exact expressions for the pairwise error probability were derived in [23] and [25]. However, the evaluation of these exact expressions can become numerically unstable because they involve the computation of residues at poles of high multiplicities [25]. A method that uses numerical integration to evaluate the exact PEP from the expression in [23] was provided in [28]. In order to avoid numerical inconvenience, bounds on the pairwise error probabilities were developed in [23,25] and [76]. In this section we provide an alternative expression for the exact pairwise error probability. Our method differs from the one presented in [23] and [25] in that it produces an expression in the form of series expansion and avoids the computation of residues. Our series expansion is absolutely convergent and hence can be used to compute the pairwise error probability up to the required degree of precision. In fact, our method will not only yield an expression for the pairwise error probability. It will also give an expression for the distribution of the multivariate random variable involved in the computation of this probability (see Appendix K). This distribution can be useful in assessing the performance of "soft-decision" based detectors.

The pairwise error probability (PEP) $P(i \to j)$ is defined as the probability that the receiver mistakes the i-th codeword, Q_{X_i}, for the j-th codeword, Q_{X_j}, given that the i-th codeword has been transmitted. In order to compute $P(i \to j)$, we will define

the matrix Γ_{ij} to be

$$\Gamma_{ij} = \begin{bmatrix} \frac{1}{2}(1+\frac{M}{\rho T})(\Sigma_{ij}^2 - I) & \frac{1}{2}\sqrt{\frac{M}{\rho T}(1+\frac{M}{\rho T})}(I-\Sigma_{ij}^2)^{1/2}\Sigma_{ij} \\ \frac{1}{2}\sqrt{\frac{M}{\rho T}(1+\frac{M}{\rho T})}(I-\Sigma_{ij}^2)^{1/2}\Sigma_{ij} & \frac{1}{2}\frac{M}{\rho T}(I-\Sigma_{ij}^2) \end{bmatrix}, \tag{5.9}$$

where $V_{ij}\Sigma_{ij}U_{ij}^{\dagger}$ is the SVD of $Q_{X_j}^{\dagger}Q_{X_i}$. Let λ_k^{ij} be the k-th eigenvalue of Γ_{ij} and $\kappa(k)$ be the multiplicity associated with this eigenvalue. Let X_{ij} be the random variable defined as,

$$X_{ij} = \sum_{k=1}^{K_{ij}} \lambda_k^{ij} \chi^2_{2\kappa(k)N}, \tag{5.10}$$

where χ_n^2 denotes a Chi-square random variable with n degrees of freedom and K_{ij} is the number of distinct eigenvalues of Γ_{ij}. We show in Appendix K that the pairwise error probability $P(i \to j)$ is given by,

$$\begin{aligned} P(i \to j) &= P(X_{ij} \geq 0) \\ &= P(X_{ij} \geq x)\big|_{x=0}. \end{aligned} \tag{5.11}$$

In order to compute $P(X_{ij} \geq x)$, we invoke the following result from [77] and [78] to find the distribution function of X_{ij}.

Lemma 5.1 *Let $X = a(\chi^2_{2n} + a_1\chi^2_{2n_1} + \cdots + a_r\chi^2_{2n_r} - b_1\chi^2_{2m_1} - \cdots - b_s\chi^2_{2m_s})$, where the Chi-square variates are independent and $a, a_1, \ldots, a_r, b_1, \ldots, b_s$ are positive constants such that $a_i \geq 1$, $b_i \geq 1$. Define constants d_j and d'_k by the identities,*

$$\prod_{i=1}^{r} a_i^{-n_i}\big(1-(1-a_i^{-1})z\big)^{-n_i} \equiv \sum d_j z^j, \tag{5.12a}$$

$$\prod_{i=1}^{s} b_i^{-m_i}\big(1-(1-b_i^{-1})z\big)^{-m_i} \equiv \sum d'_k z^k. \tag{5.12b}$$

Let $N_f = 2(n + n_1 + \ldots + n_r)$, $M_f = 2(m_1 + \ldots + m_s)$. Then for every x,

$$P(X \geq x) = \sum_{j=0}^{\infty}\sum_{k=0}^{\infty} d_j d'_k H_{M_f+2k,N_f+2j}\Big(\frac{x}{a}\Big), \tag{5.13}$$

where $H_{2n,2m}(x) = \int_{-\infty}^{x} h_{2n,2m}(u)du$,

$$h_{2n,2m}(u) = \begin{cases} \sum_{s=0}^{n-1} 2^{-(s+m)} \frac{(m)_s}{s!} f_{2n-2s}(u), & x \geq 0, \\ \sum_{s=0}^{m-1} 2^{-(s+n)} \frac{(n)_s}{s!} f_{2m-2s}(-u), & x < 0, \end{cases}$$

$f_{2n}(x) = \frac{1}{2^n(n-1)!} e^{-x/2} x^{n-1}$, $(p)_n = p(p+1)\cdots(p+n-1)$ *and* $(p)_0 = 1$.

Using (5.11) and (5.13), one can analytically compute

$$P(i \to j) = P(X_{ij} \geq 0) = \sum_{\ell=0}^{\infty} \sum_{k=0}^{\infty} d_\ell d'_k \sum_{s=0}^{N_f/2+\ell-1} 2^{-(s+M_f/2+k)} \frac{(M_f/2+k)_s}{s!}. \quad (5.14)$$

The union bound is therefore given by

$$P_U = \frac{1}{|\mathcal{C}|} \sum_{i=1}^{|\mathcal{C}|} \sum_{\substack{j=1 \\ j \neq i}}^{|\mathcal{C}|} P(i \to j) = \frac{2}{|\mathcal{C}|} \sum_{i=1}^{|\mathcal{C}|-1} \sum_{j=i+1}^{|\mathcal{C}|} P(i \to j). \quad (5.15)$$

Notice that $d_\ell \geq 0$, $d'_k \geq 0$, $\sum d_\ell = 1$ and $\sum d'_k = 1$ and hence the series in (5.12) is absolutely convergent. Moreover, for given T, M and N, the inner summation in (5.14) is independent of both the constellation size and the SNR. Hence the inner summation need only to be computed once and can be used to assess the PEP performance of the communication system at different rates and SNRs. For $T = 2M$ and constellations generated by (4.21), one can use the results of Proposition H.1 in Appendix H, to show that only half the terms of (5.15) need to be computed.

The PEP expression in (5.14) can help to identify the impact of changes in the design parameters on the asymptotic performance of the communication system. For instance, the expressions in (5.10) and (5.14) suggest that the number of receive antennas, N, has an impact on the pairwise error probability only through the number of degrees of freedom of the associated Chi-square random variables. An increase in the degree of freedom results in a Chi-square distribution that is more concentrated around its mean. Hence, if N is increased the areas of overlap between the positively weighted and the negatively weighted Chi-square variables in (5.10) is reduced, which

results in a significantly smaller PEP. Notice that the number of receive antennas does not affect the magnitude nor the multiplicity of the eigenvalues of Γ_{ij} in (5.9). The magnitude and multiplicity of eigenvalues are solely determined by the SNR and the dimensions of the transmitted codeword, namely T and M.

5.4 Numerical results

In this section we provide a few numerical results that illustrate the efficacy of our detection approach. The channel is assumed to be Rayleigh block-fading with coherence time $T = 4$. In order to achieve the maximum number of degrees of freedom of this channel (c.f., (4.1) and (4.2)), the numbers of transmit and receive antennas were chosen to be $M = N = T/2 = 2$. We consider data rates of 2 and 2.5 bits per channel use (bpcu), which require 256-point and 1024-point Grassmannian constellations respectively. These constellations were designed using the greedy algorithm in Section 4.4.

In order to assess the effectiveness of the reduced search algorithm introduced in Section 5.2, we have plotted the corresponding block error rate when different numbers of reference points are used, for systems operating at data rates of 2 and 2.5 bpcu in Figures 5.3(a) and 5.4(a), respectively. In these figures we have also plotted the block error rate of the ML detector, as well as the union bound derived from the exact expression for the pairwise error probability of Section 5.3. From these figures, we observe that when the reduced search algorithm uses multiple reference points its performance can indeed approach that of the ML detector. In addition, our expression for the pairwise error probability seems to lead to a tighter union bound than the asymptotic union bound derived in [70]. For example, at moderate-to-high SNRs the union bound derived in Section 5.3 for our 256-point constellation is about 0.23 dB away from the actual block error rate, whereas the corresponding SNR gap

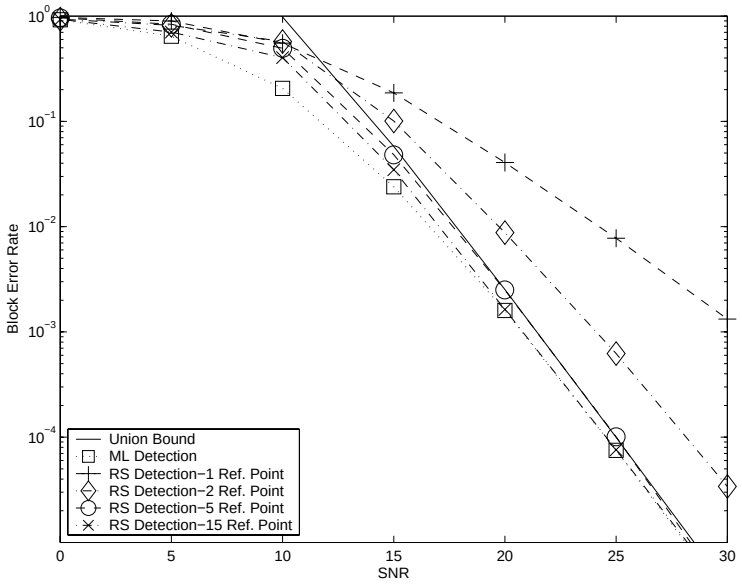

(a) Performance

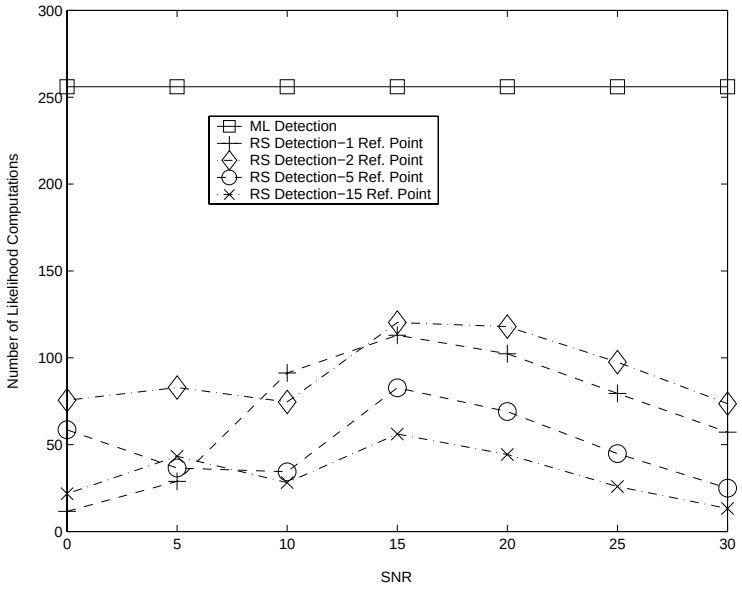

(b) Computational Cost

Figure 5.3: The performance and computational advantage of the Reduced Search detection algorithm of Section 5.2 over that of ML detection for the 256-point Grassmannian constellation.

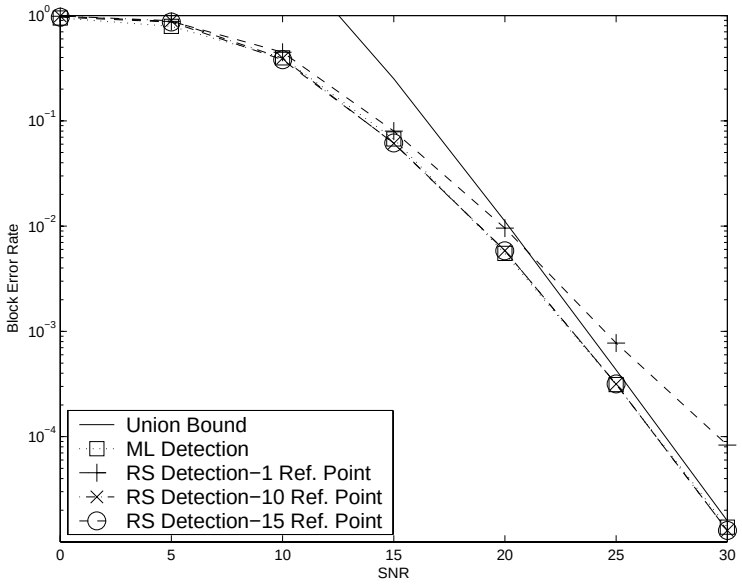

(a) Performance

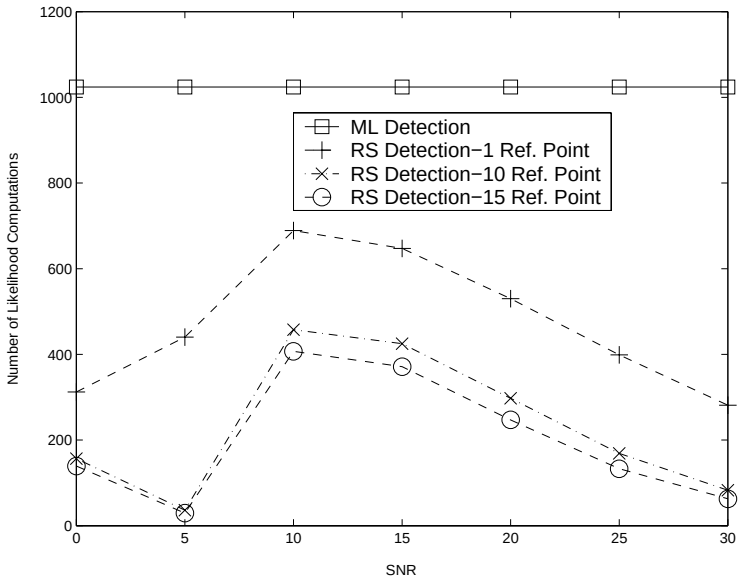

(b) Computational Cost

Figure 5.4: The performance and computational advantage of the Reduced Search detection algorithm of Section 5.2 over that of ML detection for the 1024-point Grassmannian constellation.

of the asymptotic union bound derived in [70] for the 256-point constellation in [70] is about 2 dB. In Figures 5.3(b) and 5.4(b) we have plotted the number of likelihood computations required for the reduced search algorithm. From these figures, one can conclude that an increase in the number of reference points not only results in the performance of the reduced search algorithm approaching that of the ML detector; there is also a significant reduction in the number of likelihood computations. For example, at an SNR of 30 dB, when the detector uses 15 reference points instead of 1 reference point, the average number of likelihood computations is reduced from about 75 to 25 evaluations for the 256-constellation and from about 280 to 60 likelihood computations for the 1024-constellation. Notice that for these constellations, ML detection requires the evaluation of 256 and 1024 likelihoods respectively.

5.5 Conclusion

In this chapter we have considered non-coherent MIMO communication over block Rayleigh fading channels using Grassmannian constellations. Using the perturbation analysis presented in Chapter 4 we were able to show that the information about the transmitted codeword is captured by the Q-component of the received signal matrix whereas all the channel information is contained in the R-component. We then used this result to introduce an efficient suboptimum detection strategy with a computational complexity that decays as the inverse of the square root of SNR. Finally, we have derived an exact expression for the pairwise error probability. This expression is numerically stable and was shown to be significantly tighter than other approximate expressions that have been developed in the literature. The analysis of the detection strategy and the pairwise error probability could prove valuable in identifying the role of various design parameters. For instance, while the capacity gain of choosing $N > M$ was discussed in [19], using the analyses in this chapter we are able to assess

the potential gains of choosing $N > M$ from other perspectives. In particular, we have shown in Section 5.3 how the increase in the number of receive antennas is reflected in the asymptotic error performance of the communication system. Similarly, in Appendix J.2 we have shown that this increase can offer an attractive reduction in the computational complexity of the proposed detector.

Chapter 6

Summary and future work

6.1 Summary

This thesis considered the design of space-time communication systems operating over wireless channels. Both coherent and non-coherent communication scenarios were considered.

For the coherent communication scenario, we considered the class of linear dispersion (LD) codes. This class of codes comprises a general framework that subsumes many standard designs. It was shown that, for systems with a large number of transmit antennas, constructing these codes from randomly chosen unitary matrices is asymptotically optimal from several design perspectives, including mean square error, mutual information and average pairwise error probability. Using the insight generated from the asymptotic analysis, an efficient constellation-independent design technique for finding "good" unitary coding matrices was developed for practical finite-sized systems. The resulting codes were shown to compete with and, in many instances, perform better than the best currently available codes. The asymptotic properties of unitary coded system prompted the development of a row interleaving scheme for LD codes. This scheme was shown to significantly improve the system

performance at high SNR without increasing the complexity of the detector.

For the non-coherent communication scenario, we considered space-time systems operating at moderate-to-high signal-to-noise ratios (SNRs) using Grassmannian constellations. We began by studying the manner in which the channel and noise matrices perturb the subspace spanned by the transmitted codeword matrix. This perturbation analysis was used first to determine an appropriate distance metric for constellation design and second to develop an efficient suboptimum detection strategy. The rationale behind choosing the distance metric was to quantify the perturbation that the signal subspace undergoes in a sense that conforms with the communication model. This metric was found to be the chordal Frobenius norm rather than the commonly used chordal Frobenius distance.

Having determined the appropriate distance metric, we then developed a greedy algorithm for designing Grassmannian constellations. As illustrated, the choice of the appropriate metric is reflected through the performance of these constellations. In addition to offering substantial performance gain over constellations that were designed according to other distance metrics, these constellations exhibit performance characteristics that conform to established theoretical results.

In order to promote the practical application of Grassmannian signalling, in this thesis we propose an efficient detector whose performance closely approximates that of the optimal maximum likelihood detector, but it can be implemented with a significantly less computational effort. In particular, the computational complexity of the proposed detector decays as the inverse of the square root of the SNR. The main principle on which this detector is based follows from the fact that the channel information and the transmitted codeword information can be decoupled at the receiver by performing a QR-decomposition on the received signal matrix. More specifically, using the perturbation analysis it was possible to show that the transmitted codeword information is captured by the Q-component of the received signal matrix, whereas

all the channel information is contained in the R-component.

Finally, seeing as the pairwise error probability comprises an important high SNR performance measure, an exact expression for this quantity was derived. In addition to being numerically stable, the derived expression was shown to be significantly tighter than other approximate expressions that have been developed in the literature.

The analysis of the detection strategy and the expression for the pairwise error probability provided in this thesis could prove valuable in identifying the role of various design parameters. For instance, while the capacity gain of choosing $N > M$ was discussed in [19], the analyses in this thesis made it possible to assess the potential gains of choosing $N > M$ from other perspectives. In particular, it was shown how the increase in the number of receive antennas is reflected in the asymptotic error performance of the communication system. In addition, it was shown that this increase can offer an attractive reduction in the computational complexity of the proposed detector.

6.2 Future Work

The studies conducted in this thesis have opened several research directions that appear to be worthy of exploration. In particular, one might consider the following directions for coherent communication using the LD framework.

- While in this thesis the design technique for finite size LD codes is based on optimizing the Givens rotations that were used to parametrize the unitary coding matrices, one might consider optimizing these matrices directly on the Stiefel manifold using the principles of the algorithms developed in [44].

- Instead of using numerical optimization techniques, it would be interesting to

develop an analytical method for obtaining "good" coding matrices. One approach to do that for particular block sizes is based on number theory [33].

- In this thesis, we have only considered adapting the LD framework to sphere detectors that employ a linear minimum mean squared error (MMSE) front end. However, other versions of the sphere detector that use decision-feedback equalization preprocessing stage have been shown to yield a significant reduction in complexity [38]. Adapting the LD framework to these versions of the sphere detector might be worthy of exploration.

- The fact that LD codes with unitary coding matrices exhibit several attractive performance features raises the question of whether it is possible to exploit the unitary structure of the coding matrices to simplify the detection of these codes.

- In this thesis a row interleaving scheme for LD codes was introduced. Although we have only considered one particular way to perform row interleaving, the impact of using other interleaving strategies could be investigated.

- So far we have only considered uncoded communication. Since, in practice, coding is an indispensable ingredient in the communication framework, one might want to investigate the design of LD codes in coded scenarios.

For the non-coherent channel, the work in this thesis has exposed a number of open problems that require investigation. For instance, a major contribution in this area would be to evaluate the ergodic non-coherent capacity at any SNR and to identify the distribution of the input signals that achieve this capacity. Other important potential contributions are included in the following points.

- This thesis presented a greedy technique for designing Grassmannian constellations. While the resulting constellations perform well in practice, it is expected that by designing the constellation points jointly, better performance can be

achieved. Similar to the approach adopted in the greedy technique, one way to implement joint design is to use a smooth approximation of the max(·) cost function. However, for the joint design the argument of the max(·) function is the vector containing the pairwise distance between all points in the constellation. Since the length of this vector is typically large, the approximation is required to be tighter than the one used for the greedy technique. Once an appropriate smooth approximation has been obtained, it can be minimized by applying a suitable optimization technique that is tailored to the Grassmann manifold [44].

- Since the number of constellation points grows exponentially with the data rate, direct design of Grassmannian constellations becomes excessively complex at high data rates. In order to mitigate this problem, one might consider constructing larger constellations from smaller ones. In particular, a large constellation can be viewed as the union of several subconstellations. If these subconstellations are structured so that they are well-spaced in the appropriate sense, the large constellation may exhibit favourable performance characteristics.

- Given the computational efficiency of the reduced search algorithm, it might be interesting to analytically evaluate the complexity of this type of detector in order to identify the key factors that dominate its computational cost. One strategy for doing so would be to compute the expected volume of the search region of the reduced search algorithm.

- The reduced search algorithm is based on using a number of reference points. A potential research direction is to investigate how to choose good reference points in order to guarantee affordable complexity without significant deterioration in performance. One approach to do that is to choose the reference points in such a way that minimizes the expected volume of the search region.

- The proposed reduced search detection algorithm attempts to localize the search on the Grassmann manifold. As an alternative, one might consider projecting the Grassmannian constellation points onto the Euclidean space using the coordinate representation of these points, and performing the reduced search in this space. Implementing the search algorithm in Euclidean space might provide insight for the exploration of other options to accelerate the detection procedure.

- Given the appealing performance of iterative detection techniques in coherent MIMO communication systems [12], one possible research direction is to apply these iterative techniques to non-coherent MIMO systems that use Grassmannian signalling. Some preliminary results in this direction are already available [79].

- Similar to trellis coded modulation in coherent systems, one can apply coded modulation techniques to non-coherent systems with underlying Grassmannian signalling [80]. Applying coded modulation in the Grassmannian signalling framework requires appropriate labelling of the Grassmannian symbols as well as trellis designs that take into account the geometry of the Grassmann manifold.

- While most training schemes are based on sending pilot symbols that do not contain any data to aid the receiver in identifying the channel, one might consider using Grassmannian symbols for this purpose. In particular, since the detection of Grassmannian symbols does not require channel knowledge at the receiver, one can use Grassmannian symbols during the initial communication phase. Once detected, these symbols can be used as pilot symbols for the receiver to identify the channel. Similar principles were proposed in [81].

Appendix A

Proof of Proposition 3.1

Before proceeding with the proof of Proposition 3.1, we first point out that in Lemma 3.2, the assumption of diagonal C and D matrices having non decreasing entries is without loss of generality. To show that, let $E = UCV^T$ be the singular value decomposition of an arbitrary real matrix E. Here, U and V are orthonormal and $C = \mathrm{Diag}(c_1, \ldots, c_n)$ and $c_1 \geq c_2 \geq \ldots \geq c_n \geq 0$. Now,

$$\mathrm{Tr}(E\Gamma) = \mathrm{Tr}\Big(U^T(EVV^T\Gamma)U\Big) = \mathrm{Tr}\Big((U^TEV)(V^T\Gamma U)\Big) = \mathrm{Tr}(C\Xi),$$

where $\Xi = V^T\Gamma U$. Notice that by appropriately choosing E, one can choose any entry from Γ, implying that each entry of Γ converges in distribution to a standard normal random variable. Hence, if Γ converges in distribution to the isotropic standard normal distribution then so does Ξ. (The same argument holds for D and Λ).

As mentioned in Proposition 3.1, we assume that for some $N \geq 1$, $Q \geq M$, with T/M held constant and the coding matrices are drawn at random from the group of unitary matrices. Notice that for the actual finite size coding matrices, in order to ensure the existence of coding matrices A_q that satisfy (3.17) and (3.24), the block size, T, must be restricted to be no greater than $2MQ$. However, the result in Proposition 3.1 applies for any T that grows in proportion to M. For the sake of

brevity, we will only consider square coding matrices A_q, i.e., $T/M = 1$.

We begin by observing that the (i,j)th $2T \times 2T$ block of $\frac{1}{M}\mathcal{H}\mathcal{H}^T$ is given by

$$Z_{ij} = \frac{1}{M}\sum_q \mathcal{A}_q h_i h_j^T \mathcal{A}_q^T. \tag{A.1}$$

Now the (k,ℓ)th element of this block can be written as

$$[Z_{ij}]_{k\ell} = \frac{1}{M}\sum_q \mathcal{A}_q(k,:)h_i h_j^T \mathcal{A}_q(\ell,:)^T = \frac{1}{M}\Big(h_j^T\big[\sum_q \mathcal{A}_q(\ell,:)^T\mathcal{A}_q(k,:)\big]h_i\Big), \tag{A.2}$$

where $\mathcal{A}_q(\ell,:)$ denotes the ℓ^{th} row of $\mathcal{A}_q$. Consider the following scenario. We pick $2Q$ i.i.d. random unitary coding matrices A_q from a uniform distribution with respect to the Haar measure of unitary matrices, and construct the corresponding $2M \times 2M$ matrices[1] $\mathcal{A}_q$ with the symplectic structure given in (3.6) such that $\mathcal{A}_q\mathcal{A}_q^T = \frac{M}{Q}I_{2M}$.

We note that, while the matrices A_q are uniformly distributed with respect to the Haar measure of unitary matrices, the matrices $\mathcal{A}_q$, due to their symplectic structure, are *not* uniformly distributed with respect to the Haar measure of orthogonal matrices. However, our treatment needs only the circular symmetry of A_q. By invoking the result in Lemma 3.2, we can examine the asymptotic behaviour of $[Z_{ij}]_{k\ell}$ in (A.2) as M grows. In particular, Lemma 3.2 enables us to assume independence between the entries of unitary coding matrices of sufficiently large dimensions. Using this result, we first consider the case when $|k-\ell| \neq T$ in (A.2). For that case, one can write,

$$\frac{1}{2Q}\sum_{q=1}^{2Q}\mathcal{A}_q(\ell,:)^T\mathcal{A}_q(k,:) = \frac{1}{2Q}\sum_{q=1}^{2Q}\begin{bmatrix} \mathcal{A}_q(\ell,1)\mathcal{A}_q(k,1) & \cdots & \mathcal{A}_q(\ell,1)\mathcal{A}_q(k,2M) \\ \vdots & \ddots & \vdots \\ \mathcal{A}_q(\ell,2T)\mathcal{A}_q(k,1) & \cdots & \mathcal{A}_q(\ell,2M)\mathcal{A}_q(k,2M)\end{bmatrix}. \tag{A.3}$$

Notice that for any $k \neq \ell$ or $n \neq m$, $\{\zeta_q | \zeta_q = \mathcal{A}_q(\ell,m)\mathcal{A}_q(k,n)\}_{q=1,\ldots,2Q}$ is a set of i.i.d. zero mean random variables. Thus, for $k \neq \ell$, by the strong law of large numbers, $\frac{1}{2Q}\sum_{q=1}^{2Q}\mathcal{A}_q(\ell,:)^T\mathcal{A}_q(k,:)$ converges to $0_{2M\times 2M}$ almost surely.

[1] While we have only considered square coding matrices, the generalization to rectangular matrices is straightforward.

For the case when $k = \ell$, we have for $Q \geq M$

$$\frac{1}{2Q}\sum_{q=1}^{2Q}\mathcal{A}_q(\ell,:)^T\mathcal{A}_q(\ell,:) \xrightarrow{\text{a.s.}} \rho_0 I_{2M}, \tag{A.4}$$

where $\rho_0 = \mathrm{E}\{|\mathcal{A}_q(\ell,k)|^2\} = \frac{1}{2Q}$. Next, we consider the case when $|k-\ell| = T$. In this case we notice that because of the structure in (3.6) we can no longer assume independence between the entries. In fact, for this case (c.f., (3.6)),

$$\frac{1}{2Q}\sum_{q=1}^{2Q}\mathcal{A}_q(\ell,:)^T\mathcal{A}_q(\ell,:) = \frac{1}{2Q}\sum_{q}\begin{bmatrix} A_{R,q}^T(\ell,:)A_{I,q}(\ell,:) & A_{R,q}^T(\ell,:)A_{R,q}(\ell,:) \\ -A_{I,q}^T(\ell,:)A_{I,q}(\ell,:) & A_{I,q}^T(\ell,:)A_{R,q}(\ell,:) \end{bmatrix}. \tag{A.5}$$

Now, using the independence assumption on the real and imaginary components of the entries of A_q as per Lemma 3.2, one can argue that for $Q \geq M$,

$$\frac{1}{2Q}\sum_{q=1}^{2Q}\mathcal{A}_q(\ell,:)^T\mathcal{A}_q(\ell,:) \xrightarrow{\text{a.s.}} \frac{1}{2Q}\begin{bmatrix} 0 & I_M \\ -I_M & 0 \end{bmatrix}. \tag{A.6}$$

Substituting (A.4) and (A.6) in (A.2), one obtains

$$[Z_{ij}]_{k\ell} \xrightarrow{\text{a.s.}} \frac{1}{M}\Big(h_j^T h_i \delta_{k\ell} + h_j^T \begin{bmatrix} 0 & I_M \\ -I_M & 0 \end{bmatrix} h_i \delta_{|k-\ell|,T}\Big), \tag{A.7}$$

where δ_{ij} denotes the Kronecker delta. Given our assumption on the distribution of the elements of H, it is observed that for $i \neq j$, the entries of h_i and h_j are independent. Therefore, by the strong law of large numbers, $\frac{1}{M}h_j^T h_i \xrightarrow{\text{a.s.}} 0$ and hence $[Z_{ij}]_{k\ell} \xrightarrow{\text{a.s.}} 0$. For $i = j$, the second term on the right hand side of (A.7) vanishes, and the strong law of large numbers implies that $\frac{1}{M}h_i^T h_i \xrightarrow{\text{a.s.}} 1$. Therefore,

$$[Z_{ij}]_{k\ell} \xrightarrow{\text{a.s.}} \delta_{ij}\delta_{k\ell}.$$

Thus, our claim that as M increases $\mathcal{H}\mathcal{H}^T$ converges almost surely to $\mathrm{E}\{\mathcal{H}\mathcal{H}^T\} = MI_{2NT}$ is asserted.

Appendix B

A bound on the ergodic channel capacity

Let $C(M,N,\rho)$ denote the ergodic channel capacity of a system with M transmit and N receive antennas. It is well known [2] that $C(M,N,\rho) = \mathrm{E}_H\big\{\log\det(I_N+\frac{\rho}{M}H^\dagger H)\big\}$. In order to show that the right hand side of (3.25) is an upper bound on $C(M,N,\rho)$, we point out that since $C(M,N,\rho)$ is a monotonically increasing function of M, then

$$C(M,N,\rho) \leq \lim_{\tilde{M}\to\infty} C(\tilde{M},N,\rho).$$

Furthermore,

$$\lim_{\tilde{M}\to\infty} C(\tilde{M},N,\rho) = \mathrm{E}_H\left\{\lim_{\tilde{M}\to\infty} \log\det\left(I_N + \tfrac{\rho}{\tilde{M}}\begin{bmatrix} H_1^\dagger H_1 & \cdots & H_1^\dagger H_N \\ \vdots & \ddots & \vdots \\ H_N^\dagger H_1 & \cdots & H_N^\dagger H_N \end{bmatrix}\right)\right\}, \tag{B.1}$$

$$= \mathrm{E}_H\big\{\log\det(I_N+\rho I_N)\big\}, \tag{B.2}$$

$$= N\log(1+\rho), \tag{B.3}$$

where in (B.1) we have denoted the j-th column of H by H_j. Notice that in (B.1) the mathematical expectation and the limit operations were exchanged. We will show below that this is a mathematically valid procedure. In (B.2) we have used the fact that for a richly scattered environment, the entries of the channel matrix, H, are independent identically distributed complex Gaussian random variables, $\mathcal{CN}(0,1)$, and hence for any two columns in H, H_i and H_j, we have $\lim_{\tilde{M}\to\infty} \frac{1}{\tilde{M}} H_i^\dagger H_j = \delta_{ij}$, where δ_{ij} is the Kronecker delta function.

We now show that exchanging the mathematical expectation and the limit operations in (B.1) is a valid procedure. To show that, we define a sequence of functions $\{f_{\tilde{M}}\}$, where

$$f_{\tilde{M}} = \log\det\left(I_N + \tfrac{\rho}{\tilde{M}}\begin{bmatrix} H_1^\dagger H_1 & \cdots & H_1^\dagger H_N \\ \vdots & \ddots & \vdots \\ H_N^\dagger H_1 & \cdots & H_N^\dagger H_N \end{bmatrix}\right).$$

The sequence $\{f_{\tilde{M}}\}$ is a sequence of non-negative measurable functions that satisfy $f_{\tilde{M}} \to f$ as $\tilde{M}$ tends to infinity, where

$$f = N\log(1+\rho).$$

Notice that for any $\tilde{M}$, the function $f_{\tilde{M}}$ is bounded. Hence, from the dominated convergence theorem [82, p. 67], we have that

$$\lim_{\tilde{M}\to\infty} \mathrm{E}\{f_{\tilde{M}}\} = \lim_{\tilde{M}\to\infty} \int_{-\infty}^{\infty} f_{\tilde{M}}\, p(H)dH = \int_{-\infty}^{\infty} \lim_{\tilde{M}\to\infty} f_{\tilde{M}}\, p(H)dH = \int_{-\infty}^{\infty} f\, p(H)dH, \tag{B.4}$$

where $p(H)$ is the probability density function of H. This argument confirms that exchanging the mathematical expectation and the limit operations in (B.1) is mathematically valid.

Appendix C

Gradient Computation

One way to parameterize an $M \times M$ unitary matrix, A, is through Givens rotations [48, 60, 61]. Thereby,

$$A = \Big(\prod_{m=1}^{M(M-1)/2} G_m \Big) D \Big(\prod_{m=M(M-1)/2+1}^{M(M-1)} G_m \Big), \tag{C.1}$$

where G_m is a planar rotation matrix for coordinates i_m and k_m with angle θ_m. This matrix can be constructed from the identity matrix by replacing the (i_m, i_m)th element by a, the (i_m, k_m)th element by b, the (k_m, i_m)th element by c and the (k_m, k_m)th element by d, where for Type ℓ rotations, $\ell \in \{1, 2\}$, $a = \cos(\theta_m)$, $b = \sin(\theta_m)$, $c = (-1)^{\ell} \sin(\theta_m)$ and $d = (-1)^{(\ell-1)} \cos(\theta_m)$. The matrix D is a diagonal unitary matrix; i.e, $[D]_{ii} = e^{j\phi_i}$.

If the coding matrices A_q are parameterized using (C.1), we can express the equivalent channel matrix (c.f., (3.5), (3.6)) as a function of the set of Givens rotations Θ which parameterize the matrices A_q and the physical channel H as

$$\mathcal{H}(\Theta, H) = \Big[\breve{h}_1 \quad \breve{h}_2 \quad \cdots \quad \breve{h}_{2Q} \Big],$$

where $\breve{h}_q = (I_N \otimes \mathcal{A}_q) \Big[h_1^T \quad \ldots \quad h_2^T \Big]^T$, and $\mathcal{A}_q$ is defined in (3.6). Let C denote the

matrix of cofactors of $\mathcal{H}$. Then,

$$\det(\mathcal{H}) = \sum_i [\breve{h}_j]_i C_{ij} = \breve{h}_j^T \check{C}_j,$$

where $\check{C}_j$ is the jth column of C. This expression is convenient because a given planar rotation $\theta_r \in \Theta$ affects only one coding matrix A_q. Let $q(r)$ denote the index of that matrix. Then θ_r affects only $\mathcal{A}_{q(r)}$ and $\breve{h}_{q(r)}$. That is, θ_r affects only one column of $\mathcal{H}$. Therefore,

$$\frac{\partial \det(\mathcal{H})}{\partial \theta_r} = \frac{\partial \breve{h}_{q(r)}^T}{\partial \theta_r} \check{C}_{q(r)}. \tag{C.2}$$

Since $\breve{h}_{q(r)} = \left(I_N \otimes \mathcal{A}_{q(r)}\right) \left[\begin{array}{ccc} h_1^T & \dots & h_N^T \end{array} \right]^T$, we have that

$$\frac{\partial \breve{h}_{q(r)}}{\partial \theta_r} = \left(I_N \otimes \frac{\partial \mathcal{A}_{q(r)}}{\partial \theta_r} \right) \left[\begin{array}{ccc} h_1^T & \dots & h_N^T \end{array} \right]^T. \tag{C.3}$$

Since $Q = NT$, $\mathcal{H}$ is square and hence $\det(\mathcal{H}\mathcal{H}^T) = \det(\mathcal{H})^2$. Therefore, using (C.2), (C.3) and (3.6), the chosen Givens parameterization of A_q, and the standard rules for the derivative of a composite function, the gradient is readily computed.

Appendix D

Insight into row interleaving

In this appendix we provide an intuitive argument for the effects of row interleaving on the system performance. The row interleaving operation presented in Section 3.5 offers two advantages over non-interleaved LD codes. The first advantage of row interleaving follows from the observation that row interleaving tends to increase the diagonal dominance of $\tilde{\mathcal{H}}\tilde{\mathcal{H}}^T$. The second advantage of using row interleaving is that it provides a means for increasing the diversity order.

In order to see why row interleaving tends to increase the diagonal dominance of $\tilde{\mathcal{H}}\tilde{\mathcal{H}}^T$, we write the $2T \times 2T$ blocks of $\tilde{\mathcal{H}}\tilde{\mathcal{H}}^T$ in an analogous way to the $2T \times 2T$ blocks of $\mathcal{H}\mathcal{H}^T$ in (A.1):

$$\tilde{Z}_{ij} = \sum_q \tilde{\mathcal{A}}_q \begin{bmatrix} h_i^{(1)} \\ \vdots \\ h_i^{(T)} \end{bmatrix} \begin{bmatrix} h_j^{(1)} \\ \vdots \\ h_j^{(T)} \end{bmatrix}^T \tilde{\mathcal{A}}_q^T, \qquad i,j = 1,\ldots,N. \tag{D.1}$$

The (k,ℓ)th element of this block can be written as

$$\begin{aligned} [\tilde{Z}_{ij}]_{k\ell} &= \sum_{q=1}^{2Q} \mathcal{A}_q(k,:) h_i^{(\kappa(k))} h_j^{(\kappa(\ell))^T} \mathcal{A}_q(\ell,:)^T \\ &= h_i^{(\kappa(\ell))^T} \big[\sum_{q=1}^{2Q} \mathcal{A}_q(k,:)^T \mathcal{A}_q(\ell,:)\big] h_j^{(\kappa(k))}, \end{aligned} \tag{D.2}$$

where $\kappa(i)$ was defined in (3.38).

We first consider the off-diagonal blocks of $\tilde{\mathcal{H}}\tilde{\mathcal{H}}^T$ in (3.37) and those of $\mathcal{H}\mathcal{H}^T$ in (3.5). That is, we compare entries of the blocks $\tilde{Z}_{ij}$ and Z_{ij} for which $i \neq j$ in (D.2) and (A.2) respectively. For a fixed choice of the matrices $\{\mathcal{A}_q\}$, one can easily see that these blocks are statistically equivalent since the columns h_i and h_j are independent and identically distributed Gaussian vectors.

We now compare the right hand side of (D.2) with that of (A.2) for the diagonal blocks. That is, the blocks for which $i = j$. One can see that the off-diagonal entries in (A.2) approach zero only when the coding matrices are large enough so that the summation in (A.2) vanishes. On the other hand, if we let

$$g_j^{(k,\ell)} = \big(\sum_{q=1}^{2Q} \mathcal{A}_q(k,:)^T \mathcal{A}_q(\ell,:)\big) h_j^{(\kappa(k))},$$

then the (k,ℓ)th element in (D.2) when $i = j$ can be written as

$$[\tilde{Z}_{ii}]_{k\ell} = h_i^{(\kappa(\ell))^T} g_i^{(k,\ell)}.$$

Since for $k \neq \ell$, $g_i^{(k,\ell)}$ and $h_i^{(\kappa(\ell))}$ are independent with zero-mean Gaussian distribution, we conclude that even when the coding matrices are not large enough to ensure that the summation in (A.2) vanishes, row interleaving will tend to reduce the values of the off-diagonal entries of the diagonal blocks.

We now argue that row interleaving provides a means for increasing the diversity order. In order to do that, we compare the equivalent channel expression in (3.5) with that in (3.37). To simplify the exposition, we consider the case of one receive antenna; i.e., $N = 1$. In that case, the p-th column of the equivalent channel matrix of a non-interleaved LD code can be written as $\mathcal{A}_p h$ (c.f., (3.5)), where the matrix $\mathcal{A}_p$ is of dimension $2T \times 2M$ and is specified by the code, and h is a $2M$-dimensional vector of i.i.d. Gaussian distributed entries. On the other hand, the p-th column of the equivalent channel matrix of an interleaved LD code (c.f., (3.37)) can be written

as $\tilde{\mathcal{A}}_p\tilde{h}$, where the matrix $\tilde{\mathcal{A}}_p$ is of dimension $2T \times 2TM$ and $\tilde{h}$ is a $2MT$-dimensional vector of i.i.d. Gaussian random variables that represents the channel coefficients of T independent channel realizations. Recall that the rank of the equivalent channel matrix is closely related to the diversity order of the system; see Chapter 2. We consider the ranks of both $\mathcal{H}$ and $\tilde{\mathcal{H}}$ in an extreme fading case where the channel realization H is such that $\|h\|$ falls below a small positive constant ϵ. In this case the matrix $\mathcal{H}$ in (3.5) will be in the neighbourhood of the manifold of rank-zero matrices. If this happens, the channel will be in the "out" state and no information can be reliably transfered over this particular channel realization [6]. On the other hand, if such an atypical fading event occurs for one of the channel realizations, say $H^{(t)},\ t \in \{1, \ldots, T\}$, in a row-interleaved LD coding scheme, the equivalent channel matrix $\tilde{\mathcal{H}}$ in (3.37) may still be far from becoming rank deficient. This is because the columns of $\tilde{\mathcal{H}}$ are the projections of a $2MT$-dimensional vector on $2T$-dimensional hyperplanes that are spanned by the row vectors of $\{\tilde{\mathcal{A}}_q\}$. In contrast, in the non-interleaved case, the columns of $\mathcal{H}$ are mere rotations of a $2M$-dimensional vector of i.i.d. zero-mean Gaussian entries as in the non-interleaved case. If the matrices $\{\tilde{\mathcal{A}}_q\}$ are carefully designed, using the technique outlined in Section 3.4, one can ensure that the projections of $\tilde{h}$ on the row subspaces of $\{\tilde{\mathcal{A}}_q\}$ form a set of linearly independent vectors for "almost" all channel realizations. Hence, one can see that using row interleaving provides a means for enriching the diversity of the received signal. Notice that this result holds for finite values of M and T as well as in the limit as M and T grow.

Appendix E

Proof of Lemma 4.2

Let $U_X = \begin{bmatrix} Q_X & Q_X^{\perp} \end{bmatrix}$. In order to show the desired result, we will use the following lemma.

Lemma E.1 *If G and $\hat{G}$ are defined as in* (4.9)*, then G and $\hat{G}$ are independent of each other and independent of U_X.*

Proof. Let $\Theta = \begin{bmatrix} G^{\dagger} & \hat{G}^{\dagger} \end{bmatrix}^{\dagger}$. Since the additive noise matrix V in (4.3) is isotropically distributed then $\tilde{V} = U_X^{\dagger} V = \Theta$ is also isotropically distributed with independent complex Gaussian entries. This implies that G and $\hat{G}$ are independent of each other. Furthermore, we have that

$$p(\Theta|U_X) = p(U_X^{\dagger}V|U_X) = \alpha \exp\big(-\operatorname{Tr}(V^{\dagger}U_X U_X^{\dagger}V)\big) = \alpha \exp\big(-\operatorname{Tr}(V^{\dagger}V)\big) = p(V),$$

and hence G and $\hat{G}$ are independent of U_X. Using Lemma E.1, the entries of $\big(H + \sqrt{\frac{M}{\rho T}} Q_X^{\dagger} V\big) \sim \mathcal{CN}\big(0, \frac{1}{2}(1 + \frac{M}{\rho T})\big)$ and $\sqrt{\frac{M}{\rho T}}(Q_{X_1}^{\perp})^{\dagger} V \sim \mathcal{CN}(0, \frac{M}{2\rho T})$ are statistically independent. If we let $B = \begin{bmatrix} (H + \sqrt{\frac{M}{\rho T}} G)^{\dagger} & \sqrt{\frac{M}{\rho T}} \hat{G}_1^{\dagger} \end{bmatrix}^{\dagger}$ as in (4.11), we can write

$$B = \Lambda \tilde{B}, \tag{E.1}$$

where $\Lambda = \left[\sqrt{\frac{1}{2}(1+\frac{M}{\rho T})} I_M \quad \sqrt{\frac{M}{2\rho T}} I_{N-M} \right]$ and $\tilde{B}$ is a random matrix with i.i.d. Gaussian entries. Now, for $N > M$ we have that

$$\begin{aligned} \frac{1}{\lambda_{\min}(BB^\dagger)} &= \lambda_{\max}\big((BB^\dagger)^{-1}\big), \\ &= \lambda_{\max}\big(\Lambda^{-2}(\tilde{B}\tilde{B}^\dagger)^{-1}\big), \\ &\leq \frac{2\rho T}{M\lambda_{\min}(\tilde{B}\tilde{B}^\dagger)}, \end{aligned} \tag{E.2}$$

where $\lambda_{\min}(X)$ and $\lambda_{\max}(X)$ denote the minimum and maximum eigenvalues of X. Now $\tilde{B}\tilde{B}^\dagger$ is a complex Wishart [83] matrix $\tilde{W}(N,N)$. The distribution of the minimum eigenvalue of this matrix is given by [73],

$$p_{\lambda_{\min}}(\lambda) = \frac{N}{2} e^{-\lambda N/2}. \tag{E.3}$$

Using (E.3) and (E.2), we obtain the required result. For $N = M$, the inequality in (E.2) can be replaced by equality if the scalar multiplier of $\lambda_{\min}$ in the denominator is replaced by $\frac{1}{2}(1+\frac{M}{\rho T})$.

Appendix F

Proof of Lemma 4.3

In this appendix we will use the notations of Lemma 4.1. Let K be defined such that,

$$(I_N + L^\dagger L)^{1/2} = I_N + K.$$

Using this definition of K, one can express (4.7) as

$$F = \tilde{Q}^\dagger E + K(\tilde{R} + \tilde{Q}^\dagger E).$$

From (4.8) we have

$$\begin{aligned} W &= (E - \tilde{Q}F)(\tilde{R} + F)^{-1} \\ &= (I_T - \tilde{Q}\tilde{Q}^\dagger)E(\tilde{R} + \tilde{Q}^\dagger E)^{-1}(I_N + K)^{-1} - \tilde{Q}\big(I_N - (I_N + K)^{-1}\big) \\ &= Q_2^\perp (Q_2^\perp)^\dagger E(\tilde{R} + \tilde{Q}^\dagger E)^{-1}(I_N + K)^{-1} - \tilde{Q}\big(I_N - (I_N + K)^{-1}\big) \\ &= Q_2^\perp L(I_N + L^\dagger L)^{-1/2} - \tilde{Q} + \tilde{Q}(I_N + L^\dagger L)^{-1/2} \\ &= (Q_2^\perp L + \tilde{Q})(I_N + L^\dagger L)^{-1/2} - \tilde{Q}. \end{aligned}$$

Denoting the SVD of L by $U_L \Sigma_L V_L^\dagger$ and letting $\Xi = \arccos\big((I_N + \Sigma_L^2)^{-1/2}\big)$, we obtain the desired form of W.

Appendix G

Proof of Theorem 4.1

Using Lemma 4.3 and the definition of the chordal Frobenius norm in (4.18a), one can verify that

$$\|W\| = d(Q_Y, Q_X) = 2\|\sin(\tfrac{1}{2}\Xi)\|,$$

where Ξ is defined as in Lemma 4.3. We now show that the normal and tangential components of the additive perturbation term W in (4.12) are independent of Q_X. Using (4.12), for $N = M$ we have that

$$W = \begin{bmatrix} Q_X & Q_X^{\perp} \end{bmatrix} \begin{bmatrix} 2V_L \sin^2(\frac{1}{2}\Xi)V_L^{\dagger} \\ 2U_L \sin(\frac{1}{2}\Xi)\cos(\frac{1}{2}\Xi)V_L^{\dagger} \end{bmatrix}.$$

Therefore, the tangential component is given by

$$Q_X^{\dagger} W = 2V_L \sin^2(\tfrac{1}{2}\Xi)V_L^{\dagger}, \tag{G.1}$$

and the normal component is given by

$$(Q_X^{\perp})^{\dagger} W = 2U_L \sin(\tfrac{1}{2}\Xi)\cos(\tfrac{1}{2}\Xi)V_L^{\dagger}. \tag{G.2}$$

These components are functions of Q_X through the SVD of the matrix L, which is, in turn, a random quantity that only depends on G and $\hat{G}$ in (4.9); c.f., (4.14). The

result in Lemma E.1 implies that G and $\hat{G}$ are independent of Q_X, and hence we conclude that the tangential and normal components (and hence the norm) of W are independent of Q_X as claimed.

Appendix H

Proof of Proposition 4.1

In order to prove this proposition, we begin by stating the following result.

Proposition H.1 *For $T = 2M$, if Q_{X_1}, $Q_{X_1}^{\perp}$ and Q_{X_2} belong to the codebook $\mathcal{C}$ generated by* (4.21)*, then augmenting the codebook by $Q_{X_2}^{\perp}$ does not reduce the minimum distance between constellation points.*

To prove this proposition, we merely need to show that the constellation point $Q_{X_1}^{\perp}$ does not increase the minimum chordal Frobenius norm between constellation points if those points exist as pairs of the form $(Q_{X_0}, Q_{X_0}^{\perp})$, where Q_{X_0} and $Q_{X_0}^{\perp}$ span orthogonal subspaces. Alternatively, we need to show that for $d(Q_{X_i}, Q_{X_j})$ defined as in (4.19),

$$d(Q_{X_0}, Q_{X_1}) = d(Q_{X_0}^{\perp}, Q_{X_1}^{\perp}). \tag{H.1}$$

We will use the following lemma.

Lemma H.1 *Let Q_A and Q_B be $T \times M$ unitary matrices with $T \geq 2M$. Let $Q_A^{\perp}$ be the unitary matrix whose columns span the null space of Q_A. If $U\Sigma V^{\dagger}$ denotes the SVD of $Q_A^{\dagger}Q_B$, then the SVD of $(Q_A^{\perp})^{\dagger}Q_B$ is given by $\hat{U}[(I_M - \Sigma^2)^{1/2} \;\; 0]^{\dagger}V^{\dagger}$ for some unitary matrix $\hat{U}$, where 0 denotes the all zero matrix of dimension $M \times T - 2M$.*

Proof. Observe that $Q_A^{\perp}(Q_A^{\perp})^{\dagger}$ is a projector on the null space of Q_A. The uniqueness of the projector operator [61] implies that $Q_A^{\perp}(Q_A^{\perp})^{\dagger} = I_T - Q_A Q_A^{\dagger}$. Hence,

$$\begin{aligned} Q_B^{\dagger} Q_A^{\perp}(Q_A^{\perp})^{\dagger} Q_B &= I_M - Q_B^{\dagger} Q_A Q_A^{\dagger} Q_B \\ &= I_M - V\Sigma^2 V^{\dagger} \\ &= V(I_M - \Sigma^2)V^{\dagger}. \end{aligned}$$

Using the Cholesky factorization, we conclude that the SVD of $Q_B^{\dagger}Q_A^{\perp}$ is given by $V[(I_M - \Sigma^2)^{1/2} \;\; 0]\hat{U}^{\dagger}$, for some unitary matrix $\hat{U}$.

By applying Lemma H.1 twice; first with $Q_A = Q_{X_0}$ and $Q_B = X_1$, and then with $Q_A = Q_{X_1}$ and $Q_B = Q_{X_0}^{\perp}$, we obtain the desired result.

Using the result in Proposition H.1, we now prove Proposition 4.1 by induction.

Proof. For $K = 1$, $|\mathcal{C}| = 2$, and the codebook generated by (4.21) is given by $\mathcal{C} = \{Q_{X_1}, Q_{X_1}^{\perp}\}$. Suppose that the assumption is true for $K = k$. That is, $\mathcal{C} = \{Q_{X_1}, Q_{X_1}^{\perp}, \cdots, Q_{X_k}, Q_{X_k}^{\perp}\}$. We wish to prove that the property holds for $K = k+1$. Let $Q_{X_{k+1}}$ be the $(k+1)$-th codeword generated by (4.21) with $|\mathcal{C}| = 2(k+1)$. Then by Proposition H.1, we have $Q_{X_{k+1}}^{\perp} \in \mathcal{C}$. The proof is complete.

Appendix I

Proof of Theorem 5.1

In order to prove the first statement of the theorem (c.f., (5.4)), we have from (4.7) that R_Y corresponds to a rotated version of $(\tilde{R} + F)$. Therefore, we can write,

$$R_Y = \Phi(I + LL^\dagger)^{1/2} B^{-1},$$

where $L = \hat{G}_2 B^{-1}$ (c.f., (4.14), (4.9)), B is defined in (4.11) and Φ is some unitary matrix that specifies the rotation of the basis of the subspace spanned by the columns of Q_Y. The result of Lemma E.1 in Appendix E shows that B and $\hat{G}_2$ are statistically independent of Q_X, and hence R_Y is also statistically independent of Q_X.

In order to prove the second statement (c.f., (5.5)), let $\Psi = \begin{bmatrix} \cos\big(\Xi(H)\big) V_L^\dagger \\ \sin\big(\Xi(H)\big) V_L^\dagger \end{bmatrix}$ and $U_X = \begin{bmatrix} Q_X & Q_X^\perp \end{bmatrix}$, where Ξ is defined in Lemma 4.3. The matrix Q_X and hence the matrix U_X are isotropically distributed. Then, using Lemma 4.1 and Lemma 4.3, one can write

$$Q_Y = U_X \Psi$$

In order to show that $I(Q_Y; H) = 0$, one can equivalently show that $h(Q_Y|H) = h(Q_Y)$. To that end, we have

$$h(Q_Y) \geq h(Q_Y|H) \geq h(Q_Y|\Psi). \tag{I.1}$$

The first inequality in (I.1) follows from the fact that conditioning reduces entropy [21]. The second inequality in (I.1) follows from the fact that H affects Q_Y only through Ψ. That is, Ψ contains more information about Q_Y than H because it involves information about the noise components.

We now prove that $p(Q_Y|\Psi) = p(Q_Y)$. In order to do that, we only need to show that

$$p(U_X\Psi|\Psi) = g(U_X), \tag{I.2}$$

for some function g. Let $U_\Psi = \begin{bmatrix}\Psi & \Psi^\perp\end{bmatrix}$ be a square unitary matrix, where $\Psi^\perp$ is the orthogonal complement of Ψ. Now, because U_Ψ contains more information about Q_Y than Ψ, we have

$$h(Q_Y|\Psi) \geq h(Q_Y|U_\Psi). \tag{I.3}$$

In order to evaluate the differential entropy $h(Q_Y|U_\Psi)$, we consider the marginal distribution $p(Q_Y|U_\Psi)$, which is given by

$$p(Q_Y|U_\Psi) = p\big(U_X U_\Psi \left[\begin{smallmatrix} I_M \\ 0_{T-M\times M}\end{smallmatrix}\right]|U_\Psi\big). \tag{I.4}$$

Consider the marginal probability distribution $p(U_X U_\Psi|U_\Psi)$. Since for a fixed unitary matrix U_Ψ, the matrix $U_X U_\Psi$ is unitary and isotropically distributed, we have [65]

$$\begin{aligned} p(U_X U_\Psi|U_\Psi) &= \alpha \int d\Omega e^{\imath \operatorname{Tr}\left(\Omega(U_\Psi^\dagger U_X^\dagger U_X U_\Psi - I_T)\right)} \\ &= \alpha \int d\Omega e^{\imath \operatorname{Tr}\left(U_\Psi \Omega U_\Psi^\dagger (U_X^\dagger U_X - I_T)\right)}, \end{aligned} \tag{I.5}$$

where the integration is over the space of Hermitian matrices Ω and α is a normalizing scalar. We now perform a change of variables so that Υ is the Hermitian matrix given by $\Upsilon = U_\Psi \Omega U_\Psi^\dagger$. That is, $\Omega = U_\Psi^\dagger \Upsilon U_\Psi$. Using a result in [83], it can be shown that the differential

$$d\Upsilon = d\Omega.$$

Using this result with the expression in (I.5), we have

$$p(U_X U_\Psi | U_\Psi) = \alpha \int d\Upsilon e^{\imath \operatorname{Tr}\left(\Upsilon (U_X^\dagger U_X - I_T)\right)}. \tag{I.6}$$

The right hand side of (I.6) is not a function of U_Ψ. Hence, $p(Q_Y|U_\Psi) = p(Q_Y)$. Using this result in (I.1) and (I.3) completes the proof.

Appendix J

Threshold Values Computations

This appendix proposes a method for determining the threshold values A_Y and B_Y for the reduced search quasi-ML detection strategy described in Section 5.2.2. As pointed out in that section, proper selection of these values is critical in controlling the trade-off between complexity and performance of the reduced search detection strategy. Our method for selecting A_Y and B_Y is based on using Chebychev's inequality to bound the probability of missing the correct codeword in the set of candidate codewords. In the initial development we will first focus on the $N = M$ case. Later, we will discuss the extension to the case when $N > M$.

J.1 $N = M$ case

Let P_m be the probability of missing the correct symbol Q_X in the set of candidate points. That is, P_m denotes the probability that $Q_X \notin \mathcal{C}'$, where Q_X is the transmitted symbol, $\mathcal{C}' \triangleq \{Q_{X_i} | A_Y \leq d_D(Q_{X_i}, Q_{\text{ref},1}) - d_D(Q_Y, Q_{\text{ref},1}) < B_Y\}$ and $d_D(\cdot, \cdot)$ is the distance metric used by the detector. For convenience we choose the squared projection Frobenius norm for the distance metric; c.f. (4.20). That is,

$$d_D(Q_{X_2}, Q_{X_1}) = d_p^2(Q_{X_2}, Q_{X_1}) = \|Q_{X_2} Q_{X_2}^\dagger - Q_{X_1} Q_{X_1}^\dagger\|_F^2.$$

Define ξ to be the following function of the transmitted signal matrix Q_X, the received signal matrix $Y = Q_X H + \sqrt{\frac{M}{\rho T}} V = Q_Y R_Y$ and the reference point $Q_{\text{ref},1}$.

$$\begin{aligned}
\xi &= \frac{1}{2}\|Q_Y Q_Y^\dagger - Q_{\text{ref},1} Q_{\text{ref},1}^\dagger\|^2 - \frac{1}{2}\|Q_X Q_X^\dagger - Q_{\text{ref},1} Q_{\text{ref},1}^\dagger\|^2 \\
&= \|Q_Y^\dagger Q_{\text{ref},1}\|^2 - \|Q_X^\dagger Q_{\text{ref},1}\|^2 \\
&= \|(Q_X + W)^\dagger Q_{\text{ref},1}\|^2 - \|Q_X^\dagger Q_{\text{ref},1}\|^2 \qquad \text{(J.1)} \\
&= \text{Tr}\big(Q_{\text{ref},1}^\dagger (W + Q_X)(W + Q_X)^\dagger Q_{\text{ref},1}\big) - \text{Tr}\big(Q_{\text{ref},1}^\dagger Q_X Q_X^\dagger Q_{\text{ref},1}\big), \qquad \text{(J.2)}
\end{aligned}$$

where the equality in (J.1) follows from Lemma 4.1. Let $\bar{\xi} = \text{E}\{\xi|Y\}$ and $\sigma_\xi^2 = \text{Var}\{\xi|Y\}$, where the expectation is taken with respect to the isotropically distributed transmitted signal Q_X, the channel H and noise V. For some strap width $\tau > 0$, the probability of missing P_m can be expressed as,

$$P_m = P\big(|\xi - \bar{\xi}| > \tau\big). \qquad \text{(J.3)}$$

Direct computation of the probability in (J.3) is quite complicated and depends on the choice of the reference point. Using Chebyshev's inequality, we have, for any $\tau > 0$,

$$P(|\xi - \bar{\xi}| \geq \tau) \leq \frac{\sigma_\xi^2}{\tau^2}. \qquad \text{(J.4)}$$

This inequality suggests that for P_m to be bounded by a certain constant, a good choice of τ scales with σ_ξ, i.e.,

$$\tau = k\sigma_\xi. \qquad \text{(J.5)}$$

(We will discuss later in this section how to choose the value of k.) The corresponding threshold values, A_Y and B_Y, are given by

$$A_Y = -\tau + \bar{\xi}, \qquad B_Y = \tau + \bar{\xi}. \qquad \text{(J.6)}$$

In order to determine the values of A_Y and B_Y, we need to find $\bar{\xi}$ and σ_ξ. To do so, we will first show that $\bar{\xi}$ and σ_ξ are independent of the actual choice of the

reference point. We will then proceed to compute $\bar{\xi}$ and σ_ξ. Since the transmitted signal, Q_X, the channel realizations, H, and noise, V, are all independent random processes, we can compute $\bar{\xi}$ and σ_ξ by first performing the expectation over Q_X and then the expectations over H and V.

We begin by using Lemma 4.1 to expose the dependency of ξ on H, V and Q_X. From (4.5) we have $(W+Q_X)R_Y = Q_XH + \sqrt{\frac{M}{\rho T}}V$. Let $U_X = \begin{bmatrix} Q_X & Q_X^{\perp} \end{bmatrix}$, $G = \sqrt{\frac{M}{\rho T}}Q_X^{\dagger}V$ and $\hat{G} = \sqrt{\frac{M}{\rho T}}(Q_X^{\perp})^{\dagger}V$; c.f., (4.9). Substituting into (J.2) we obtain

$$\begin{aligned}\xi &= \mathrm{Tr}\big(Q_{\mathrm{ref},1}^{\dagger}U_XU_X^{\dagger}(Q_XH+E)R_Y^{-1}R_Y^{-\dagger}(Q_XH+E)^{\dagger}U_XU_X^{\dagger}Q_{\mathrm{ref},1}\big)\\ &\quad - \mathrm{Tr}\big(Q_{\mathrm{ref},1}^{\dagger}U_XU_X^{\dagger}Q_XQ_X^{\dagger}U_XU_X^{\dagger}Q_{\mathrm{ref},1}\big) \qquad \text{(J.7)}\\ &= \mathrm{Tr}\left((Q'_{\mathrm{ref},1})^{\dagger}\begin{bmatrix} H+G \\ \hat{G}\end{bmatrix}R_Y^{-1}R_Y^{-\dagger}\begin{bmatrix}(H+G)^{\dagger} & \hat{G}^{\dagger}\end{bmatrix}Q'_{\mathrm{ref},1}\right)\\ &\quad - \mathrm{Tr}\left((Q'_{\mathrm{ref},1})^{\dagger}\begin{bmatrix} I_M & 0 \\ 0 & 0\end{bmatrix}Q'_{\mathrm{ref},1}\right), \qquad \text{(J.8)}\end{aligned}$$

where $Q'_{\mathrm{ref},1} = U_X^{\dagger}Q_{\mathrm{ref},1}$. Observe that the averaging over Q_X has been absorbed into averaging over the reference point. This indicates that as far as the moments of ξ are concerned, the reference points are identical.

The noise matrices G, $\hat{G}$ and the channel matrix H are independent Gaussian random matrices. In particular, $G \sim \mathcal{CN}(0, \frac{M}{2\rho T})$, $\hat{G} \sim \mathcal{CN}(0, \frac{M}{2\rho T})$, $H \sim \mathcal{CN}(0, \frac{1}{2})$ and $H+G \sim \mathcal{CN}(0, \frac{1}{2}(1+\frac{M}{\rho T}))$. Observe that G is the component of noise that adds directly to the channel. That is, G contributes additively to the received signal power. However, at high SNR, the variance of this component decays as $1/\rho$, and hence the effect becomes negligible.

Assuming that the channel matrix H is nonsingular, from Lemma 4.1 we have

that at high SNR,

$$\begin{aligned} R_Y &= \Phi\big(I + (H+G)^{-\dagger}\hat{G}^{\dagger}\hat{G}(H+G)^{-1}\big)^{-1/2}(H+G) \\ &\approx \Phi\big(I + H^{-\dagger}\hat{G}^{\dagger}\hat{G}H^{-1}\big)^{-1/2}H \\ &= \Phi\Big(H^{-\dagger}\big(H^{\dagger}H + \hat{G}^{\dagger}\hat{G}\big)H^{-1}\Big)^{-1/2}H \\ &\approx \Phi H, \end{aligned} \tag{J.9}$$

where we have used the fact that at high SNR, the variance of both G and $\hat{G}$ decays as $1/\rho$, and Φ is a unitary matrix that specifies the orientation of the basis within the subspace[1]. Substituting (J.9) into (J.8), we obtain,

$$\xi \approx \mathrm{Tr}\left((Q'_{\mathrm{ref},1})^{\dagger}\begin{bmatrix} 0 & R_Y^{-\dagger}\hat{G}^{\dagger} \\ \hat{G}R_Y^{-1} & \hat{G}R_Y^{-1}R_Y^{-\dagger}\hat{G}^{\dagger}\end{bmatrix}Q'_{\mathrm{ref},1}\right). \tag{J.10}$$

Using the result in (J.9), we can assume that R_Y is independent of $Q'_{\mathrm{ref},1}$ and $\hat{G}$, which enables us to compute $\bar{\xi}$ and σ_{ξ}^2 based on the approximate expression in (J.10). To begin with, we will compute the conditional expectations $\bar{\xi}_{|\hat{G}}$ and $\sigma_{\xi|\hat{G}}$ and then we will compute the expectation over $\hat{G}$. If we let

$$P = \begin{bmatrix} 0 & R_Y^{-\dagger}\hat{G}^{\dagger} \\ \hat{G}R_Y^{-1} & \hat{G}R_Y^{-1}R_Y^{-\dagger}\hat{G}^{\dagger}\end{bmatrix}, \tag{J.11}$$

then,

$$\bar{\xi}_{|\hat{G}} = \mathrm{E}\{\mathrm{Tr}\big(Q'_{\mathrm{ref},1}(Q'_{\mathrm{ref},1})^{\dagger}P\big)\} = \frac{M}{T}\,\mathrm{Tr}\big(\hat{G}R_Y^{-1}R_Y^{-\dagger}\hat{G}^{\dagger}\big), \tag{J.12}$$

where we have used the fact that for isotropically distributed $Q'_{\mathrm{ref},1}$, a result in [84] implies that

$$\mathrm{E}\{Q'_{\mathrm{ref},1}(Q'_{\mathrm{ref},1})^{\dagger}\} = \frac{M}{T}I_T.$$

[1]Note that the receiver has no access to Φ. That is, the receiver does not know the rotation of the QR decomposition that corresponds to the signal propagation through the channel.

In order to compute $\sigma_{\xi|\hat{G}}$, we begin by finding

$$\begin{aligned}\mathrm{E}\{\xi^2|\hat{G}\} &= \mathrm{E}\{\mathrm{Tr}^2\big((Q'_{\mathrm{ref},1})^\dagger P Q'_{\mathrm{ref},1}\big)\},\\ &= \sum_{j,k,m,n=1}^{T} p_{jk}p_{mn} \sum_{i,\ell=1}^{M} \mathrm{E}\{q^*_{ji}q_{ki}q^*_{ml}q_{nm}\}, \end{aligned} \tag{J.13}$$

where q_{ij} and p_{ij} are ij-th entries of $Q'_{\mathrm{ref},1}$ and P, respectively. Notice that our result here complements the result in [64] in which the variance of the same quadratic term is computed for Gaussian matrices rather than the isotropically distributed unitary matrices. In order to compute the statistical expectation in (J.13), we make use of the following lemma from [84], which we have extended to the case of complex unitary matrices.

Lemma J.1 *Let Q be a $T \times M$ random isotropically distributed unitary matrix. The following statements hold.*

(i) The multiplication of a fixed row or column of Q by $e^{i\theta}$ does not destroy the isotropic distribution. Consequently, the mixed moments of elements of a random unitary matrix are zero unless each index occurs an even number of times in the product of which we take expectation.

(ii) For all $i \in [1,T]$ and $j \in [1,M]$, $\alpha_1 \stackrel{\triangle}{=} \mathrm{E}\{|q_{ij}|^4\} = \frac{2}{T(T+1)}$.

(iii) For all $i \in [1,T]$, $j \in [1,M]$ and $k \in [1,M], k \neq j$, $\alpha_2 \stackrel{\triangle}{=} \mathrm{E}\{|q_{ij}|^2|q_{ik}|^2\} = \frac{1}{T(T+1)}$.

(iv) For all $i \in [1,T]$, $\ell \in [1,T], \ell \neq i$ and $j \in [1,M]$, $\mathrm{E}\{|q_{ij}|^2|q_{\ell j}|^2\} = \frac{1}{T(T+1)} = \alpha_2$.

(v) For all $i \in [1,T]$, $\ell \in [1,T], \ell \neq i$, $j \in [1,M]$ and $k \in [1,M], k \neq j$, $\alpha_3 \stackrel{\triangle}{=} \mathrm{E}\{|q_{ij}|^2|q_{\ell k}|^2\} = \frac{1}{(T-1)(T+1)}$.

(vi) For all $i \in [1,T]$, $\ell \in [1,T], \ell \neq i$, $j \in [1,M]$ and $k \in [1,M], k \neq j$, $\alpha_4 \stackrel{\triangle}{=} \mathrm{E}\{q^*_{ij}q_{ik}q_{\ell j}q^*_{\ell k}\} = \frac{-1}{(T-1)T(T+1)}$.

It follows from (i), that only the terms with the following indices will be non-zeros in the expectation: $\{j = k = m = n, i = \ell\}$, $\{j = k \neq m = n, i = \ell\}$, $\{j = n \neq k = m, i = \ell\}$, $\{j = k = m = n, i \neq \ell\}$, $\{j = k \neq m = n, i \neq \ell\}$ and $\{j = n \neq k = m, i \neq \ell\}$.

Using the results in Lemma J.1, after regrouping and arranging terms, we can express $\mathrm{E}\{\xi^2|\hat{G}\}$ as,

$$\mathrm{E}\{\xi^2|\hat{G}\} = (\alpha_2 M + \alpha_4 M(M-1))\,\mathrm{Tr}(P^2) + (\alpha_2 M + \alpha_3 M(M-1))\big(\mathrm{Tr}(P)\big)^2. \quad \text{(J.14)}$$

In order to compute $\bar{\xi}$ and σ_ξ, we still need to average the expressions in (J.12) and (J.14) over $\hat{G}$. To that end, we observe that $\hat{G}$ is an isotropically distributed Gaussian random matrix. Hence, using the SVD of $R_Y^{-1} = U_Y \Sigma_Y V_Y^\dagger$,

$$\bar{\xi}_{|\hat{G}} = \frac{M}{T}\,\mathrm{Tr}\big(\hat{G} R_Y^{-1} R_Y^{-\dagger} \hat{G}^\dagger\big) = \frac{M}{T}\sum_{i=1}^{M} \sigma_i^2 \|g_i\|^2,$$

where we have used the fact that $\hat{G}U_Y \overset{d}{=} \hat{G}$, where $\overset{d}{=}$ denotes equality in distribution and the i-th column of $\hat{G}$ is denoted as g_i and the i-th diagonal entry of Σ_Y as σ_i. Similarly, using (J.11),

$$\begin{aligned}
\mathrm{Tr}(P^2) &= 2\,\mathrm{Tr}\big(\hat{G}\Sigma_Y^2\hat{G}^\dagger\big) + \mathrm{Tr}\big(\Sigma_Y\hat{G}^\dagger\hat{G}\Sigma_Y^2\hat{G}^\dagger\hat{G}\Sigma_Y\big) \\
&= 2\sum_{i=1}^{M}\sigma_i^2\|g_i\|^2 + \|\Sigma_Y\hat{G}^\dagger\hat{G}\Sigma_Y\|^2 \\
&= 2\sum_{i=1}^{M}\sigma_i^2\|g_i\|^2 + \sum_{i=1}^{M}\sigma_i^4\|g_i\|^4 + \sum_{i=1}^{M}\sum_{\substack{j=1\\ j\neq i}}^{M}\sigma_i^2\sigma_j^2\|g_i\|^2\|g_j\|^2.
\end{aligned}$$

Likewise,

$$\big(\mathrm{Tr}(P)\big)^2 \overset{d}{=} \sum_{i=1}^{M}\sigma_i^4\|g_i\|^4 + \sum_{i=1}^{M}\sum_{\substack{j=1\\ j\neq i}}^{M}\sigma_i^2\sigma_j^2\|g_i\|^2\|g_j\|^2. \quad \text{(J.15)}$$

Now, $\|g_i\|^2$ is a Chi-square random variable with $2(T-M)$ degrees of freedom and

Gaussian variance equal to $\frac{M}{2\rho T}$. Hence,

$$\bar{\xi} = \frac{M^2(T-M)}{T^2\rho}\sum_{i=1}^{M}\sigma_i^2. \tag{J.16}$$

$$\begin{aligned}\mathrm{E}\{\mathrm{Tr}(P^2)\} &= 2\frac{M(T-M)}{T\rho}\sum_{i=1}^{M}\sigma_i^2 \\ &\quad + \frac{M^2(T-M)(T-M+1)}{T^2\rho^2}\sum_{i=1}^{M}\sigma_i^4 + \frac{M^2(T-M)^2}{T^2\rho^2}\sum_{i=1}^{M}\sum_{\substack{j=1\\ j\neq i}}^{M}\sigma_i^2\sigma_j^2.\end{aligned} \tag{J.17}$$

$$\mathrm{E}\{\big(\mathrm{Tr}(P)\big)^2\} = \frac{M^2(T-M)(T-M+1)}{T^2\rho^2}\sum_{i=1}^{M}\sigma_i^4 + \frac{M^2(T-M)^2}{T^2\rho^2}\sum_{i=1}^{M}\sum_{\substack{j=1\\ j\neq i}}^{M}\sigma_i^2\sigma_j^2. \tag{J.18}$$

Using (J.17), (J.18), (J.14), (J.16) and the fact that

$$\sigma_\xi^2 = \mathrm{E}\big\{\mathrm{E}\{\xi^2|\hat{G}\}\big\} - \bar{\xi}^2,$$

one can readily compute the proposed values of A_Y and B_Y given in (J.6) for any given R_Y.

We now make a few remarks regarding the values computed for A_Y and B_Y.

- The high SNR asymptotic result in (J.9) conforms with the result of Theorem 5.1 that the channel information is captured by the R-component of the received signal. However, Theorem 5.1 asserts a stronger claim; at any SNR the channel information is contained in R_Y.

- Notice the dependence of A_Y and B_Y on the the singular values of R_Y. Specifically, as the singular values of R_Y^{-1} grow, indicating that the channel is close to singularity (c.f., (J.9)), the width of the search region should be increased in order to maintain a reasonable likelihood of the transmitted codeword being within the search region.

- Notice that, as a consequence of Theorem 5.1, the values of A_Y and B_Y turn out to be independent of the received signal subspace spanned by Q_Y.

- As the SNR, $\rho \to \infty$, σ_ξ^2 goes to zero as fast as $1/\rho$. Therefore, $P_m \to 0$, (c.f., (J.4)), which indicates that the width of the search region approaches zero. In that case, if more than one reference point is used, no likelihoods need to be computed. Hence the computation cost of the reduced search detector is simply the cost of computing $d_D(Q_Y, Q_{\text{ref},i})$, which involves a small number of computations that depends linearly on the number of reference points.

It remains to determine an appropriate choice for the parameter k in (J.5). To that end we have the following comments.

(i) The above analysis was based on using one reference point. When increasing the number of reference points, we found it beneficial to slightly increase the scaling parameter (J.5). Since the distribution of ξ in (J.8) seems complicated to compute, even in the case of one reference point, the computation of an exact scaling parameter does not seem feasible. We will therefore assume that ξ is a zero-mean Gaussian random variable, and determine a method for adjusting the scaling factor according to the number of reference points, N_{ref}. Suppose that k_1 in (J.5) is the parameter used when one reference point is used and we wish to find the corresponding value $k_{N_{\text{ref}}}$ associated with a choice of N_{ref} different reference points. For N_{ref} points, the event of missing occurs if the correct codeword does not lie in the prescribed strap associated with the first reference point or it does not lie in the prescribed strap associated with the second reference point, and so on. Since our estimation of the missing probability is based on the moments of ξ (c.f., (J.4)), which are invariant under the choice of the reference point, we conclude that the estimate of the probability of missing is simply the sum of probabilities that the correct codeword does not lie in one

of the prescribed strap. That is, $P_m = N_{\text{ref}} P_{m_0}$, where P_{m_0} is the probability of missing with respect to the first reference point, $Q_{\text{ref},1}$. Our goal is to find $k_{N_{\text{ref}}}$ such that

$$N_{\text{ref}} P_{m_0}(k_{N_{\text{ref}}}) = P_{m_0}(k_1). \tag{J.19}$$

Under the Gaussian assumption on ξ, and with the choice of τ in (J.5), we have from (J.19), that

$$k_{N_{\text{ref}}} = \sqrt{2}\,\text{erfc}^{-1}\big(\tfrac{1}{N_{\text{ref}}}\,\text{erfc}(k_1/\sqrt{2})\big). \tag{J.20}$$

This choice of $k_{N_{\text{ref}}}$, though approximate, provides reasonable guidance as to how k should be adjusted with the number of reference points.

(ii) It is well known that the bound given by Chebychev's inequality (J.4) is quite loose. A better bound can be derived using the Chernoff bound. However, the latter involves computations that require the distribution of the entries of random unitary matrices. One approach might be to assume Gaussianity of the entries, which is an asymptotically tight assumption [84], but this is beyond our current scope.

(iii) We now consider the effect of choosing a particular k on the probability of error and the detection complexity. Let the probability of error be denoted as $P_e(\rho)$. The probability of error is the probability that the codeword in $\mathcal{C}'$ with the highest likelihood, say $\hat{Q}_X$, is not the transmitted codeword, Q_X. This probability can be written as,

$$\begin{aligned} P_e(\rho) &= P(\hat{Q}_X \neq Q_X | Q_X \in \mathcal{C}') \times P(Q_X \in \mathcal{C}') + P(Q_X \notin \mathcal{C}'), \\ &= (1 - P_m) P(\hat{Q}_X \neq Q_X | Q_X \in \mathcal{C}') + P_m, \\ &\approx P(\hat{Q}_X \neq Q_X | Q_X \in \mathcal{C}') + P_m, \end{aligned} \tag{J.21}$$

where the approximation in (J.21) is based on the assumption that $P_m \ll 1$. The first term on the right hand side of (J.21) denotes the inherent probability

of error due to ML detection, whereas the second term is the probability of error due to the correct codeword falling outside the reduced search region $\mathcal{C}'$. In order to ensure that our choice of k does not result in significant deterioration in the performance of the receiver, P_m must be maintained small with respect to $P(\hat{Q}_X \neq Q_X | Q_X \in \mathcal{C}')$. We note that for a given value of k, the Chebychev bound in (J.4) asserts that P_m is upper bounded by $1/k^2$. However, this bound is generally loose [22] and one can afford to use values of k smaller than those predicted by this bound without significantly affecting the overall probability of error. In particular, at high SNR the probability of missing P_m can be large compared to the inherent probability of error of ML detection. This suggests that in order to ensure that the performance of the reduced search detector continues to be essentially the same as that of the ML detector, larger values of k must be chosen at higher SNRs. That is, we should allow the scaling parameter k to be a function of the SNR. However, we would still like to have $|\mathcal{C}'| \to 1$ as $\rho \to \infty$. Since σ_ξ decays as fast as $\frac{1}{\sqrt{\rho}}$, we seek a function that grows no faster than $\sqrt{\rho}$. One such function is the $\log(\cdot)$ function which results in an overall decay in the strap width at a rate of $\frac{\log(\rho)}{\sqrt{\rho}}$. In Section 4.5 we show that this choice of k yields good trade-off in performance versus decoding complexity.

J.2 $N > M$ case

In this case, the channel matrix, $H \in \mathbb{C}^{M\times N}$ is fat. Let H be partitioned as $H_1 \in \mathbb{C}^{M\times M}$ and $H_2 \in \mathbb{C}^{M\times(N-M)}$, $V \in \mathbb{C}^{T\times N}$ be partitioned as $V_1 \in \mathbb{C}^{T\times M}$ and $V_2 \in \mathbb{C}^{T\times(N-M)}$. Assume that the receiver performs the unique QR-decomposition of Y

such that R_Y is an upper triangular matrix. That is,

$$Y = Q_Y R_Y = \begin{bmatrix} Q_{Y_1} & Q_{Y_2} \end{bmatrix} \begin{bmatrix} R_{Y_{11}} & R_{Y_{12}} \\ 0 & R_{Y_{22}} \end{bmatrix} \tag{J.22}$$

$$= Q_X \begin{bmatrix} H_1 & H_2 \end{bmatrix} + \sqrt{\tfrac{M}{\rho T}} \begin{bmatrix} V_1 & V_2 \end{bmatrix}. \tag{J.23}$$

Therefore, using (J.22) and (J.23), we have

$$Q_{Y_1} R_{Y_{11}} = Q_X H_1 + \sqrt{\tfrac{M}{\rho T}} V_1, \tag{J.24}$$

$$Q_{Y_1} R_{Y_{12}} + Q_{Y_2} R_{Y_{22}} = Q_X H_2 + \sqrt{\tfrac{M}{\rho T}} V_2. \tag{J.25}$$

From (J.24), it is clear that we could determine the search region by simply applying the previous algorithm to the first M columns of Y. In that case, the probability of missing the correct codeword in $\mathcal{C}'$ would be the same as that when $N = M$, but the information from the additional antennas is naturally incorporated into the likelihoods; c.f., (5.7). The performance of that approach can be significantly improved by first permuting Y so that the diagonal entries of R_Y are arranged in non-increasing order of their absolute values [61]. The results in Section J.1 suggest that the width of the search region is dominated by the inverse of the square of the minimum singular value of R_Y; i.e., the minimum eigenvalue of $R_Y R_Y^\dagger$. Since the eigenvalues of a positive semidefinite matrix strongly majorize the absolute values of its diagonal entries [48], we conclude that subsequent to the permutation of Y, the width of the search region that corresponds to the upper left $M \times M$ block of R_Y is typically less than the width of the search region that corresponds to blocks of smaller diagonal entries. That is, the diversity gain offered by the increase in the number of receive antennas can be used to reduce the adverse effect of atypically weak channel realizations on the detection complexity. In that way, the additional receive antennas play a role in both the selection of the candidate codewords and in the values of the likelihoods; something that improves the trade-off between the probability of missing and the

number of likelihood computations. This trade-off could be more tightly controlled by exploiting the information in (J.25). However, such an algorithm would need to compute the distance not only between codewords and reference points but also the distance between the $(N-M)$-dimensional null spaces of the $T \times M$ codewords and the reference points. That is, the look-up table would have to be augmented in order to include the distance to reference points from all possible $(N-M)$-dimensional null spaces of the $T \times M$ codewords. Since there are $\binom{T-M}{N-M}$ possible null spaces associated with each $T \times M$ codeword and $T \geq \min\{M,N\}+N = M+N$, attempting to reduce the probability of missing the correct codeword in $\mathcal{C}'$ by exploiting the null space information contained in (J.25) would require an increase in memory size that would be hard to justify. Fortunately, the probability of missing can be easily controlled via the scaling factor k in (J.6) and the number of reference points at a small storage cost.

Appendix K

Pairwise error probability

The pairwise error probability (PEP) $P(i \to j)$ is defined as the probability that the receiver mistakes the i-th codeword for the j-th one given that the i-th codeword has been transmitted. Assuming that the receiver employs an ML detector[1] (c.f., (5.2)), then the PEP is given by,

$$P(i \to j) = P\big(\mathrm{Tr}(Y^\dagger Q_{X_i} Q_{X_i}^\dagger Y) \leq \mathrm{Tr}(Y^\dagger Q_{X_j} Q_{X_j}^\dagger Y)\big). \tag{K.1}$$

Since we assume Q_{X_i} to be the transmitted codeword, then the received signal can be expressed as $Y = Q_{X_i} H + \sqrt{\frac{M}{\rho T}} V$, where H is the $M \times N$ isotropically distributed (i.d.) complex Gaussian channel matrix and V is the $T \times N$ i.d. complex Gaussian additive noise matrix.

Now consider the first term in the probability argument in (K.1). Let G and $\hat{G}$ be defined as in (4.9). Then,

$$\mathrm{Tr}(Y^\dagger Q_{X_i} Q_{X_i}^\dagger Y) = \mathrm{Tr}\big((H^\dagger + \sqrt{\tfrac{M}{\rho T}} G^\dagger)(H + \sqrt{\tfrac{M}{\rho T}} G)\big) = \|S\|_F^2, \tag{K.2}$$

where $S = (H + \sqrt{\frac{M}{\rho T}} G)$ is a zero mean isotropically distributed complex Gaussian

[1] Notice that the performance of the reduced search detector in Section 5.2.2 is very similar to that of the ML detector.

random matrix with variance $\frac{1}{2}(1+\frac{M}{\rho T})$ per real dimension. Similarly,

$$\mathrm{Tr}(Y^\dagger Q_{X_j} Q_{X_j}^\dagger Y) = \|H^\dagger Q_{X_i}^\dagger Q_{X_j} + \sqrt{\tfrac{M}{\rho T}} V^\dagger Q_{X_j}\|_F^2 \tag{K.3}$$

$$= \left\| H^\dagger Q_{X_i}^\dagger Q_{X_j} + \sqrt{\tfrac{M}{\rho T}} V^\dagger \begin{bmatrix} Q_{X_i} & Q_{X_i}^\perp \end{bmatrix} \begin{bmatrix} Q_{X_i}^\dagger \\ (Q_{X_i}^\perp)^\dagger \end{bmatrix} Q_{X_j} \right\|_F^2 \tag{K.4}$$

$$= \|S^\dagger Q_{X_i}^\dagger Q_{X_j} + \hat{G}^\dagger (Q_{X_i}^\perp)^\dagger Q_{X_j}\|_F^2. \tag{K.5}$$

The $(T-M)\times N$ random matrix $\hat{G}$ is zero mean isotropically distributed (i.d.) complex Gaussian with variance of $\frac{1}{2}\frac{M}{\rho T}$ per real dimension. From Lemma E.1 in Appendix E, we have that $\hat{G}$ and G are statistically independent. Using the result of Lemma H.1 in Appendix H and equation (K.5), the PEP in (K.1) can be written as,

$$P(i\to j) = P\Big(\|S\|^2 \le \|V_{ij}\Sigma_{ij}U_{ij}^\dagger S + V_{ij}[(I-\Sigma_{ij}^2)^{1/2} \;\; 0]\hat{U}_{ij}^\dagger \hat{G}\|^2\Big) \tag{K.6}$$

$$= P\Big(\|S\|^2 \le \|V_{ij}\big((\Sigma_{ij}U_{ij}^\dagger S + [(I-\Sigma_{ij}^2)^{1/2} \;\; 0]\hat{U}_{ij}^\dagger \hat{G}\big)\|^2\Big) \tag{K.7}$$

$$= P\Big(\|U_{ij}^\dagger S\|^2 \le \|(\Sigma_{ij}U_{ij}^\dagger S + [(I-\Sigma_{ij}^2)^{1/2} \;\; 0]\hat{U}_{ij}^\dagger \hat{G})\|^2\Big) \tag{K.8}$$

$$= P\Big(\|S_A\|^2 \le \|\Sigma_{ij}S_A + (I-\Sigma_{ij}^2)^{1/2}S_B\|^2\Big), \tag{K.9}$$

where $V_{ij}\Sigma_{ij}U_{ij}^\dagger$ and $V_{ij}\Sigma_{ij}\hat{U}_{ij}^\dagger$ denote the SVD of $Q_{X_j}^\dagger Q_{X_i}$ and $Q_{X_j}^\dagger Q_{X_i}^\perp$ respectively, $S_A = U_{ij}^\dagger S$ and $S_B = [I_M \;\; 0]\hat{U}_{ij}^\dagger \hat{G}$. Notice that because $T \ge 2M$ (c.f., (4.1)), S_A and S_B are independent $M\times N$ i.d. Gaussian random matrices with respective variances $\frac{1}{2}(1+\frac{M}{\rho T})$ and $\frac{1}{2}\frac{M}{\rho T}$ per real dimension . The equality in (K.8) follows from the invariance of the norm under unitary transformation. Now,

$$P(i\to j) = P\Big(\mathrm{Tr}(S_A^\dagger S_A) \le \mathrm{Tr}(S_A^\dagger \Sigma_{ij}^2 S_A + S_A^\dagger \Sigma_{ij}(I-\Sigma_{ij}^2)^{1/2}S_B + S_B^\dagger \Sigma_{ij}(I-\Sigma_{ij}^2)^{1/2}S_A + S_B^\dagger (I-\Sigma_{ij}^2)S_B\Big), \tag{K.10}$$

$$= P\Big(0 \le \mathrm{Tr}(S_A^\dagger(\Sigma_{ij}^2 - I)S_A + S_A^\dagger \Sigma_{ij}(I-\Sigma_{ij}^2)^{1/2}S_B + S_B^\dagger \Sigma_{ij}(I-\Sigma_{ij}^2)^{1/2}S_A + S_B^\dagger (I-\Sigma_{ij}^2)S_B)\Big). \tag{K.11}$$

Let $\tilde{S}_A$ and $\tilde{S}_B$ be the zero mean and unit variance i.d Gaussian random matrices $\sqrt{\frac{2\rho T}{\rho T+M}}S_A$ and $\sqrt{\frac{2\rho T}{M}}S_B$, respectively. If we let S_C be the i.d. random Gaussian matrix with i.i.d. zero mean unit variance entries given by $S_C = \begin{bmatrix} \tilde{S}_A^\dagger & \tilde{S}_B^\dagger \end{bmatrix}$, and let Γ_{ij} be given by

$$\Gamma_{ij} = \begin{bmatrix} \frac{1}{2}(1+\frac{M}{\rho T})(\Sigma_{ij}^2 - I) & \frac{1}{2}\sqrt{\frac{M}{\rho T}(1+\frac{M}{\rho T})}(I-\Sigma_{ij}^2)^{1/2}\Sigma_{ij} \\ \frac{1}{2}\sqrt{\frac{M}{\rho T}(1+\frac{M}{\rho T})}(I-\Sigma_{ij}^2)^{1/2}\Sigma_{ij} & \frac{1}{2}\frac{M}{\rho T}(I-\Sigma_{ij}^2) \end{bmatrix},$$

then one can express the argument of the trace in (K.11) as

$$S_A^\dagger(\Sigma_{ij}^2-I)S_A+S_A^\dagger\Sigma_{ij}(I-\Sigma_{ij}^2)^{1/2}S_B+S_B^\dagger\Sigma_{ij}(I-\Sigma_{ij}^2)^{1/2}S_A+S_B^\dagger(I-\Sigma_{ij}^2)S_B = S_C\Gamma_{ij}S_C^\dagger. \tag{K.12}$$

Notice that Γ_{ij} is symmetric and hence using the eigen decomposition of Γ_{ij} we obtain, $\Gamma_{ij} = Q_{ij}\Lambda_{ij}Q_{ij}^\dagger$. Since S_C is i.d., then $S_C \overset{d}{=} \tilde{S}_C = S_C Q_{ij}$ and the expression in (K.11) reduces to

$$P(i\to j) = P\big(0 \le \mathrm{Tr}(\tilde{S}_C\Lambda_{ij}\tilde{S}_C^\dagger)\big) \tag{K.13}$$

$$= P\Big(0 \le \sum_{k=1}^{2M}\lambda_k^{ij}\|S_{C_k}\|^2\Big), \tag{K.14}$$

where S_{C_k} is the k-th column of $\tilde{S}_C$. Since $\|S_{C_k}\|^2$ is a Chi-square distributed random variable with $2N$ degrees of freedom, then if we denote the multiplicity of λ_k^{ij} by $\kappa(k)$, the expression in (5.11) follows.

It remains to determine the eigenvalues of Γ_{ij} in terms of Σ_{ij}. For brevity, we will use the following notation, $\gamma_{11} = \frac{1}{2}(1+\frac{M}{\rho T})$, $\gamma_{22} = \frac{1}{2}\frac{M}{\rho T}$ and $\gamma_{12} = \sqrt{\gamma_{11}\gamma_{22}}$. Furthermore, we will suppress the subscript ij in Γ_{ij} and Σ_{ij}, and we will define $\Theta = (I-\Sigma^2)^{1/2}$. Using these notations we obtain

$$\Gamma = \begin{bmatrix} -\gamma_{11}\Theta^2 & \gamma_{12}\Theta\Sigma \\ \gamma_{12}\Theta\Sigma & \gamma_{22}\Theta^2 \end{bmatrix}, \tag{K.15}$$

where Θ and Σ are both diagonal matrices with non negative entries given by θ_ℓ and σ_ℓ, respectively. In order to compute λ_k for $k \in \{1, 2, \ldots, 2M\}$, we need to find the roots of $\det(\Gamma - \lambda I)$. Assuming that $-\gamma_{11}\Theta^2 - \lambda I$ is nonsingular, an expression for those roots can be obtained by using the expression for the determinant of a block partitioned matrix [48] and the diagonal structure of Θ and Σ. Specifically, one can show that

$$\begin{aligned}
\det(\Gamma - \lambda I) &= \det\big(-\gamma_{12}^2\Theta^4 + \frac{\lambda}{2}\Theta^2 + \lambda^2 I - \gamma_{12}^2\Theta^2\Sigma^2\big) \\
&= (-1)^M \det\big(\gamma_{12}^2\Theta^2(\Theta^2 + \Sigma^2) - \frac{\lambda}{2}\Theta^2 - \lambda^2 I\big) \\
&= (-1)^M \det\big(\gamma_{12}^2\Theta^2 - \frac{\lambda}{2}\Theta^2 - \lambda^2 I\big) \\
&= \prod_{i=1}^{M}\big(\lambda^2 + \frac{\lambda}{2}\theta_i^2 - \gamma_{12}^2\theta_i^2\big).
\end{aligned}$$

Therefore, the eigenvalues of Γ are given by,

$$\lambda_i = \frac{\theta_i}{4}\Big(-\theta_i \pm \sqrt{\theta_i^2 + 16\gamma_{12}^2}\Big),$$

and hence one can see that Γ has M non-positive eigenvalues.

Bibliography

[1] S. N. Diggavi, N. Al-Dhahir, A. Stamoulis, and A. R. Calderbank, "Great expectations: the value of spatial diversity in wireless networks," *IEEE Proc.*, vol. 92, pp. 219–270, Feb. 2004.

[2] I. E. Telatar, "Capacity of multiantenna Gaussian channels," *Eur. Trans. Telecom.*, vol. 10, pp. 585–595, Nov. 1999.

[3] S. Barabarossa, *Multiantenna Wireless Communication Systems*. Boston: Artech House, 2005.

[4] E. Biglieri, J. Proakis, and S. Shamai, "Fading channels: Information-theoretic and communication aspects," *IEEE Trans. Informat. Theory*, vol. 44, pp. 2619–2692, Oct. 1998.

[5] J. G. Proakis, *Digital Communications*. New York: McGraw-Hill, 3rd ed., 1995.

[6] L. Zheng and D. N. C. Tse, "Diversity and multiplexing: A fundamental tradeoff in multiple antenna channels," *IEEE Trans. Informat. Theory*, vol. 49, pp. 1073–1096, May 2003.

[7] K. Azarian and H. E. Gamal, "The throughput-reliability tradeoff in MIMO channels," Sept. 2005. Submitted to *IEEE Trans. Informat. Theory*. Also available at `http://arxiv.org/abs/cs.IT/0509021`.

[8] A. Scaglione, P. Stoica, S. Barbarossa, G. B. Giannakis, and H. Sampath, "Optimal designs for space-time linear precoders and decoders," *IEEE Trans. Signal Processing*, vol. 50, pp. 1051–1064, May 2002.

[9] Z. Liu, Y. Xin, and G. B. Giannakis, "Space-time-frequency coded OFDM over frequency-selective fading channels," *IEEE Trans. Signal Processing*, vol. 50, pp. 2465–2476, Oct. 2002.

[10] G. J. Foschini and M. J. Gans, "On limits of wireless communication in a fading environment when using multiple antennas," *Wireless Personal Commun.*, vol. 6, pp. 311–335, Mar. 1998.

[11] J. Ling, D. Chizhik, P. W. R. Valenzuela, N. Costa, and K. Huber, "Multiple transmit multiple receive (MTMR) capacity survey in Manhattan," *IEEE Electron. Lett.*, vol. 37, pp. 1041–1042, Aug. 2001.

[12] B. M. Hochwald and S. ten Brink, "Achieving near-capacity on a multiple-antenna channel," *IEEE Trans. Commun.* , vol. 51, pp. 389–399, Mar. 2003.

[13] A. Goldsmith, S. A. Jafar, N. Jindal, and S. Vishwanath, "Capacity limits of MIMO channels," *IEEE J. Select. Areas Commun.*, vol. 21, pp. 684–701, June 2003.

[14] B. Hassibi and B. M. Hochwald, "High-rate codes that are linear in space and time," *IEEE Trans. Informat. Theory*, vol. 48, pp. 1804–1824, July 2002.

[15] G. J. Foschini, "Layered space-time architecture for wireless communication in a fading environment when using multielement antennas," *Bell Labs Tech. J.* , vol. 1, Autumn 1996.

[16] T. L. Marzetta and B. M. Hochwald, "Capacity of a mobile multiple-antenna communication link in Rayleigh flat fading," *IEEE Trans. Informat. Theory*, vol. 45, pp. 139–157, Jan. 1999.

[17] E. Visotsky and U. Madhow, "Space-time transmit precoding with imperfect feedback," *IEEE Trans. Informat. Theory*, vol. 47, pp. 2632–2639, Sept. 2001.

[18] U. Fincke and M. Pohst, "Improved methods for calculating vectors of short length in a lattice, including a complexity analysis," *Math. Comput.*, vol. 44, pp. 463–471, Apr. 1985.

[19] L. Zheng and D. N. C. Tse, "Communication on the Grassmann manifold: A geometric approach to the noncoherent multiple-antenna channel," *IEEE Trans. Informat. Theory*, vol. 48, pp. 359–383, Feb. 2002.

[20] V. Tarokh, N. Seshadri, and A. R. Calderbank, "Space-time codes for high data rate wireless communication: Performance criterion and code construction," *IEEE Trans. Informat. Theory*, vol. 44, pp. 744–765, 1998.

[21] T. M. Cover and J. A. Thomas, *Elements of Information Theory*. New York: Wiley, 1991.

[22] A. Papoulis, *Probability, Random Variables and Stochastic Processes*. New York: McGraw-Hill, 2nd ed., 1984.

[23] B. M. Hochwald and T. L. Marzetta, "Unitary space-time modulation multiple-antenna communications in Rayleigh flat fading," *IEEE Trans. Informat. Theory*, vol. 46, pp. 543–564, Mar. 2000.

[24] B. Hassibi and B. M. Hochwald, "How much training is needed in multiple-antenna wireless links?," *IEEE Trans. Informat. Theory*, vol. 49, pp. 951–963, Apr. 2003.

[25] M. Brehler and M. K. Varanasi, "Asymptotic error probability analysis of quadratic receivers in Rayleigh-fading channels with applications to a unified analysis of coherent and noncoherent space-time receivers," *IEEE Trans. Informat. Theory*, vol. 47, pp. 2383–2399, Sept. 2001.

[26] V. Tarokh, H. Jafarkhani, and A. R. Calderbank, "Space-time block codes from orthogonal designs," *IEEE Trans. Informat. Theory*, vol. 45, pp. 1456–1467, July 1999.

[27] X. Ma and G. B. Giannakis, "Full-diversity full-rate complex-field space-time coding," *IEEE Trans. Signal Processing*, vol. 51, pp. 2917–2930, Nov. 2003.

[28] B. M. Hochwald, T. L. Marzetta, and B. Hassibi, "Space-time autocoding," *IEEE Trans. Informat. Theory*, vol. 47, pp. 2761–2781, Nov. 2001.

[29] S. M. Alamouti, "A simple transmitter diversity scheme for wireless communications," *IEEE J. Select. Areas Commun.*, vol. 16, pp. 1451–1458, Oct. 1998.

[30] X.-B. Liang, "Orthogonal designs with maximal rates," *IEEE Trans. Informat. Theory*, vol. 49, pp. 2468–2503, Oct. 2003.

[31] G. Foschini, G. Golden, R. Valenzuela, and P. Wolniansky, "Simplified processing for high spectral efficiency wireless communication employing multi-element arrays," *IEEE J. Select. Areas Commun.*, vol. 17, pp. 1841–1852, Nov. 1999.

[32] H. El Gamal and M. O. Damen, "Universal space-time coding," *IEEE Trans. Informat. Theory*, vol. 49, pp. 1097–1119, May 2003.

[33] J.-K. Zhang, K. M. Wong, and T. N. Davidson, "Information lossless full rate full diversity cyclotomic linear dispersion codes," in *Proc. IEEE Int. Conf. Acoustics, Speech, and Signal Processing*, (Montreal), May 2004.

[34] B. Hassibi, "An efficient square-root algorithm for BLAST," in *Proc. IEEE Int. Conf. Acoustics, Speech, and Signal Processing*, vol. 2, (Istanbul, Turkey), pp. II737–II740, June 2000.

[35] G. Ginis and J. M. Cioffi, "On the relation between V-BLAST and the GDFE," *IEEE Commun. Lett.*, vol. 5, pp. 364–366, Sept. 2001.

[36] E. Viterbo and J. Boutros, "A universal lattice code decoder for fading channels," *IEEE Trans. Informat. Theory*, vol. 45, July 1999.

[37] B. Hassibi and H. Vikalo, "On sphere decoding algorithm. I. Expected complexity," *IEEE Trans. Signal Processing*, vol. 53, pp. 2806–2818, Aug. 2005.

[38] M. O. Damen, H. El Gamal, and G. Caire, "On maximum-likelihood detection and the search of the closest lattice point," *IEEE Trans. Informat. Theory*, vol. 49, pp. 2389–2402, Oct. 2003.

[39] M. O. Damen, K. Abed-Meraim, and J. C. Belfiore, "Generalised sphere decoder for asymmetrical space-time communication architecture," *Electronics Letters*, vol. 36, pp. 166–167, Jan. 2000.

[40] E. Agrell, T. Eriksson, A. Vardy, and K. Zeger, "Closest point search in lattices," *IEEE Trans. Informat. Theory*, vol. 48, pp. 2201–2214, Aug. 2002.

[41] J. Jaldén and B. Ottersten, "On the complexity of sphere decoding in digital communications," *IEEE Trans. Signal Processing*, vol. 53, pp. 1474–1484, Apr. 2005.

[42] A. Murugan, H. E. Gamal, M. O. Damen, and G. Caire, "A unified framework for tree search decoding: Rediscovering the sequential decoder." Submitted to the *IEEE Trans. Informat. Theory*. Also available at `http://arxiv.org/abs/cs.IT/0506029`.

[43] J. Luo, K. R. Pattipati, P. Willet, and G. M. Levchuk, "Fast optimal and suboptimal any-time algorithms for CDMA multiuser detection based on branch and bound," *IEEE Trans. Commun.* , vol. 52, pp. 632–642, Apr. 2004.

[44] A. Edelman, T. Arias, and S. Smith, "The geometry of algorithms with orthogonality constraints," *SIAM J. Matrix Anal. Appl.*, vol. 20, no. 2, pp. 303–353, 1998.

[45] H. El Gamal, M. O. Damen, and N. C. Beaulieu, "Linear threaded algebraic space-time constellations," *IEEE Trans. Informat. Theory*, vol. 49, pp. 2372–2388, Oct. 2003.

[46] R. W. Heath and A. J. Paulraj, "Linear dispersion codes for MIMO systems based on frame theory," *IEEE Trans. Signal Processing*, vol. 50, pp. 2429–2441, Oct. 2002.

[47] J.-K. Zhang, J. Liu, and K. M. Wong, "Trace-Orthogonal Full Diversity Cyclotomic Space-Time Codes," in *Space-Time Processing for MIMO Communications* (A. Gershman and N. Sidiropoulos, eds.), New York: Wiley, June 2005.

[48] R. A. Horn and C. R. Johnson, *Topics in Matrix Analysis*. Cambridge: Cambridge University Press, 1994.

[49] J. C. Belfiore and G. Rekaya, "Quaternionic lattices for space-time coding," in *Proc. IEEE Informat. Theory Wkshp*, (Paris), pp. 267–270, Apr. 2003.

[50] F. A. Graybill, *Matrices with Applications in Statistics*. Belmont, CA: Wadsworth, second ed., 1983.

[51] A. Paulraj, R. Nabar, and D. Gore, *Introduction to Space-Time Wireless Communications*. Cambridge, UK: Cambridge Univ. Press, 2003.

[52] N. Piskunov, *Differential and Integral Calculus*. Moscow: MIR Press, 1969.

[53] A. D. Aristotile, P. Diaconis, and C. M. Newman, "Brownian motion and the classical groups," Tech. Rep. 2002-18, Stanford University, Dept. of Statistics, Stanford, California, Aug. 2002.

[54] L. Nachbin, *The Haar Integral*. Princeton, New Jersey: D. Van Nostrand Company, Inc., 1965.

[55] R. Kashaev and O. Tirkkonen, "Linear matrix modulators from group representation theory," in *Proc. IEEE Informat. Theory Wkshp*, (Paris), pp. 42–45, Apr. 2003.

[56] H. El Gamal and A. Hammons, "On the design of algebraic space-time codes for MIMO block-fading channels," *IEEE Trans. Informat. Theory*, vol. 49, pp. 151–163, Jan. 2003.

[57] A. Graham, *Kronecker Products and Matrix Calculus: with Applications*. New York: Elis Horwood Ltd., 1981.

[58] A. Gaivoronski, "Stochastic Quasigradient Methods and Their Implementation," in *Numerical Techniques for Stochastic Optimization*, ch. 16, pp. 313–351, New York: Springer-Verlag, 1988.

[59] J. H. Manton, "Optimization algorithms exploiting unitary constraints," *IEEE Trans. Signal Processing*, vol. 50, pp. 635–650, Mar. 2002.

[60] B. Hassibi and B. M. Hochwald, "Cayley differential unitary space-time codes," *IEEE Trans. Informat. Theory*, vol. 48, pp. 1485–1503, June 2002.

[61] G. H. Golub and C. F. van Loan, *Matrix Computations*. Baltimore, MD: The Johns Hopkins University Press, third ed., 1996.

[62] M. C. Jeruchim, P. Balaban, and K. S. Shanmugan, *Simulation of Communication Systems*. New York: Plenum Press, 1992.

[63] Y. Xin, Z. Wang, and G. B. Giannakis, "Space-time diversity systems based on linear constellation precoding," *IEEE Trans. Wireless Commun.*, vol. 2, pp. 294–309, Mar. 2003.

[64] C. Rao and B. Hassibi, "Analysis of multiple antenna wireless links at low SNR," *IEEE Trans. Informat. Theory*, vol. 50, pp. 2123–2130, Sept. 2004.

[65] B. Hassibi and T. L. Marzetta, "Multiple-antennas and isotropically random unitary inputs: the received signal density in closed form," *IEEE Trans. Informat. Theory*, vol. 48, pp. 1473–1484, June 2002.

[66] A. Lapidoth and S. M. Moser, "Capacity bounds via duality with applications to muliple-antenna systems on flat-fading channels," *IEEE Trans. Informat. Theory*, vol. 49, pp. 2426–2467, Oct. 2003.

[67] D. Agrawal, T. Richardson, and R. Urbanke, "Multiple-antenna signal constellations for fading channels," *IEEE Trans. Informat. Theory*, vol. 47, pp. 2618–2626, Sept. 2001.

[68] P. Dayal, M. Brehler, and M. K. Varanasi, "Leveraging coherent space-time codes for noncoherent communication via training," *IEEE Trans. Informat. Theory*, vol. 50, pp. 2058–2080, Sept. 2004.

[69] A. Barg and D. Y. Nogin, "Bounds on packings of spheres in the Grassmann manifold," *IEEE Trans. Informat. Theory*, vol. 48, pp. 2450–2454, Sept. 2002.

[70] M. L. McCloud, M. Brehler, and M. K. Varanasi, "Signal design and convolutional coding for noncoherent space-time communication on the block-Rayleigh-fading channel," *IEEE Trans. Informat. Theory*, vol. 48, pp. 1186–1194, May 2002.

[71] M. J. Borran, A. Sabharwal, and B. Aazhang, "On design criteria and construction of noncoherent space-time constellations," *IEEE Trans. Informat. Theory*, vol. 49, pp. 2332–2351, Oct. 2003.

[72] G. W. Stewart, "Perturbation bounds for the QR factorization of a matrix," *SIAM J. Num. Anal.*, vol. 14, pp. 509–518, June 1977.

[73] A. Edelman, "Eigenvalues and condition numbers of random matrices," *SIAM J. Matrix Anal. Appl.*, vol. 9, pp. 543–560, Oct. 1988.

[74] I. Kammoun and J.-C. Belfiore, "A new family of Grassmann space-time codes for non-coherent MIMO systems," *IEEE Commun. Lett.*, vol. 7, pp. 528–530, Nov. 2003.

[75] J. H. Conway, R. H. Hardin, and N. J. A. Sloane, "Packing lines, planes, etc.: Packings in Grassmannian spaces," *Exper. Math.*, vol. 5, no. 2, pp. 139–159, 1996.

[76] R. Li and P. Y. Kam, "New tight bounds on the pairwise error probability for unitary space-time modulations," *IEEE Commun. Lett.*, vol. 4, pp. 289–291, Apr. 2005.

[77] J. Robinson, "The distribution of a general quadratic form in normal variates," *Austral. J. Statist.*, vol. 7, no. 3, pp. 110–114, 1965.

[78] N. Johnson and S. Kotz, *Distributions in Statistics: Continuous Univariate Distributions–2*. New York: Wiley, 1970.

[79] M. A. El-Azizy, R. H. Gohary, and T. N. Davidson, "A BICM scheme with iterative demapping and decoding for non-coherent MIMO communication," 2006. To appear in *Proc. IEEE Int. Conf. Commun.*

[80] W. Zhao, G. Leus, and G. B. Giannakis, "Orthogonal design of unitary constellations for uncoded and trellis-coded noncoherent space-time systems," *IEEE Trans. Informat. Theory*, vol. 50, pp. 1319–1327, June 2004.

[81] Y. Yu, G. B. Giannakis, and N. Jindal, "Noncoherent modulation for MIMO training and related capacity analysis," June 2005. Submitted to the *IEEE Trans. Informat. Theory*.

[82] E. M. Stein and R. Shakarchi, *Real Analysis*. Princeton, New Jersey: Princeton Univ. Press, 2005.

[83] R. J. Muirhead, *Aspects of Multivariate Statistical Theory*. New York: Wiley, 1982.

[84] C. Stein, "The accuracy of the normal approximation to the distribution of the traces of powers of random orthogonal matrices," Tech. Rep. 470, Stanford University, Dept. of Statistics, Stanford, California, Mar. 1995.